Mathematical Modelling of Brain Haemodynamics and Pressure-Volume Compensation

Ka Hing Chu
Supervised by Dr Peter Smielewski

Hughes Hall

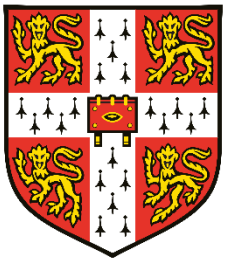

UNIVERSITY OF CAMBRIDGE

This thesis is submitted for the degree of
Doctor of Philosophy

February 2024

Preface

This thesis is the result of my own work and includes nothing which is the outcome of work done in collaboration except as declared in the preface and specified in the text. It is not substantially the same as any work that has already been submitted, or, is being concurrently submitted, for any degree, diploma or other qualification at the University of Cambridge or any other University or similar institution except as declared in the preface and specified in the text. It does not exceed the prescribed word limit for the relevant Degree Committee.

Ka Hing Chu

29/02/2024

Summary

Traumatic brain injury (TBI) is a major global health issue with diverse demographics and a dynamic clinical profile. Modern care of a pathology with such variabilities involves individualised treatment, which requires an accurate understanding of pressure-volume interactions inside the cranium. This thesis used a hydrodynamic model representing the circulation of cerebral fluids to investigate the relationships between intracranial pressure (ICP) and cerebral blood volume (CBV) changes. The effects of these relationships on the performance of indices describing vascular dynamics were also examined.

The background of this project is discussed in Chapters 1 to 4 of this thesis. **Chapter 1** provides a description of the anatomical and physiological aspects of the cerebrospinal space, including the circulation of cerebral fluids and the pressure-volume interactions among different compartments within the cranium. **Chapter 2** introduces the pathophysiology of cerebral hydrodynamics in patients with TBI, and the important role of neuro-monitoring in its management. **Chapter 3** specifies the aims and hypotheses of this project, while **Chapter 4** includes a literature review of previous modelling work in cerebral blood flow (CBF) and cerebrospinal fluid (CSF) dynamics.

In this project, a computer programme was written to create an implementation of the electrical equivalence of the hydrodynamic model. With a set of model parameters and imported data, the programme was used to simulate the pressures and flows of fluids in different intracranial compartments. Details of the programme were specified in **Chapter 5**, while experiments with the model were included in Chapters 6 to 9.

In **Chapter 6**, the validity of an existing model was tested with a series of experiments simulating various clinical phenomena. The simulations include pathophysiological features caused by dynamic variations in cerebrovascular properties, as well as prolonged changes in CBV.

In **Chapter 7**, the existing model was modified to include a compartment representing the bulk flow of cerebral interstitial fluid (ISF), coupled with the cerebrovascular compartment. The new model was tested using the same sets of experiments in the previous chapter, with its results compared to the original model.

In **Chapter 8**, the modified model was used to assess the performance of common autoregulation indices in response to changing strength of cerebral autoregulation (CA), thus identifying the physiological factors determining the reliability of CA assessments.

In **Chapter 9**, the modified model was used to explore the interplay between brain compliances and vascular reactivity, and its influence on pressure reactivity indices. The ability of the model to replicate clinical features observed in TBI patients was also investigated.

In conclusion, the model has proved to be a robust tool to study the pressure-volume interactions among various intracranial compartments, as well as the performance of CA and pressure reactivity indices in different scenarios. The work in this thesis has laid the foundation of creating a 'digital twin' of cerebral hydrodynamics, with the potential of improving the individualisation of treatments in neuro-intensive care, particularly in dynamic pathologies such as TBI.

Acknowledgements

I would like to start by expressing my gratitude to my supervisor, Dr Peter Smielewski, for his incredible guidance and generous support throughout my postgraduate journey. From writing the first line of source code to the final paragraph of this thesis, his tireless and professional supervisions have equipped me with the knowledge and mindset as a researcher, allowing me to begin my first steps towards original investigations in the exciting field of Clinical Neuroscience. I am also very grateful to my advisor, Prof Marek Czosnyka for his encouragement and valuable advice to my project, and Dr Zofia Czosnyka who has imparted to me the clinical skills essential for biomedical research.

Many thanks to my colleagues of the Brain Physics Laboratory and Addenbrooke's Hospital: Dr Erta Beqiri, Dr Michal Placek, Dr Xiuyun Liu, Dr Leanne Calviello, Dr Afroditi Lalou, Mr Manuel Cabeleira, Ms Ihsane Olakorede, and Ms Kate Lee. Our collaborations and friendship, especially at the most challenging times of the COVID-19 pandemic, remain the most memorable and heart-warming elements of my life in Cambridge.

Finally, I would like to extend the deepest thanks to my parents for their everlasting love and care in every possible way, especially during the writing of this thesis.

Table of Contents

List of Publications

First-Authored Publications

1. K. H. Chu, I. Olakorede, E. Beqiri, M. Czosnyka, and P. Smielewski, “Mathematical modelling of cerebral haemodynamics and their effects on ICP,” *Brain and Spine*, vol. 4, January 2024, Art. no. 102772, doi: 10.1016/j.bas.2024.102772.
2. K. H. Chu, E. Beqiri, M. Czosnyka, and P. Smielewski, “Comparison of Two Intracranial Pressure Calculation Methods and Their Effects on the Mean Intracranial Pressure and Intracranial Pressure Dose,” *Acta Neurochir. Suppl.*, vol. 131, pp. 31–33, 2021, doi: 10.1007/978-3-030-59436-7_7.

Co-Authored Publications

1. E. Beqiri, M. Placek, K. H. Chu, J. Donnelly, G. Cucciolini, V. Motroni, C.A. Smith, M. Czosnyka, P. Hutchinson, and P. Smielewski, “Exploration of uncertainty of PRx time trends,” *Brain and Spine*, vol. 4, January 2024, Art. no. 102795, doi: 10.1016/J.BAS.2024.102795.
2. J. Chabrosa, M. Placek, K.H. Chu, E. Beqiri, P. Hutchinson, Z. Czosnyka, M. Czosnyka, A. Joannides, and P. Smielewski, “Embracing Uncertainty in Cerebrospinal Fluid Dynamics: A Bayesian Approach to Analysing Infusion Studies,” *Brain and Spine*, vol. 4, January 2024, Art. no. 102837, doi: 10.1016/J.BAS.2024.102837.

3. V. Motroni, G. Cucciolini, E. Beqiri, C.A. Smith, M. Placek, K.H. Chu, M. Czosnyka, and P. Smielewski, "Reliability and Variability of pressure reactivity index (PRx) during oscillatory pattern in arterial blood pressure and intracranial pressure in traumatic brain injured patients," *Brain and Spine*, vol. 4, January 2024, Art. no. 102850, doi: 10.1016/J.BAS.2024.102850.
4. E. Beqiri, A. Ercole, M. J. Aries, M. Cabeleira, A. Czigler, A. Liberti, J. Tas, J. Donnelly, X. Liu, M. Fedriga, K. H. Chu, F. A. Zeiler, M. Czosnyka, and P. Smielewski, "Optimal Cerebral Perfusion Pressure Assessed with a Multi-Window Weighted Approach Adapted for Prospective Use: A Validation Study," *Acta Neurochir. Suppl.*, vol. 131, pp. 181–185, 2021, doi: 10.1007/978-3-030-59436-7_36.

Conference Presentations

International Symposium on Intracranial Pressure and Neuromonitoring XVII

September 2019, Leuven, Belgium

(funded by the Edwin Leong Travel Grant)

Poster 1: A Comparison of Two ICP Calculation Methods and Their Effects on Mean-ICP and ICP Dose

International Symposium on Intracranial Pressure and Brain Monitoring XVIII

November 2022, Cape Town, South Africa

Poster 1: Mathematical Modelling of Cerebral Haemodynamics and Their Effects on ICP

Poster 2: The Influence of ICP on Autoregulation Indices

List of Figures

List of Tables

List of Abbreviations

ABP	Arterial Blood Pressure
ACA	Anterior Cerebral Artery
ACoA	Anterior Communicating Artery
AMP	Fundamental Amplitude of ICP
ARI	Autoregulation Index
C_a	Compliance of the Cerebral Arterial Bed
CA	Cerebral Autoregulation
CaO_2	Arterial Oxygen Content
CBF (F_a)	Cerebral Blood Flow
CBFV (FV)	Cerebral Blood Flow Velocity
CBV	Cerebral Blood Volume
C_i	Compliance of the Cerebrospinal Space
CO_2	Carbon Dioxide
COGiTATE	CPPopt Guided Therapy: Assessment of Target Effectiveness
CPP	Cerebral Perfusion Pressure
CPP_m	Mean CPP
CPPopt	Optimal CPP

CR	Compensatory Reserve
CSF	Cerebrospinal Fluid
C_v	Venous Compliance
CVR	Cerebrovascular Resistance
CW	Circle of Willis
DC	Decompressive Craniectomy
E	Elasticity of the Cerebrospinal Space
FFT	Fast Fourier Transformation
GCS	Glasgow Coma Scale
ICA	Internal Carotid Artery
ICP (P_i)	Intracranial Pressure
IR	Impulse Response
ISF	Interstitial Fluid
LLA	Lower Limit of Autoregulation
MAP	Mean ABP
MCA	Middle Cerebral Artery
MRI	Magnetic Resonance Imaging
Mx	Mean Flow Index (Correlation between CPP and CBFV)
Mxa	Mean Flow Index (Correlation between AMP and CBFV)

NIRS	Near-Infrared Spectroscopy
P_a	Cerebral Arterial Pressure
PAx	Pressure Amplitude Index (Correlation between AMP and ABP)
$PaCO_2$	Partial Pressure of CO_2 in Arterial Blood
PaO_2	Partial Pressure of Oxygen
$PbtO_2$	Brain Tissue Oxygenation
PCA	Posterior Cerebral Artery
PCoA	Posterior Communicating Artery
P_{opt}	Optimal Pressure
PRx	Pressure Reactivity Index
P_v	Pial Venous Pressure
R_a	Resistance at the Large Cerebral Arteries
RAC	Autoregulation Index (Correlation between AMP and CPP)
RAP	CR Index (Correlation between AMP and ICP)
R_b	Resistance of Venous Outflow
RBC	Red Blood Cell
R_{CSF}	Resistance of CSF Outflow
R_{ISF}	Resistance of ISF Bulk Flow
RK4	4^{th} Order Runge-Kutta Method

SIBICC	Seattle International Brain Injury Consensus Conference
TBI	Traumatic Brain Injury
TCD	Transcranial Doppler
TFA	Transfer Function Analysis
THRT	Transient Hyperaemic Response Test
ULA	Upper Limit of Autoregulation

Chapter 1

Anatomy and Physiology of Cerebral Circulation

This project focuses on the mathematical modelling of cerebral blood flow (CBF) and cerebrospinal fluid (CSF) circulation in patients with traumatic brain injuries (TBI); the anatomical and physiological bases of the model are discussed in this chapter.

As an integral part of the central nervous system, the brain is the centre of information processing enabling motor and cognitive activities. Consisting of billions of neurons, the human brain has a mass of about 1.4 kg [1] and a volume of approximately 1200 mL [2]. It is encased within the intracranial space, which is defined by the skull and meninges (consisting of the layers: dura mater, arachnoid mater, and pia mater). The brain is permeated with an intricate and dense, tree-like, network of blood vessels. Blood flows through body tissues and delivers oxygen and nutrients while removing carbon dioxide among other metabolites. The importance of such functions in the brain is highlighted by the abundance of blood and oxygen supply: approximately 15% of cardiac blood and 20% of oxygen in the body are drawn to the brain, despite that it only constitutes about 2% of total body weight [3]. The total blood flow through the brain is 750 – 1000 mL/min, with the flow per unit mass of white matter about a quarter that of grey matter [4]. The intracranial space is also filled with CSF: with a volume of

about 150 mL [5], it circulates in the cranial and spinal subarachnoid spaces, as well as in the brain ventricles (**Figure 1.1** [6]).

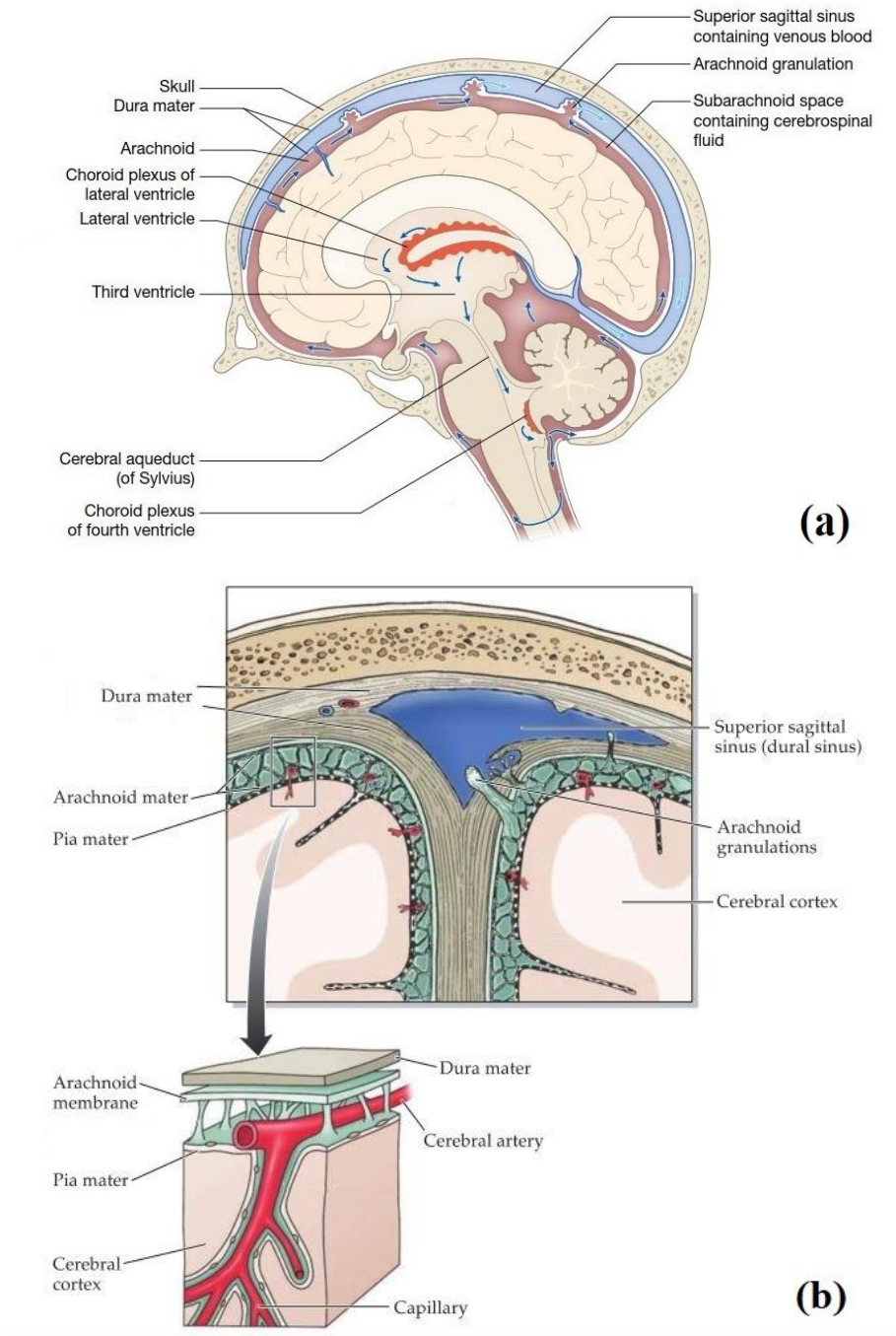

Figure 1.1. [6] (a) Cross-section of the human intracranial space, with brain tissue and cerebrospinal fluid (CSF) enclosed by the meninges (dura mater, arachnoid, and pia mater) and the skull; (b) magnified view of the intracranial space, showing vascular invagination of the brain.

1.1 Fluid Flow in the Intracranial Space

1.1.1 Blood Supply from the Large Arteries

Cardiac blood is supplied to the brain through anterior and posterior circulations. In the anterior circulation system, blood flows through the neck via the common carotid artery, before passing through the internal carotid artery (ICA) which enters the cranium (**Figure 1.2** [7]). The ICA branches into the anterior (ACA) and middle (MCA) cerebral arteries. The posterior circulation system, on the other hand, consists of the basilar artery which receives blood from the vertebral arteries at the pontomedullary junction, and bifurcates as two posterior cerebral arteries (PCA) at the pons-midbrain border.

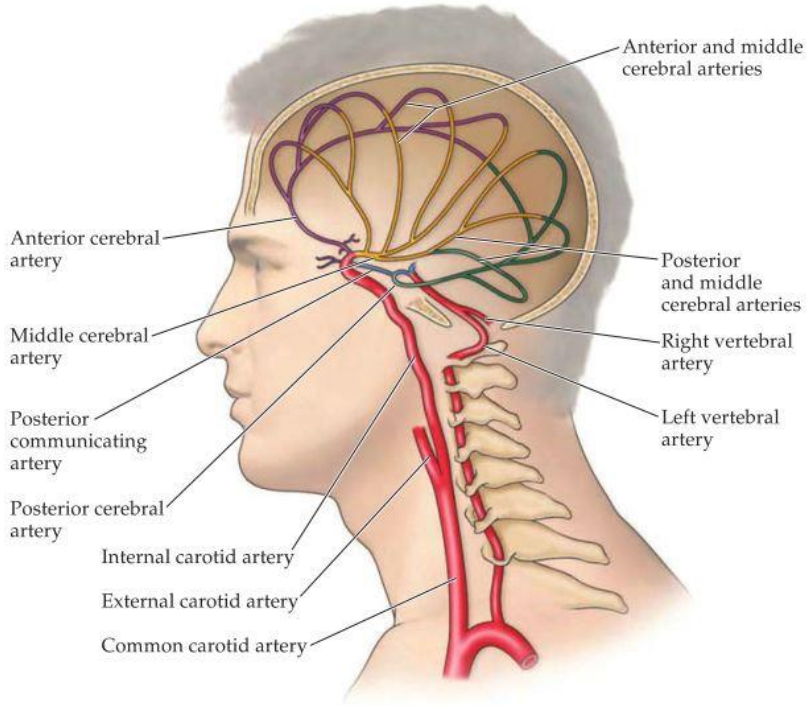

Figure 1.2. [7] Paths of the anterior circulation system (common carotid artery, internal carotid artery, anterior cerebral artery, and middle cerebral artery) and the posterior circulation system (vertebral artery, basilar artery, and posterior cerebral artery).

The anterior and posterior circulation systems are connected by the circle of Willis (CW); this structure protects the brain from regional ischaemia by providing an overlapping blood supply. CW consists of anterior communicating arteries (ACoA), which connects the two ACA, and posterior communicating arteries (PCoA) linking MCA with PCA.

1.1.2 Arterioles and Capillaries

The arteries bifurcates and lead to cerebral arterioles with smaller diameters. The walls of these resistive vessels are lined with three concentric layers (**Figure 1.3**): the outermost layer of tunica adventitia, consisting primarily of collagen fibres and fibroblasts; the central layer of tunica media, containing mostly smooth muscle cells; and the innermost layer of tunica intima, composed of endothelial cells and the internal elastic lamina [8].

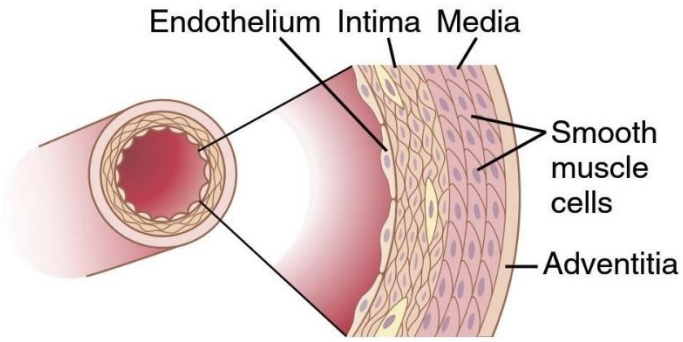

Figure 1.3. [9] Composition of cerebral arterioles, with concentric layers of tunica adventitia, tunica media, and tunica intima.

The arterial circulation terminates at the level of capillaries, where the transfer of nutrients and waste between neurons and blood takes place. The capillaries have vessel walls consisting of endothelial cells. However, in contrast to the leaky intercellular spaces between adjacent endothelial cells in other vascular structures, the junctions between capillary endothelial cells are much tighter [7], which excludes large molecules from passing through. Together with another type of cells known as astrocytes, they form a highly selective 'blood-brain barrier' to prevent the permeation of harmful substances.

1.1.3 Vascular Reactivity and Cerebral Autoregulation

Cerebral arterioles from the parenchymal or pial part of the arterial circulation have a high proportion of smooth muscle cells [10], [11], and play a crucial role in the mechanism of cerebral autoregulation (CA). Autoregulation maintains homeostasis of the circulation system by stabilising cerebral blood flow (CBF) in spite of fluctuations in cerebral perfusion pressure (CPP), which is the difference between systemic arterial blood pressure (ABP) and intracranial pressure (ICP). The arterioles react to variations in CPP through active changes in muscle tone of the vessel walls, in order to dilate or constrict. This alters the cerebrovascular resistance of the vessels and hence the flow rate of blood. However, the regulatory response has lower and upper limits, corresponding to maximal extent of vasodilation and vasoconstriction respectively. Beyond the range of autoregulation, the vessels distend or collapse passively. The

changes in CBF in response to increasing CPP can be plotted as the so-called 'Lassen curve' (**Figure 1.4** (a)) [12], named after the paper that first described the 'autoregulatory plateau' of CBF [13].

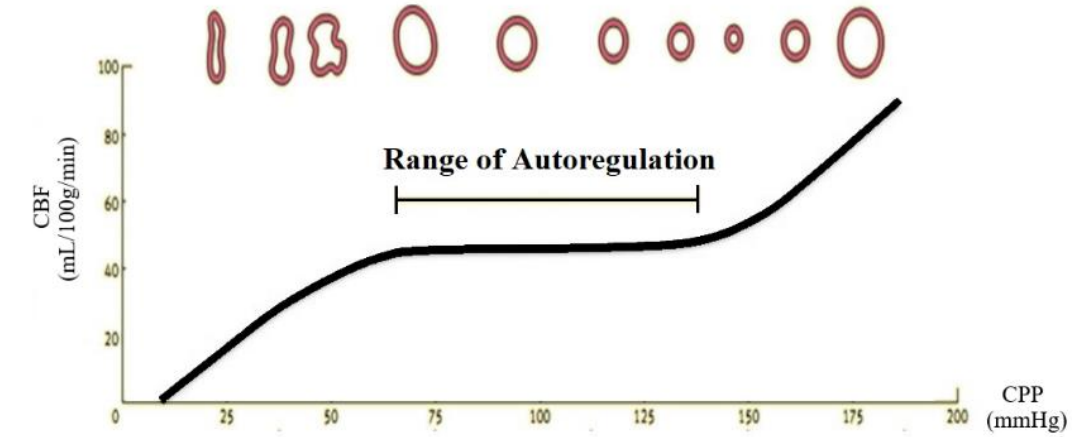

(a)

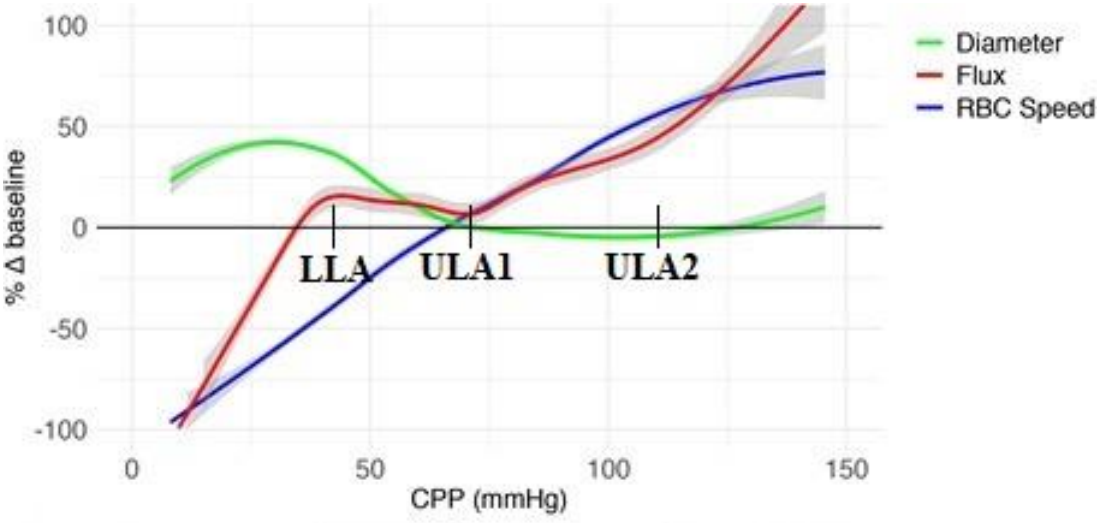

(b)

Figure 1.4. (a) The classical Lassen curve, with a plateau in CBF within the range of autoregulation [12]; (b) the effect of CPP on red blood cell (RBC) flux, pial arteriole diameter, and RBC velocity for experiments involving hypotensive and hypertensive pial arterioles [14]. LLA denotes the lower limit of autoregulation and ULA denotes the upper limit of autoregulation, which in this work was postulated to be bi-phasic. The mildly sloped CBF-CPP relationship between ULA1 and ULA2 indicates progressive failure of CA.

According to the classic textbooks, CBF in healthy, normoxic and normocapnic adults with mean ABP of 60 to 150 mmHg is stabilised at around 50 mL/100g brain tissue/min [15]–[20]. Recent studies [14] have suggested that the autoregulatory capability of arterioles varies with sizes; this allows two upper limits of autoregulation (ULA) to be defined (**Figure 1.4** (b)). An autoregulatory plateau can be observed between the lower limit of autoregulation (LLA) and ULA1. As CPP is raised above ULA1, failure of CA begins to take place (resulting in a mildly sloped CBF-CPP relationship), starting from the smallest arterioles and progressively towards the larger ones. At ULA2, all arterioles have exhausted their regulatory capacity and being passively dilated by the transmural pressure; further rises in CPP would lead to a rapid increase in CBF. Reduction in CPP below the range of autoregulation (such as during intracranial hypertension) can deprive the brain of oxygen (cerebral ischaemia) and potentially result in cell death. In contrast, an elevated CPP above ULA can cause hyperaemia which raises the pressure in the arterioles and capillaries. This may disrupt the blood-brain barrier, as the fragile wall structures of the capillaries are prone to damage under excessive pressure [21]–[24]. The consequent reduction in resistance through the blood-brain barrier can produce brain swelling [25]–[27] and elevate ICP.

In addition to CPP, the arterioles are also sensitive to changes in metabolic stimuli. For example, an increase in CBF can be observed with hypoxia: as the partial pressure of oxygen (PaO_2)

drops below about 50 mmHg [28], a 1% decrease in arterial oxygen content (CaO_2) raises the CBF by 2% [29]. CBF also varies with the partial pressure of carbon dioxide, reducing by 1-4% or rising by 4-8% with every 1-mmHg decrease or increase in $PaCO_2$ respectively [30], [31]. As clinical studies have related hypocapnia with deteriorations in cerebral oxygen delivery [32], the vascular reactivity to both oxygen and carbon dioxide levels are vital to maintaining oxygen delivery to the cerebral vascular bed at the level appropriate for metabolic needs and preventing the onset of hypoxic-ischaemic brain injuries [33].

1.1.4 Venous Outflow

After exiting the capillary bed, cerebral blood circulates through the venous compartment. Cerebral veins have very thin walls and lack the muscular tunica commonly seen in other vascular structures (**Figure 1.5** [34]); they also do not contain valves [8], [35].

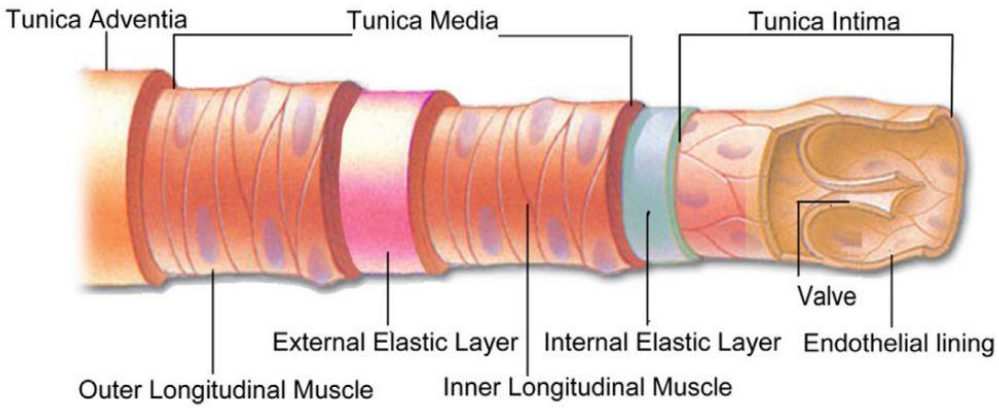

Figure 1.5. [34] The wall structure of a typical vein, with three concentric layers (tunica adventitia, tunica media, and tunica intima) which are also seen in arteries. Cerebral veins differ from other veins in that they lack the smooth muscle layers, and also have no valves.

The venous compartment begins with the small venules, which receive blood from multiple capillaries and join to form a series of intracranial bridging veins. Cerebral blood flows through the bridging veins and arrive at the dural sinuses, before being drained to the internal jugular veins at the neck. The bridging veins are highly elastic due to their thin walls and the lack of smooth muscles [36]. This makes them compressible by the pressure in the adjacent subarachnoid space, and thus exhibiting a Starling resistor effect [37], [38], as illustrated in **Figure 1.6**. While venous resistance is dependent on ICP, it does not contribute much to cerebral blood flow due to the waterfall effects of the bridging veins, where flow becomes independent of downstream pressure gradients as it is compressed by an external pressure. This is a characteristic behaviour of Starling resistors.

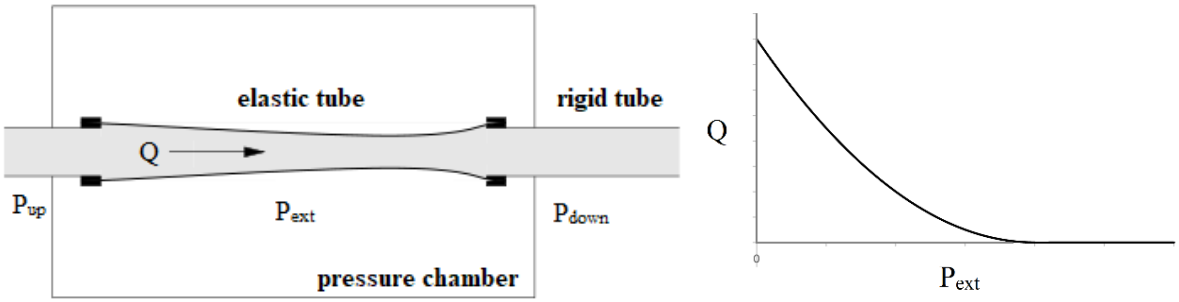

Figure 1.6. Diagram of a Starling resistor, consisting of a fluid-filled collapsible elastic tube mounted inside a chamber filled with air. The external pressure of the chamber (P_{ext}) governs the degree of collapse (and hence the resistance of fluid flow) of the elastic tube. As the tube collapses, fluid flow (Q) becomes independent of the downstream pressure (P_{down}), and is only regulated by the difference between the upstream pressure (P_{up}) and P_{ext}.

1.1.5 Circulation of Cerebrospinal Fluid

Another important fluid in the skull is the cerebrospinal fluid (CSF), which surrounds the brain and protects it from impact by equalising the pressure gradient throughout the cranial cavity [3]. According to the mainstream textbook understanding, CSF is mainly secreted by the choroid plexuses in the cerebral ventricles (**Figure 1.7** [7]). It flows into the third ventricle, and through the aqueduct of Sylvius into the fourth ventricle. The CSF is then drained into the subarachnoid space through several apertures in the fourth ventricle. Located between the arachnoid and pia mater, the subarachnoid space encompasses both the brain and the spinal cord. CSF pools in dilated regions in the subarachnoid space known as cisterns (which exists both in the intracranial and spinal subarachnoid spaces), where the main portion of the cerebrospinal compliance resides. CSF is ultimately absorbed into the dural sinuses via the arachnoid villi. Reabsorption only occurs if ICP rises above an ‘opening pressure’, which is the pressure in the sinuses where CSF drains into [39].

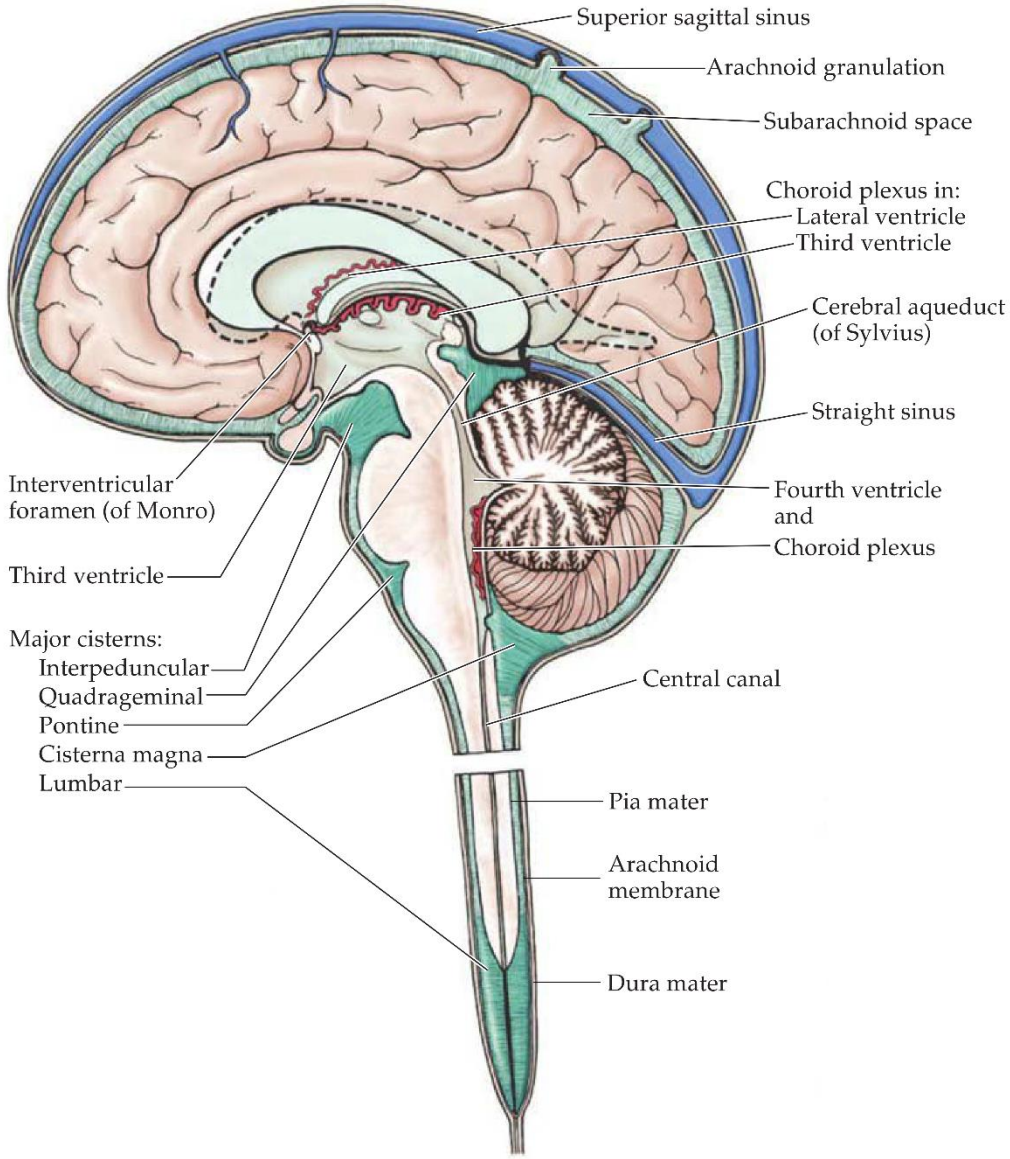

Figure 1.7. [7] Circulation pathways of cerebrospinal fluid. CSF is mainly produced in the choroid plexus, which resides in the third, the fourth, and the lateral ventricles. It then circulates into the subarachnoid space and pools in dilated locations known as cisterns, which exists both in the intracranial space (cisterna magna, interpeduncular, quadrigeminal, and pontine cisterns) and in the caudal end of the spinal canal (lumbar cistern).

1.1.6 The Glymphatic System

The section above has introduced the pathways of CSF circulation according to classical understanding. However, recent studies [40], [41] have proposed another possible pathway of intracranial fluid flow known as the glymphatic system. This involves the perivascular space, which encompasses the vascular structures of arterioles, capillaries, and venules. As the arterioles narrow in diameter, the periarterial space becomes continuous with the basal lamina, which is a thin sheet of extracellular matrix (**Figure 1.8** [42]) filled with interstitial fluid (ISF). CSF is drawn into the perivascular space from the subarachnoid space, before flowing into the brain parenchyma through channels in astrocytic endfeet. This drives the ISF toward the perivenous spaces, creating a continuous and rapid interchange between CSF and ISF.

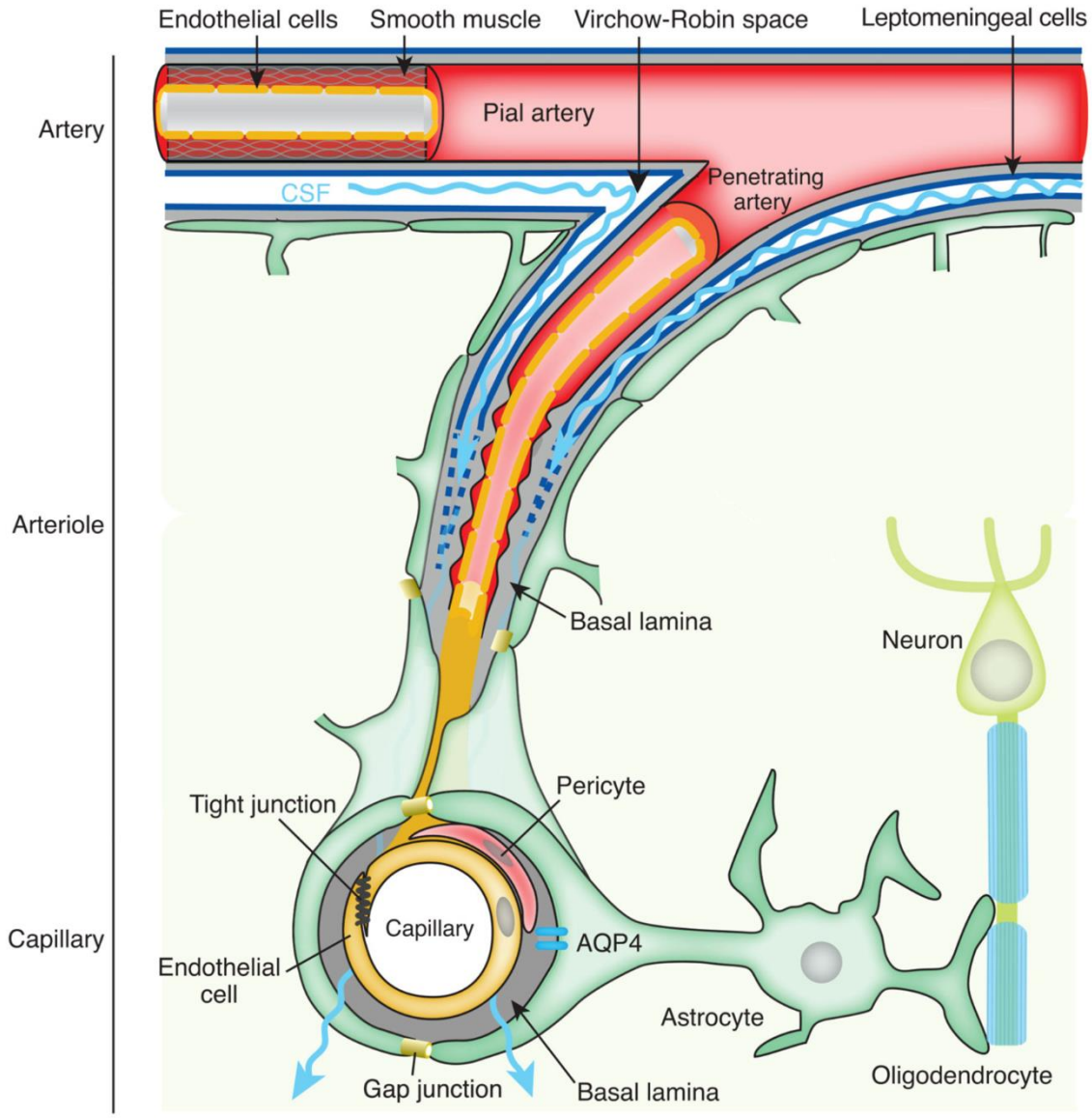

Figure 1.8. [42] Schematic depicting the glymphatic system. The boundary of the perivascular spaces is defined by astrocytic endfeet which encapsulate the vasculature. The periarterial space (Virchow-Robin space) surrounds the penetrating arteries; it disappears before the level of capillaries, where the perivascular space is composed of the basal lamina only. CSF flows into the brain parenchyma through channels in astrocytic endfeet (AQP4), driving ISF through the perivascular spaces.

1.2 Volume and Pressure of the Intracranial Space

In the late 18th to early 19th centuries, studies by Monro and Kellie [43], [44] have revealed the important relationship between volume and pressure within the cranium. This relationship (known as the Monro-Kellie doctrine) states that the volume sum of intracranial contents (blood, CSF and brain tissue) is conserved, due to the rigidity of the dura mater and skull structures. As the volume of one compartment increases, contents of the remaining compartments may be displaced as compensation. However, if the compartment expands beyond a certain threshold, the compensation would eventually be exhausted, resulting in a rapid rise in the intracranial pressure (ICP). ICP refers to the hydrostatic and filling pressures acting within the cranial cavity relative to atmospheric pressure [45]. The relationship between the volume of an intracranial compartment and ICP is illustrated in **Figure 1.9** [46], [47].

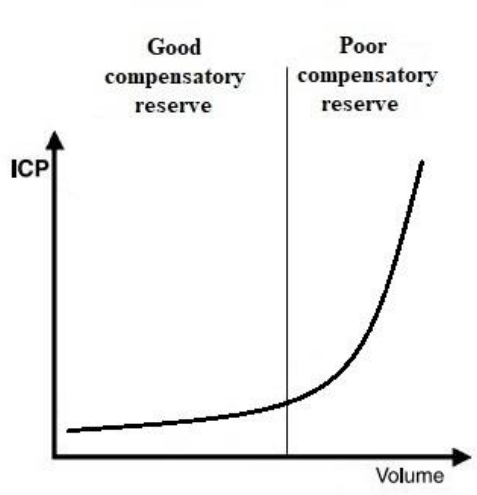

Figure 1.9. [46], [47] The pressure-volume curve of the intracranial space. An increase in volume is initially accompanied by a mild and linear rise in ICP. However, as the compensatory reserve becomes exhausted, ICP begins to surge exponentially in response to expanding volume.

The capacity of pressure-volume compensation in a compartment can be described by its compliance; it is defined as the change in volume in response to a unit change in pressure of the compartment (reciprocal of the pressure-volume curve's slope). The compliance of the CSF space (C_i) is understood to be approximately constant at low levels of ICP. When ICP is raised above a limit (also termed 'optimal pressure' [48], [49]), the compensatory reserve of the CSF space becomes exhausted, and C_i starts to decrease (**Figure 1.10** (a)). As the intracranial compliance describes the influence of intracranial volume variations on ICP changes, a higher value of C_i effectively attenuates the transmission of pressure changes from the vascular compartments to the intracranial space. As introduced in the 'CSF circulation' section, the lumbar cistern in the spinal subarachnoid space can accommodate some shift in CSF volume from the brain, and therefore also contributes to C_i. It has been shown [50] that the contributions of cranial and spinal compliances to C_i vary with posture, meaning that the spinal canal helps to modulate ICP during postural changes.

Compliance of the arterial bed (C_a) represents the temporary storage of inflowing cerebral blood in the large arteries. It plays an important role in the transmission of pulsatile pattern from ABP to ICP, as it determines the alterations in cerebral blood volume due to pressure changes in the arteries [51], [52]. With decreasing CPP, C_a rises gradually to a maximum value

due to the reduction in vascular myogenic tone [53] (**Figure 1.10** (b)). As CPP falls below the critical closing pressure, the arteries begin to collapse, causing C_a to drop sharply.

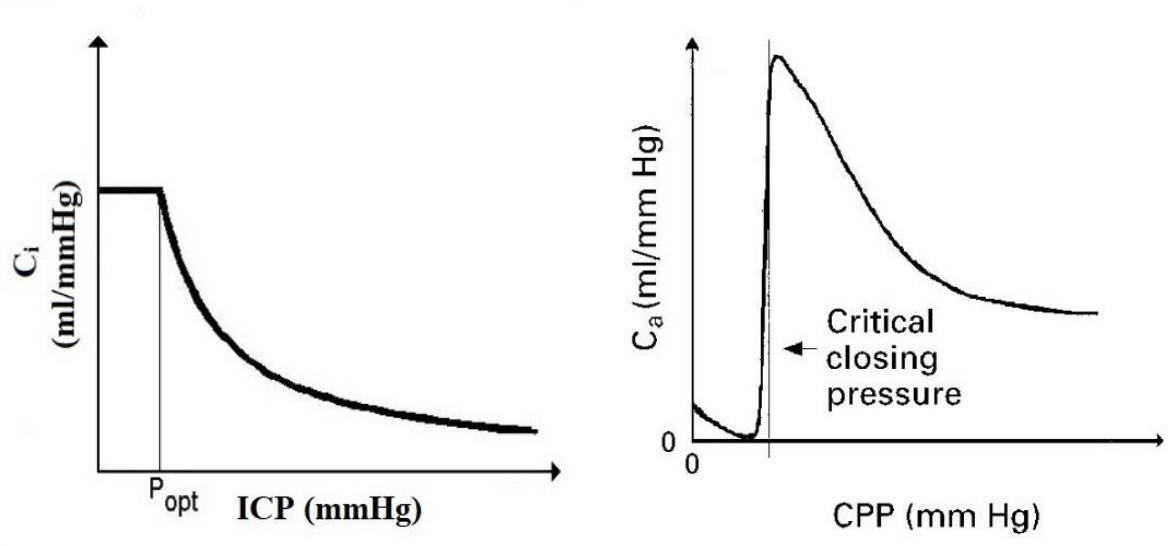

(a) (b)

Figure 1.10. [48] Effects of pressures on the intracranial compartments. (a) with rising ICP, compliance of the CSF space (C_i) remains constant until the compensatory reserve is exhausted at the optimal pressure (P_{opt}), where it starts to decrease; (b) arterial compliance (C_a) increases with reducing CPP until reaching the critical closing pressure, below which it begins to fall.

The majority of cerebral blood (estimated at about 70% of total cerebral blood volume [54]) is stored in the venous compartment. With the thin and highly elastic vascular walls, the venous bed acts as a compliant pool and contribute significantly to the overall compliance of the intracranial space. Venous and intracranial pressures are linked through mechanisms with different time scales. This includes the bridging veins, which transmit dynamic changes in central venous pressure to the intracranial space through their elastic walls. In addition, the

pathway of CSF reabsorption into the venous bed also influences ICP; these effects are more sustained due to the slow circulation of CSF. This can be seen during the obstruction of venous drainage, which produces extra resistance to CSF outflow and consequently elevation in ICP, as observed in patients with idiopathic intracranial hypertension.

Chapter 2

Pathophysiology of Cerebrospinal Dynamics in TBI and the Role of Neuromonitoring in Its Management

Traumatic brain injury (TBI) is defined as the alterations in functions or pathologies of the brain, caused by mechanical energy from external forces to the head [55], [56]. It is a common cerebral pathology affecting more than 50 million people globally every year [57]. While TBI is most frequently attributed to traffic accidents in low- and middle-income countries [58], falls have become its leading cause in high-income countries due to their ageing population [59]. Apart from the initial tears and contusions of the brain, TBI can lead to secondary injuries such as stroke and epilepsy, and neuronal degeneration in the long term; these give rise to the high mortality rate of patients with severe injuries (30 – 40% as observed on unselected populations [60]). The resulting disabilities have a profound impact on the quality of life of the survivors; this often poses a heavy mental burden on their caretakers and incurs huge costs to the society.

The severity of TBI is commonly characterised by the Glasgow Coma Scale (GCS), which quantifies the responses in the eye, motor, and verbal domains [61]. However, this single-parameter approach cannot describe the symptoms of individual patients accurately. Although neuroimaging and genetic analyses have improved the characterisation of the nature of TBI,

their progress is slow due to poor understanding of the underlying biomarker biology, and the lack of reference standards [62]. It is proposed that a multidimensional assessment should be developed for a comprehensive evaluation of the patient's status, accounting in particular for psychological health and cognitive deficits [63], [64].

The initial period after a severe head injury is often accompanied by intracranial hypertension due to the swelling of brain tissues. This may impede the cerebral blood circulation, and potentially causing cell death due to the starvation of oxygen in parts of the brain. In more extreme cases, intracranial hypertension can lead to brain herniation, with brain tissue squeezed under pressure through the rigid dura and skull structures (such as the cerebellar tentorium and falx cerebri), resulting in fatal damage to the brain [62], [65]. Therefore, intracranial pressure (ICP) is a vital quantity to be monitored for TBI patients. The measurement of ICP with high temporal resolution provides clinicians with a dynamic window into the physiology and pathological abnormalities relevant to cerebral circulation, thus allowing them to track the development of pathology or changes in the patient's state. As there are currently no non-invasive methods allowing ICP to be measured with high accuracy, bedside monitoring commonly resorts to invasive intracranial access devices (**Figure 2.1** [62]). In addition to ICP sensors, it allows other monitoring devices to be inserted into the intracranial space. One of

such devices is the $PbtO_2$ probe, which measures the partial pressure of brain tissue oxygen and is believed to be instrumental in preventing the onset of ischaemic hypoxia in TBI patients.

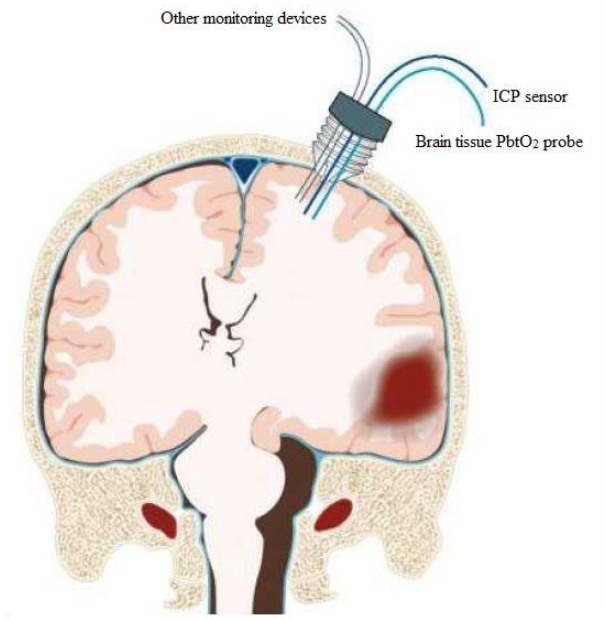

Figure 2.1. [62] An intracranial access device allowing the simultaneous measurements of multiple physiological signals. ICP sensors and $PbtO_2$ probes are among the most commonly monitoring devices to be inserted.

As elevated ICP has been shown to correlate strongly with mortality, stabilising mean ICP below a threshold of 20 – 25 mmHg has become a widely adopted clinical practice [66]. Retrospective studies have also associated low levels of $PbtO_2$ with unfavourable clinical outcome [67]. These findings have encouraged the establishment of treatment protocols based on ICP and brain oxygenation [68]. However, recent studies have cast doubt on the clinical benefits of basing clinical decisions solely on mean values and fixed thresholds of

physiological measures. For instance, maintaining monitored ICP below a universal threshold does not result in significant improvements in recovery when compared to management delivered without ICP monitoring [69]. Similarly, a trial involving the monitoring of ICP and $PbtO_2$ failed to reduce the proportion of TBI patients with poor outcome [70]. These evidences have highlighted the limitations of treatments based on unidimensional clinical targets, and the importance of data integration with multimodal monitoring has become apparent [62].

2.1 Cerebrovascular Pressure Reactivity

A crucial step of integration and interpretation of multimodal monitoring is to develop metrics of physiological processes. One of such metrics is the state of cerebral autoregulation (CA), which has proved to be a strong indicator of clinical outcome for TBI patients [71]–[76]. The slow waves in ICP can be used as a surrogate measure of CA via the pressure reactivity index (PRx): by correlating the slow changes (commonly defined as a 10-second averaging period [77], [78]) in arterial blood pressure (ABP) with ICP, this index is able to reflect the state of vascular reactivity (further discussed in **Chapter 8**) [74], [79]. As PRx has been demonstrated to be highly predictive of poor outcome following TBI [80], [81], it has become an important index to be monitored continuously in neuro-intensive care [78].

When plotting PRx against cerebral perfusion pressure (CPP) a U-shaped curve can be observed. As improved clinical outcome is associated with the minimisation of PRx, an optimal level of cerebral perfusion pressure (CPPopt, corresponding to the minimum value of PRx) can be chosen as a therapeutic target. Since CPPopt points to the CPP level at which CA is best preserved, aiming at that value allows in theory to optimise conditions for the protection of cerebral perfusion. Using this concept, an approach to manage patients according to individualised CPP targets based on the state of pressure reactivity has been proposed and validated in retrospective studies [82], [83], as well as in a randomised trial of safety and feasibility [84]. However, this approach has not yet been included as part of the routine clinical practice, partly because the assumptions of current methods used for CA assessments are often violated [85].

2.2 Intracranial Compensatory Reserve

The state of compensatory reserve (CR) of the intracranial space is another important metric to be assessed for head-injured patients, as it determines the variations in ICP in response to changes in intracranial volume (illustrated in the pressure-volume curve in **Figure 1.9**). It was observed that the relationship between mean ICP and its pulse amplitude (AMP, defined as the fundamental harmonic of the pulse component in a Fourier decomposition of the ICP signal) carries information of CR. The index RAP (correlation (R) between the slow changes (10-

second averaging period [86]) in AMP (A) and mean ICP (P)) was therefore proposed, with values close to zero at low ICP representing good CR. As ICP increases, RAP rises to +1 as changes in AMP becomes more synchronised with ICP, indicating exhausted CR. At this stage, the intracranial compliance begins to fall, so that an increase in intracranial volume leads to rapid rises in ICP. For most TBI patients, RAP indicates intact CR at the initial stages of hospital admissions, but often approaches +1 with the onset of cerebral oedema [78].

2.3 ICP Waveform Analysis

Serial measurements of ICP reveal rich patterns when examined at high resolution (100 Hz). Using Fourier spectral analysis, ICP waveforms can be studied in the frequency domain and separated into individual components related to different physiological mechanisms (**Figure 2.2** (a)). These include the arterial pulse (0.83 – 1.33 Hz), respiratory waves (0.13 – 0.33 Hz), and 'slow' vasogenic waves (0.005 – 0.05 Hz) [78]. The pulse waves are represented in frequency as several peaks due to their complex, non-sinusoidal nature. Because of this, they are more often analysed in the time domain, where they form characteristic shapes with three pronounced peaks (**Figure 2.2** (b)). Investigating the relationships between these peaks may provide metrics of clinical importance. For example, the ratio of P1 and P2 peak-to-peak amplitudes is thought to be related to intracranial compliance [45].

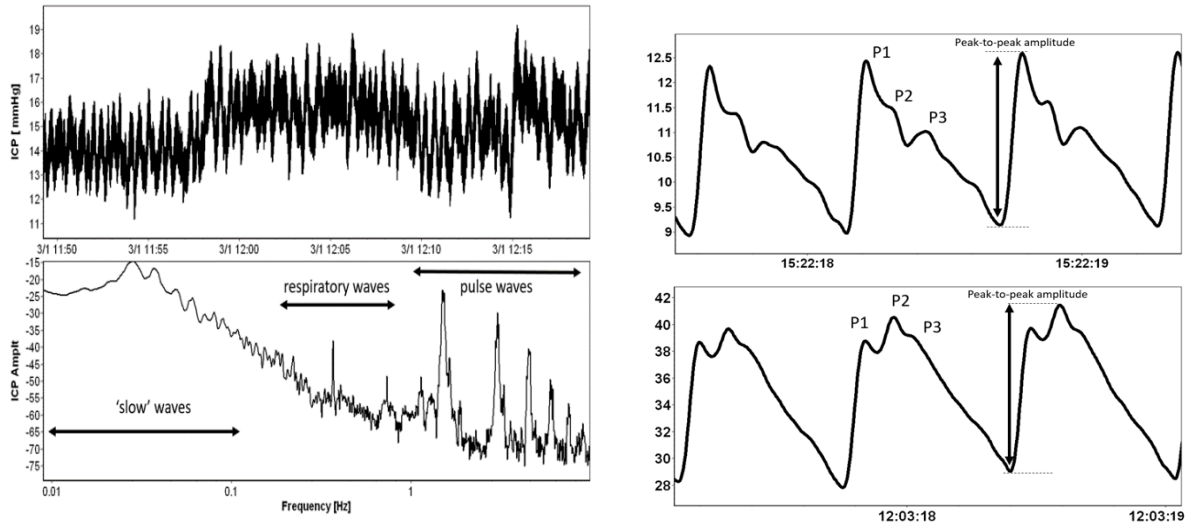

(a) (b)

Figure 2.2. [45] (a) A 30-minute recording of ICP, plotted against time (above) and as a Fourier frequency spectrum (below), showing three types of decomposed waves (arterial pulse, respiratory, and 'slow' waves). (b) Patterns of ICP pulse wave; three peaks (P1, P2 and P3) can be observed, related to percussion, tidal, and dicrotic waves respectively.

In general, a better understanding of the relationships among the flows, volumes and pressures in the intracranial space is required to improve the reliability of the indices derived from ICP. This can be achieved through studying the mathematical models of cerebral fluid circulation, as it helps to extract physiological information from physiological measurements, and facilitates the interpretation, calibration and filtering of such indices.

Chapter 3

Aims and Objectives

As discussed in **Chapter 2**, a number of indices are commonly used for monitoring the cerebral dynamics of TBI patients. However, their reliability depends crucially on various physiological factors. While mathematical modelling is proven to be a useful tool to study fluid circulation in the cerebrospinal space, an investigation of the significance of these factors has not been attempted with this approach. This thesis aims to explore the influences of brain compliances and intracranial pressure (ICP) on the performance of cerebrospinal dynamics indices using computer-supported mathematical modelling. On the other hand, the capability of previously proposed models to simulate the effects of such factors is uncertain. Therefore, this project also seeks to elucidate the underlying mechanisms involved in pressure-volume interactions among intracranial compartments, thus ensuring the validity of this approach. The main hypothesis investigated is that the incorporation of a pressure-volume interaction mechanism in the model improves its accuracy of reflecting physiological phenomena, particularly in the context of TBI where abnormal patterns of ICP is expected. In particular, I postulate that this interaction contributes significantly to the variability and reliability of calculated autoregulation indices, and should therefore be taken into account in any future work aiming to improve their accuracy.

Chapter 4

Modelling of CBF and CSF Dynamics: a Literature Review

4.1 Introduction

In neuro-intensive care for sedated and paralysed patients, clinicians have to make therapeutic decisions using measurements of physical and biochemical properties from the body instead of neurological examination. Moreover, the conditions in the brain may change rapidly requiring frequent reassessments in pathologies such as traumatic brain injury (TBI). Therefore, it is now common in modern neuro-critical care units to use sensors (both invasive and non-invasive) to continuously monitor intracranial properties such as intracranial pressure (ICP), cerebral blood flow (CBF), and brain oxygenation with high temporal resolution.

While this method helps to capture features of clinical interest, the interpretation of continuously monitored variables at high temporal resolution exceeds the capacity of a human brain, especially if the information is encoded in the relationship across multiple signals. One way to make sense of such quantities of data is the application of data-driven modelling, i.e. machine learning models. Considered as an approach of ‘dimensionality reduction’, these models search for the best representation of data in a small number of parameters. This is

achieved by embedding the data into a low-dimensional latent space, which could then be used to create criteria for clinical purposes (such as bedside alarms for decision making). However, this approach requires a vast amount of data to train such models, in order to ensure that all possible permutations of measurements and patient states have been covered. Without this laborious training process, the models would not be able to generalise well; this can potentially lead to inaccurate interpretation of data.

On the other hand, if the characteristics of an underlying relationship can be captured by a set of equations based on the laws of physics and evidence acquired through studies of human physiology and pathology, such models only need a modest amount of data to be tuned. Techniques already exist to promote machine learning support for biomechanical modelling, as in Neural-ODE approaches. However, their foundation lies in a mathematical, physical, model that captures the current understanding of physiology. It is therefore essential to continue the development of such models, hand in hand with the progress of data-driven methodologies.

This thesis aims to explore and improve a mechanistic model of cerebrospinal hydrodynamics. However, before focusing on a particular approach, it is prudent to take stock of previous investigations in this field. Over the last decades, a multitude of models have been designed to simulate cerebral blood flow (CBF) and the circulation of cerebrospinal fluid (CSF). These

efforts have helped establish physiological parameters of clinical importance, relate them to measurable signals, and enable the interpretation of phenomena observed in clinical recordings. Of the models proposed, some focused on the physiological properties (such as volume, flow and pressure) of particular components in the intracranial circulatory system, while others described the interactions between them. This chapter sought to provide a summary of such attempts with a scoping review.

4.2 Methods

A detailed literature search was performed on PubMed, Scopus, and the Web of Knowledge for articles up to 30th September 2023, using the search strings ‘cerebrovascular model’, ‘cerebral blood flow model’ and ‘cerebrospinal fluid model’. Search results were filtered to exclude unpublished work, abstracts without a corresponding paper, and non-English articles. During subsequent screening of the search results, only studies proposing an original model or modifications to a previous model were included.

4.3 Results

A total of 3,097 articles were found upon the literature search. Of these studies, 2,707 were rejected during an initial scan, and a further 349 were excluded after a full abstract screening,

leaving 41 included articles in total. The model characteristics, queries, and main findings of the included studies are summarised in **Table 4.1**.

Table 4.1. Summary of literature describing the models of CBF and CSF dynamics.

Author	Model Characteristics	Query	Main Findings
Agarwal 1969 [87]	Hydraulic, electrical multi-compartmental	Accuracy of describing cerebral fluid dynamics with compartmental model	ICP pulse could be attributed to pressure transmittances from arterial and venous compartments. This inter-compartmental transmission mechanism was described mathematically.
Tym 1972 [88]	Physical, hydraulic	Behaviour of CBF during extreme intracranial hypertension	CBF was reduced but never completely ceased, even with ICP elevated as high as inflow ABP.
Hakim 1976 [89]	Physical, mathematical	Changes in physical properties of the brain following the development of hydrocephalus	The model described the effects of the force expanding the ventricles on brain parenchyma and the CSF/venous system. It also identified increased resistance to the reabsorption of CSF as a cause of hydrocephalus.

Marmarou 1978 [90]	Electrical, CSF space	Relationships between parameters describing CSF dynamics and ICP	The model showed exponential relationship between pressure and volume of the CSF compartment. Pressure response to changes in CSF volume simulated by the model agreed closely to experimental results.
Hoffmann 1982-87 [91], [92]	Pulsatile, non-linear computer model	The effects of ABP on ICP dynamics	The influence of ABP in CSF bolus tests became significant for ICP > 30 mmHg. Relationships of ICP pulse amplitude with ABP and intracranial compliance were established.
Takemae 1987 [93]	Electrical, multi-compartmental	The basis of variations in ICP pulsatile waves	ICP pulsatility rose with increasing venous outflow resistance, decreasing intracranial compliance, and fell with arterial resistance.
Rekate 1988-94 [94], [95]	Electrical, multi-compartmental, CSF space	Depiction of CSF dynamics in terms of volume and pressure distribution among intracranial compartments	Model parameters were found using computer simulations to replicate the clinical aspects of hydrocephalus, including changes in ICP and

			CSF volume due to obstruction of CSF flow in the ventricular system.
Sorek 1989 [96]	Lumped parameter, multi-compartmental	Reliability of predicting clinical observations of the intracranial space using compartmental model	With seven compartments each described by its compliance and resistance, the model estimated the degree of average deformation in CSF space; results were consistent with experimental measurements.
Nishimura 1991 [97]	Physical and electrical, multi-compartmental	The origins of arterial and ICP pulse waveforms	Arterial circulation transforms simple arterial pulse waves into waveforms with multiple peaks; it may determine the shape of ICP pulses. The relationship of mean ICP to its amplitude is dependent on intracranial phenomena related to CSF circulation.
Ursino 1991 [98]	Electrical, multi-compartmental	Effects of autoregulation and CSF dynamics on the nature of ICP instability	The model showed that instabilities in ICP (as observed in plateau waves) could be generated

			with intact autoregulation, compromised CSF outflow and reduced intracranial compliance.
Ursino 1995 [99]	Electrical, multi-compartmental	ICP patterns of patients with acute head injuries, and underlying intracranial biomechanical factors	Impaired flow regulatory mechanisms reduced the rate of CSF production. This could alter cerebral blood volume and lead to delayed ICP responses to bolus injection and withdrawal manoeuvres.
Czosnyka 1997 [48]	Electrical, multi-compartmental	Differences in blood flow patterns for subjects with intact and compromised autoregulation capacities	Simulations with intact (but not impaired) autoregulation showed hyperaemic response in transient hyperaemic response test, and increased CBF pulse amplitude during arterial hypotension and intracranial hypertension.
Ursino 1997 [100]	Electrical, multi-compartmental	Benefits and shortcomings compared to a more detailed model developed previously	Combining arterial segments prevented the model from simulating different resistances in large arteries and small arterioles. However, its simple structure allowed convenient data

			fitting from clinical measurements, and hence a more rapid diagnosis.
Thoman 1997 [101]	Multi-compartmental volumetric	Combined effects of physiologic variables on intracranial dynamics	Using physiologic inputs of a simulator, the model evaluated the volumes of different cerebral components, and provided real-time display of measures such as intracranial pressure and cerebral blood volume.
Ursino, Lodi 1998 [102], [103]	Electrical, multi-compartmental	Relationships among CO_2 reactivity, autoregulation and ICP	A representation of CO_2 reactivity was added to a previously developed model. Simulations with changing CO_2 levels revealed significant correlation between CBF and ICP dynamics, and successfully reproduced the ICP and CBFV tracings in clinical data.
Panerai 1999 [104]	Mathematical Pressure-flow	Performance of linear and non-linear models for cerebral autoregulation	Accuracy of models varied in different tests. The model with quadratic kernels

			outperformed linear models in supine tests, but not in thigh cuff tests.
Kirkham 2001 [105]	Mathematical	Accuracy of modelling CBF with two parameters only (rate of restoration and time delay)	Simulations of oscillatory variations and step changes in ABP reflected features of autoregulation observed in experiments.
Piechnik 2001 [106]	Hydraulic, venous outflow	Relationship of pressure along cerebral veins with cerebral blood flow and ICP	Upstream vascular bed had flow-regulating capacity. Disturbances to this regulation could modulate venous outflow, and potentially contribute to additional ICP slow wave activities.
Olufsen 2002 [107]	Windkessel model, middle cerebral artery and peripheral cerebrovascular bed	Cardiovascular response to sudden hypotension during posture changes	Using data of young subjects, the model showed initial increase, followed by reduction in cerebrovascular resistance as posture changed from sitting to standing. Results indicated the presence of autoregulatory vasodilation.

Yang 2003 [108]	Mechanical, electrochemical	Myogenic mechanisms of arterial resistance vessels	The model described the activation of smooth muscle cells in terms of mechanical, electrical, and chemical factors. Simulated relationships against transmural pressure resembled clinical data accurately.
Piechnik 2003 [109]	Electrical, bilateral	Nature of the effect of intracerebral steal	ICP and CBF changes were less substantial with improved cross-circulation through ACoA. With cerebrovascular reactivity in one hemisphere only, ACoA size determined the flow difference in internal carotid arteries, but not in middle cerebral arteries.
David 2003 [110]	Computational fluid dynamics	Feasibility of detecting small arteries with computer simulation	Relationship between geometrical variations of arteries and peripheral resistance was established. The model could provide guidelines to improve the protocol of the imaging process in MRI studies.

Banaji 2005 [111]	Mechanical, biochemical, electrical	Contribution of cerebral metabolism and vascular smooth muscles on the feedback pathways of CBF regulation	The model successfully reproduced CBF-ABP and CBF-$PaCO_2$ relationships from literature. It offered the potential to predict intracellular pH by feeding real patient data.
Payne 2005 [112]	Haemodynamic, biochemical, electrical	Autoregulatory responses to changes in blood pressure	Mechanical, electrical and biochemical properties of smooth muscle cells were incorporated in a haemodynamic model. Simulated CBF responses to blood pressure changes suggested autoregulatory processes with different time scales.
Alastruey 2007 [113]	1D arterial coupled with 0D flow-pressure	Alterations in arterial haemodynamics after carotid occlusion	Various anatomical variations of the circle of Willis were compared; absence of the first segment of the contralateral anterior cerebral artery was most detrimental to the restoration of cerebral blood flow.

Piechnik 2007 [114]	Cerebrovascular, multi-compartmental	Relationship between vascular volume and CBF	Volume-flow relationship in the cerebro-vascular bed was simulated using three models, each with a different vascular topology. Distribution of the regulating vessels has a strong influence on the slope of the relationship.
Giannessi 2008 [115]	Electrical, multi-compartmental	Effects of cerebral blood flow and CSF dynamics on ICP of patients with intracranial haemorrhage	The manoeuvre of elevating the head of a head-injured patient could help lower ICP, but may jeopardise cerebral perfusion. CO_2 level and intracranial compliance were related to the generation of ICP plateau waves.
Zheng 2009 [116]	Windkessel, venous compartment	Viscoelasticity of cerebral veins	The model was designed such that a hysteresis is produced in the pressure-volume relationship of blood vessels. It was able to simulate the viscoelastic properties of cerebral

			veins, and predict the CBV-CBF differences observed in clinical data.
Pope 2009 [117]	Electrical, multi-compartmental vascular	Practicality of estimating parameters of a cerebrovascular model with sensitivity analysis and subset selection	Through ranking parameters by sensitivity and identifying a set of candidate parameters that can be estimated using ABP and CBFV data, simulations revealed the changes in arterial resistance and compliance with age.
Chan 2011 [118]	Electrical, Arterial Windkessel	The role of arterial Windkessel properties in autoregulation	Simulations of transient hypertension and hypotension with the model fitted well to clinical data, revealing the contribution of resistance and compliance elements in modulating low-frequency CBF responses.
Kashif 2012 [119]	Electrical, multi-compartmental	Feasibility of non-invasive ICP estimations of TBI patients without the need of calibration or training	Beat-to-beat ICP estimations with the model were compared to measurements of TBI patients. While able to identify elevated ICP with high sensitivity and specificity, it did not

			take into account the effects of cerebrovascular compliance and resistance.
Marmarelis 2012 [120]	Mathematical	Effects of CO_2 tension on cerebral flow autoregulation	Modelling autoregulation process requires non-linear methodologies; including CO_2-dependent inputs improves the accuracy of autoregulation models, when compared to models with pressure-dependent inputs only.
Spronck 2012 [121]	Electrical, vascular	Effects of autoregulation and neurovascular coupling on cerebral blood flow	The model successfully identified the myogenic and neurogenic mechanisms of blood flow regulation in healthy subjects undergoing squat-stand manoeuvres and visual stimulation challenges.
Mader 2014 [122]	Mechanical, haemodynamic	Ability to predict CBFV as a function of ABP using a viscoelastic model	The stress-strain relationship observed in viscoelastic materials was used to model CBFV responses to ABP changes. It was

			successful in simulating CBF dynamics in response to sitting-to-standing manoeuvres.
Lampe 2014 [123]	Hydrodynamic, vascular	Performance of a cerebrovascular model combining characteristics of hierarchical vascular structure and autoregulation	The model included the representation of a vascular pressure-radius relationship, and hysteretic behaviour in the autoregulation curve. It was able to demonstrate the dependence of regulating capabilities on CO_2 levels.
Panunzi 2015 [124]	Mathematical, vascular	Cardiovascular factors describing cerebral autoregulation	By introducing four control mechanisms on components of cerebral circulation, the model was able to reproduce mean arterial pressure and cerebral blood flow velocity responses after postural changes.
Henley 2015-17 [125], [126]	Electrical, haemodynamic	Linear and non-linear relationships between dynamic cerebral	The model represents the pressure-flow relationship as a combination of linear and non-linear components with different time

	autoregulation and CO_2-vasomotor reactivity	scales. Simulations of vascular responses to changes in CPP and CO_2 tension resembled experimental results.

4.4 Discussion

4.4.1 Mathematical Models

A mathematical model uses a set of parameters to relate various physiological measures. This approach is commonly used to evaluate CBF with different strengths of cerebral autoregulation in response to changes in blood pressure. In order to test the accuracy of these models, clinical data of patients at different states (e.g. at supine position or during cuff tests) are collected and compared to the simulated results. Some models include parameters that describe the mathematical characteristics of the signals (such as gain and time delay) [104], [105], while others use parameters with a more direct physiological implication (such as CO_2 level) [120], [124]. While this type of models is relatively simple to construct, it is difficult to capture the effects of different anatomical structures on the measured variables.

4.4.2 Hydrodynamic Models

Hydrodynamic models help to assess the contribution of individual anatomical structures to the overall changes in CBF and ICP. By lumping intracranial structures as different compartments and describing them in terms of mechanical properties (such as resistance and compliance), a multi-compartmental model can be used to examine the interactions of pressure and fluid flow among the compartments. While some studies of this approach involved the construction of physical hydraulic models [87]–[89], [97], [106], others used computer simulations as an

alternative. A multi-compartmental model commonly includes elements representing the large cerebral arteries, resistive arterioles, bridging veins, and the intracranial space through which CSF circulates. Using this method, the models are able to predict the behaviour of CBF during extreme intracranial hypertension [88], estimate the degree of deformation in the CSF space [96], identify the mechanical cause of hydrocephalus [89], and establish the relationship of pressure along the cerebral veins with CBF and ICP [106].

4.4.3 Electrical Equivalent Models

The advancement of computing technology allows equivalent circuit models to be constructed conveniently, reducing the importance of their physical hydrodynamic counterparts. A circuit model includes electrical components analogous to their respective hydrodynamic properties:

Table 4.2. Properties of hydrodynamic models and their counterparts in electrical equivalent models

Hydrodynamic Quantities	**Electrical Equivalent**
Flow Rate (mL/min)	Electric Current (A)
Fluid Pressure (mmHg)	Potential Difference (V)
Flow Resistance (mmHg*min/mL)	Electric Resistance (Ω)
Compliance of Tube Wall (mL/mmHg)	Capacitance (F)
Inertia of flow (mmHg*min^2/mL)	Inductance (H)

Apart from the ease of construction, an electrical model also contains parameters that can be altered conveniently, and is able to avoid errors caused by measurements of parameters. Using the laws of electric circuits, ordinary differential equations can be derived from these models; solving them give the values of current and electrical potential at various nodes of the circuit (which represent the flow and pressure of the respective compartments). Since most of these equations cannot be solved analytically due to the non-linear dependence of its parameters, the solutions are approximated using numerical methods.

Some studies designed with this approach have incorporated parameters describing the mechanical and biochemical properties of arterial smooth muscle cells based on previously proposed electrical models, in order to reflect the myogenic and neurogenic mechanisms of CBF regulation [108], [111], [112], [121]. Although most electrical models are unilateral, a few studies have designed bilateral models to simulate the differences in vascular properties between hemispheres and assess their effects on CBF [109], [113]. Some electrical models have focused on the behaviour of individual compartments such as the CSF space [90], [94], [95], while others have demonstrated the influence of vascular properties on ICP. This includes studies examining the role of cerebral autoregulation on mean ICP after acute brain injuries [48], [98], [100], [102], [103], [115], and the effects of vascular pressure transmission on ICP pulse waveforms [87], [93], [97]. However, most articles that included ICP in the context of

mathematical modelling has not mentioned its influence on continuous indices describing cerebrovascular dynamics. Of the few studies that did [48], only a qualitative description of their relationships have been suggested, and none has used the model to test the performance of the indices by simulating pathologies involving intracranial hypertension (such as TBI).

4.5 Conclusions

Mathematical, hydrodynamic, and electrical analogue models have been proposed to simulate the circulation of cerebral fluids. While these models are generally successful in replicating a multitude of individual pathophysiological events, their use in studying cerebrospinal hydrodynamics, and in particular the continuous indices of cerebral autoregulation in the context of elevated ICP has been limited. The application of indices describing cerebrospinal dynamics in personalised management of TBI patients necessitates better scrutiny of the confounding factors. This can only be achieved in conditions that ensures causality, as models do.

Chapter 5

Methods

This project used computer-supported mathematical modelling to study the physiological effects of cerebral fluids circulation. The aim of the project was to create a model implementation in software that can ultimately be integrated into the ICM+ software, allowing real time clinical data to be fed from bedside monitors to the model, which calculates parameters of clinical importance and sends them back to ICM+ for display. Therefore, instead of using universal environments such as MATLAB Simulink, a standalone software application for Windows was written. This chapter provides detailed descriptions of the software developed.

5.1 The Cerebrospinal Dynamics Modelling Software

A computer programme was written in Object Pascal (Embarcadero Delphi 10.2) with the RAD studio; it was designed to be run on Windows 10. This programme was used throughout the project to simulate the pressures and flows of fluids in various intracranial compartments, based on a number of model parameters and imported data. Upon opening the programme, the main menu appears (**Figure 5.1**).

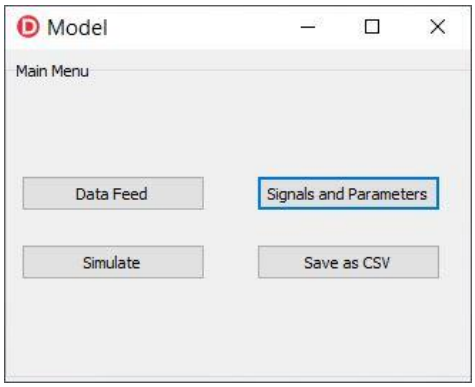

Figure 5.1. Main menu of the programme, allowing the user to choose the signals and parameters used by the model ('Signals and Parameters'), generate simulated signals using the model ('Simulate'), and save the signals in csv format ('Save as CSV').

The parameters and signals used by the model must first be set by clicking the 'Signals and Parameters' button, which opens a new window (**Figure 5.2**).

Figure 5.2. The 'Signals and Parameters' window, for users to set the parameters (left) and ABP signals (right) used by the model.

The model parameters can be set on the left side of the window, while the ABP signals are selected on the right. Users can set the ABP signal manually by specifying its baseline value and duration. Changes in ABP can be simulated by inputting additional baseline values with corresponding durations. Sinusoidal waveforms can also be added by specifying their amplitudes and frequencies. Alternatively, the model can use ABP data imported as a csv file.

By clicking the 'Simulate' button on the main menu, the programme generates simulated signals and plots them against time (**Figure 5.3**), with a time step of 40 ms. The choice of the time step was made as a balance of numerical performance of the programme and the necessity to represent information carrying frequency components normally present in the pressure and flow signals recorded in adult patients. The chosen time step corresponds to 25 Hz; while this may not be able to represent the full shape of a pressure/flow pulse, it is sufficient to study the effects of the fundamental frequency pulse amplitude, which are explored in the following chapters.

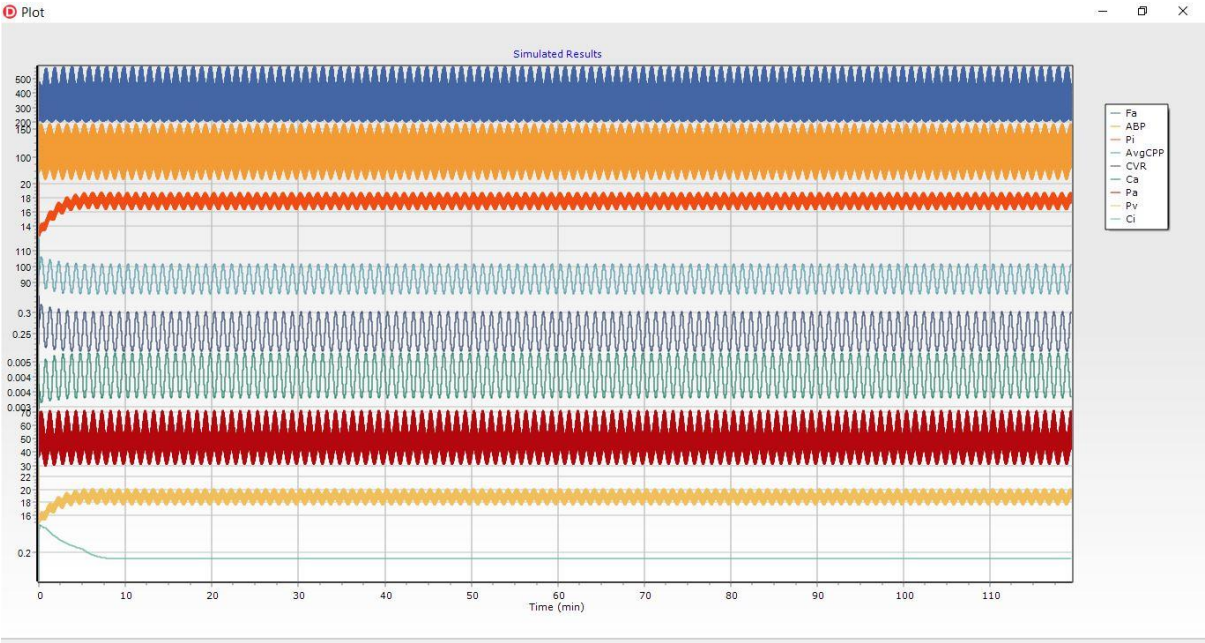

Figure 5.3. The window plotting simulated signals against time, opened by clicking the 'Simulate' button on the main menu. Note that there is a 'burn-in' period at the beginning of each simulation, where the modelled signals change from the initial values (set in the Signals and Parameters section) to their stabilised levels. Formal definitions of the variables are given in **section 6.1**.

While the programme was efficient in running simulations (about five seconds needed for a simulation of 120 minutes), substantial time and effort were required to finetune the model parameters by trial and error. About 1,400 simulations were run in the finetuning process, involving parameters of the Arteries and Veins (R_a, R_{b0}, C_{aSpan}, $C_{aBaseline}$, C_v), CSF ($P_{optimal}$, P_0, R_{CSF}, Elasticity), and ISF (R_{ISFa}, R_{ISFb}) compartments. Without a combination of physiologically reasonable parameters, the generated signals can diverge to infinity. This would result in mathematical errors, prompting the programme to display the message 'Values NaN'.

After a simulation is completed, the user can save the generated signals in csv format by clicking the 'Save as CSV' button on the main menu.

5.2 The Runge-Kutta Method and Its Validity in Simulations

The models used in this project are described with several first-order differential equations, which have no analytic solutions due to the non-linear dependence of some of its parameters. Instead, the solutions were approximated by numerical integration, using the 4th order Runge-Kutta method (RK4). RK4 is an effective and accurate method for solving initial-value problems of differential equations (its principle is illustrated in **Figure 5.4**). For an initial value problem

$$\frac{dy}{dt} = f(t, y), \qquad y(t_0) = y_0 \qquad \textbf{(Equation 5.1)}$$

the solution at the next step (y_{n+1}) is evaluated with the recursion formulae

$$y_{n+1} = y_n + \frac{h}{6}(k_1 + 2k_2 + 2k_3 + k_4) \qquad \textbf{(Equation 5.2)}$$

$$t_{n+1} = t_n + h \qquad \textbf{(Equation 5.3)}$$

where

$$k_1 = f(t_n, y_n) \quad \textbf{(Equation 5.4)}$$

$$k_2 = f\left(t_n + \frac{h}{2}, y_n + \frac{h}{2}k_1\right) \quad \textbf{(Equation 5.5)}$$

$$k_3 = f\left(t_n + \frac{h}{2}, y_n + \frac{h}{2}k_2\right) \quad \textbf{(Equation 5.6)}$$

$$k_4 = f(t_n + h, y_n + hk_3) \quad \textbf{(Equation 5.7)}$$

h is the step size (the time interval between two simulated data points); it was set as 40 ms in the programme.

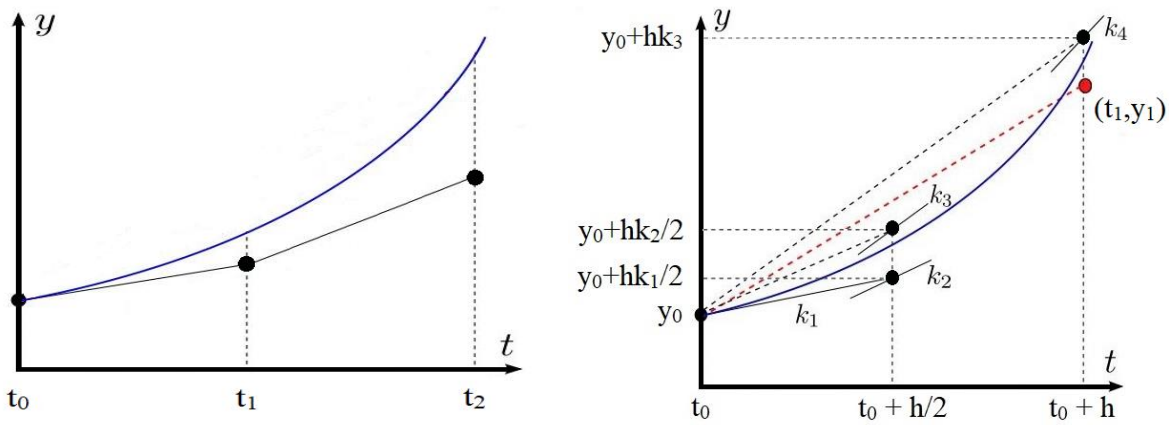

(a) (b)

Figure 5.4. Numerical approximation of a function curve (in blue) using (a) the Euler method and (b) the 4th order Runge-Kutta method (RK4). RK4 uses the weighted average of four slope-related increments, with greater weight given to the increments at the midpoint. This gives the method a greater accuracy of estimation when compared to the Euler method, which only considered the slope of one tangent curve at each time step.

5.3 Verification of the Model Solver

Using a model of CSF dynamics proposed by Marmarou [90] (which is described by a differential equation without non-linear parameter dependencies), the validity of RK4 in

simulations can be tested by comparing its results with those obtained using analytical integration. This model consists of a current source representing the formation of CSF, a capacitor modelling the intracranial compliance, and a resistive element simulating the resistance of CSF outflow (**Figure 5.5**).

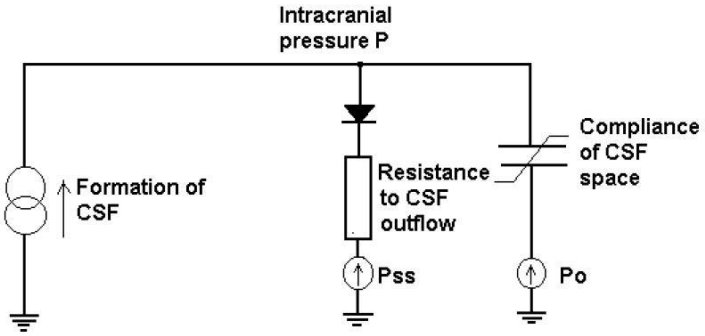

Figure 5.5. [90] The model of CSF space proposed by Marmarou, simulating the formation of CSF, compliance of CSF space, and resistance to CSF outflow. P_{ss} is the sagittal sinus pressure, and P_0 is a modelling constant. This model is used to analyse the CSF dynamics of patients during infusion studies, a diagnostic test for hydrocephalus.

The effect of an infusion test on intracranial pressure was simulated using this model. A state equation describing the current flow in the CSF model can be written:

$$\frac{dP_i}{dt} = E \cdot (P_i - P_0) \cdot \left(I_p + I_{inf} - \frac{P_i - P_b}{R_{CSF}}\right) \qquad \textbf{(Equation 5.8)}$$

where

R_{CSF} is the resistance of CSF outflow,

I_p is the rate of CSF production,

I_{inf} is the rate of infusion,

P_i is the intracranial pressure,

P_b is the 'baseline ICP', i.e. the ICP before starting the infusion,

P_0 is a constant ('equilibrium pressure'), and

E is the elasticity of the CSF space.

The equation was first solved numerically with RK4. The analytical solution is:

$$P_i = P_0 + \frac{\left(I_p + I_{inf} + \frac{P_b - P_0}{R_{csf}}\right) \cdot (P_b - P_0)}{\frac{P_b - P_0}{R_{csf}} + (I_p + I_{inf}) \cdot \exp\left[-E \cdot \left(I_p + I_{inf} + \frac{P_b - P_0}{R_{csf}}\right) \cdot t\right]} \quad \textbf{(Equation 5.9)}$$

The pressure values obtained analytically were compared to the results evaluated numerically and plotted in **Figure 5.6**.

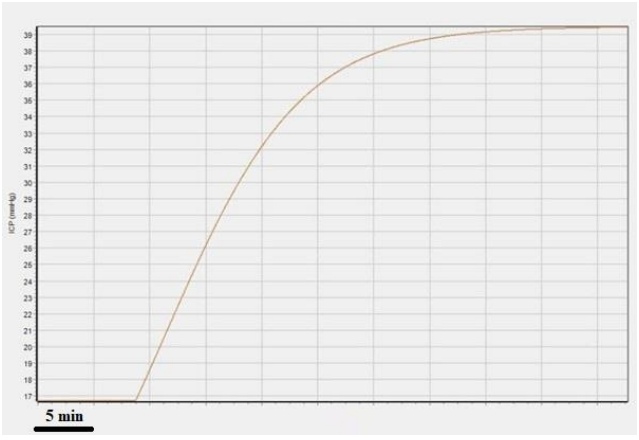

Figure 5.6. A comparison of ICP values generated during a simulated infusion test, obtained with analytical integration (in blue) and numerical estimation (in orange). The two curves overlapped each other completely.

The two curves overlapped each other completely (with a mean error of 1.64×10^{-13}). This suggests that the numerical method provides an accurate estimation of ICP, and is suitable to be employed for simulations in subsequent chapters (as results are not recorded beyond the units digit).

5.4 Additional Work in Preparation for the ICM+ Real Time Pipeline

ICM+ (Cambridge Enterprise Ltd, Cambridge, UK, https://icmplus.neurosurg.cam.ac.uk) is a clinical research software developed for neuro-intensive care monitoring; it is capable of collecting high-resolution data and performing real time analyses. By employing the principle of moving calculation window, the real time data processing engine of ICM+ allows the construction of computation pipelines with multiple analysis layers (outlined in **Figure 5.7**). This technique has facilitated the derivation of various diagnostic metrics with clinical significance.

The model software has also been prepared for real time use within the ICM+ calculation pipeline. Although completion of this work turned out to be out of the scope for this project, the real time data feed from the model into ICM+ has been implemented. For this purpose, data

generated by the model was used instead of clinical signals, so that the model also acted as the signal source.

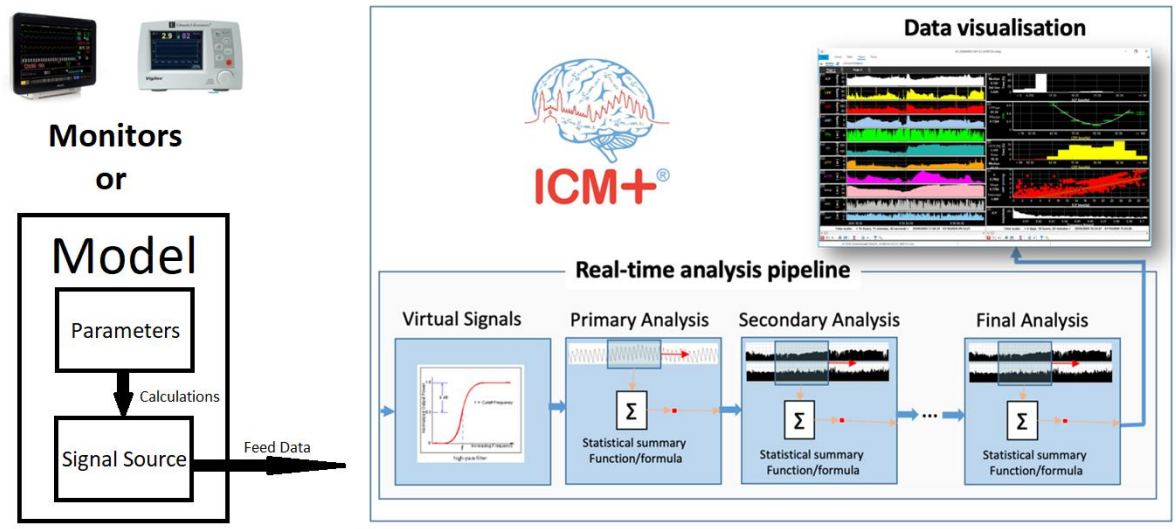

Figure 5.7. Schematic diagram of the data integration and real time processing engine of ICM+. Live data from the monitors are fed to ICM+ (in this project, the model software generates the data and acts as the signal source). The data streams are processed with moving calculation windows at multiple analysis layers of the computation pipeline, with each layer receiving data from the output of the previous one.

A serial communication protocol was used, and a simple ASCII-based data export protocol was implemented to stream the simulated signals in real time. After choosing the appropriate data feed settings with the 'Data Feed' menu of the model software (**Figure 5.8** (a)), ICM+ was used to match the respective settings and protocol (**Figure 5.8** (b)) in order to receive the data. **Figure 5.8** (c) shows the signal generated by the model and its simultaneous display in ICM+.

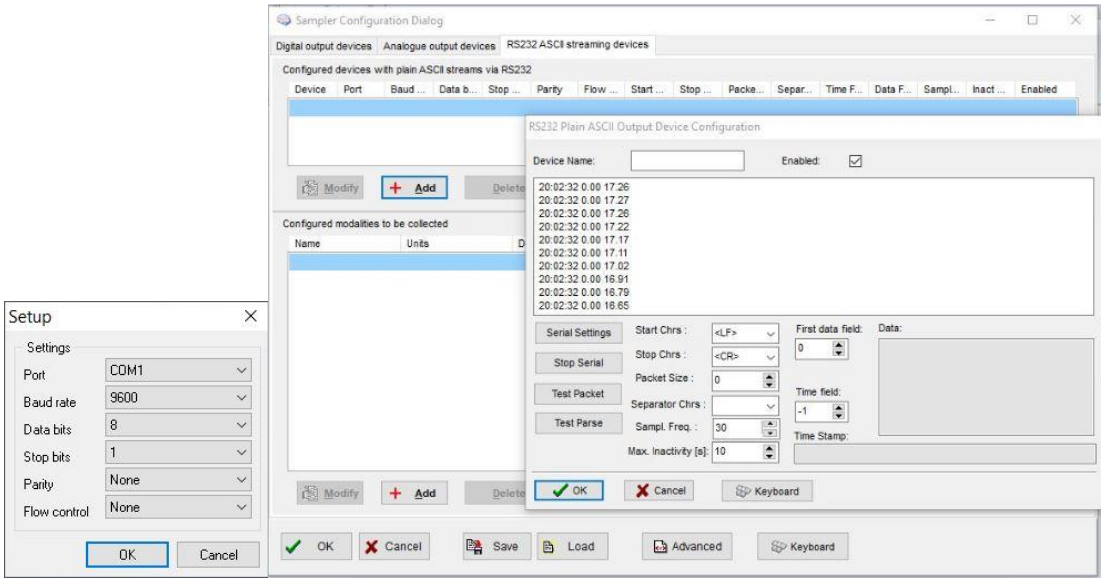

(a) (b)

(c)

Figure 5.8. (a) 'Data Feed' window of the model software, allowing users to select the appropriate settings to stream real time simulation data; (b) setup page allowing ICM+ to receive data generated by the model; (c) signal generated by the model (above), and the simultaneous display of the signal received by ICM+ (below).

5.5 Off-line Data Analysis with ICM+

Although ICM+ was, in the end, not used in this thesis for real-time data streaming from the model, it has been used extensively for calculating trends of cerebrovascular reactivity metrics

in the following chapters. However, for the sake of performance the data from the model was stored in a temporary file, before being fed in one go into ICM+ using its 're-analysis' mode. The principles of the off-line analysis pipeline are identical to its real-time counterpart as outlined in **Figure 5.7**. An example of such analysis is illustrated in **Figure 5.9** below:

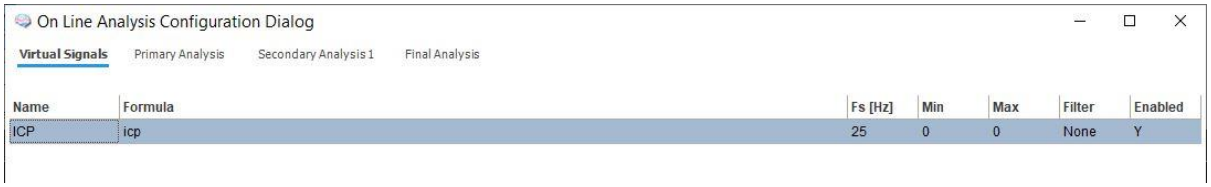

(a)

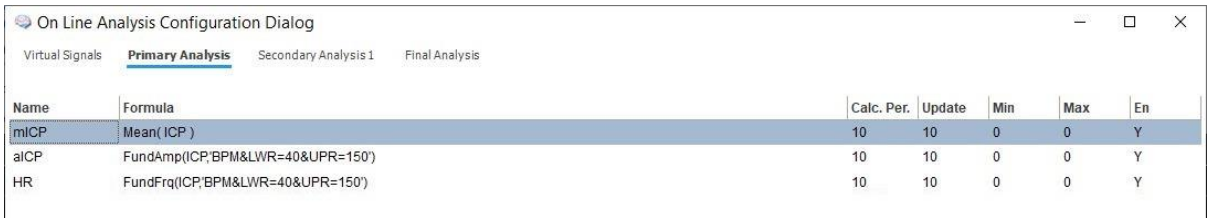

(b)

(c)

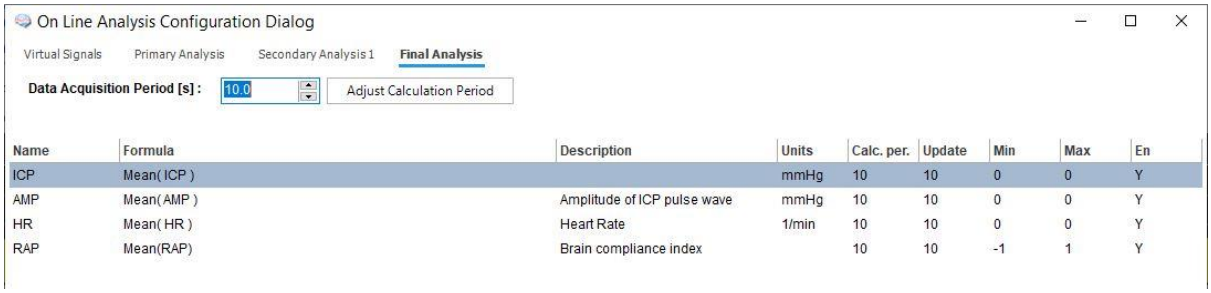

(d)

Figure 5.9. The analysis configuration dialogue of ICM+, showing (a) the virtual signal fed to the software and (b) the primary, (c) the secondary, and (d) the final stages of the analysis pipeline.

In this example, ICP with a sampling frequency of 25 Hz was used as the virtual signal (**Figure 5.9** (a)). In the primary analysis (**Figure 5.9** (b)), the fundamental amplitude and fundamental frequency of ICP were used to calculate the ICP amplitude (aICP or AMP) and heart rate (HR) respectively. Mean ICP (mICP), aICP and HR were evaluated with a calculation window of 10 seconds and updated every 10 seconds. The brain compliance index RAP was calculated in the secondary analysis (**Figure 5.9** (c)) through the correlation between aICP and mICP, using a calculation window of 240 seconds and updated every 10 seconds. Based on the calculations specified in final analysis (**Figure 5.9** (d)), the time series of ICP, HR, AMP and RAP were plotted in **Figure 5.10**.

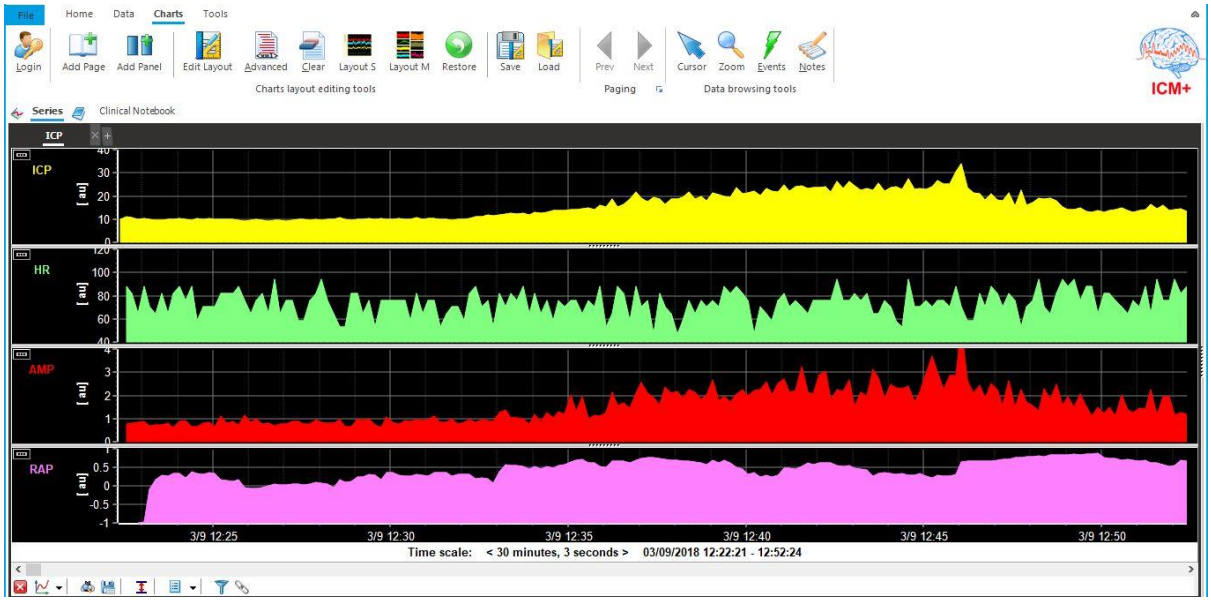

Figure 5.10. The imported signal (ICP) and indices calculated by ICM+.

Chapter 6

Validation of an Existing Model of Cerebral Hydrodynamics

Part of the work in this chapter formed the basis of the following publication:

K. H. Chu, I. Olakorede, E. Beqiri, M. Czosnyka, and P. Smielewski, "Mathematical modelling of cerebral haemodynamics and their effects on ICP," *Brain and Spine*, vol. 4, January 2024, Art. no. 102772, doi: 10.1016/j.bas.2024.102772.

6.1 Introduction

Intracranial pressure (ICP) is a vital quantity to be monitored for clinical decisions in neurointensive care, and substantial effort has been made to investigate its dynamics with mathematical modelling. Works by Monro and Kellie [43], [44] described the volume conservation of fluids and brain matter within the skull due to the unique intracranial structure: the systems of cerebral blood flow (CBF) and cerebrospinal fluid (CSF) circulation are embedded in the brain tissue, which in turn is constrained by the rigid dura and cranium. This indicates that the changes in fluid flow at different time scales contribute to ICP variations in different ways. Subsequent studies have explored the transient and sustained effects of CSF

flow on ICP. Notably, Davson [127] attributed the steady-state changes in ICP to the formation rate of CSF, the resistance of CSF outflow through the skull, and the pressure at the sagittal sinus where CSF absorption occurs. On the other hand, Marmarou [90], [128] introduced the concept of intracranial compliance in his modelling studies, and demonstrated its role on the dynamic aspects of ICP.

The interactions between cerebral haemodynamics and ICP is of much interest, particularly in scenarios like traumatic brain injury. Importantly, Ursino [100], [129], [130] included in his model a representation of cerebrovascular circulation; this enabled the simulations of physiological phenomena involving vascular dilation and constriction such as cerebral autoregulation. It is common for modelling studies to integrate compartments of CBF and CSF circulation to explore their combined effects on ICP. To examine such effects, this study initially replicated the unilateral hydrodynamic model proposed by Czosnyka [48] (**Figure 6.1** (a)).

The electrical analogue of the model (**Figure 6.1** (b)) consists of four resistive (R_a, CVR, R_b, and R_{CSF}) and three capacitive (C_a, C_v, and C_i) components, the meaning of which will be described in detail below. It also includes two input voltage sources ABP and P_{ss}, representing the systemic arterial blood pressure and the venous pressure in the dural sinuses respectively.

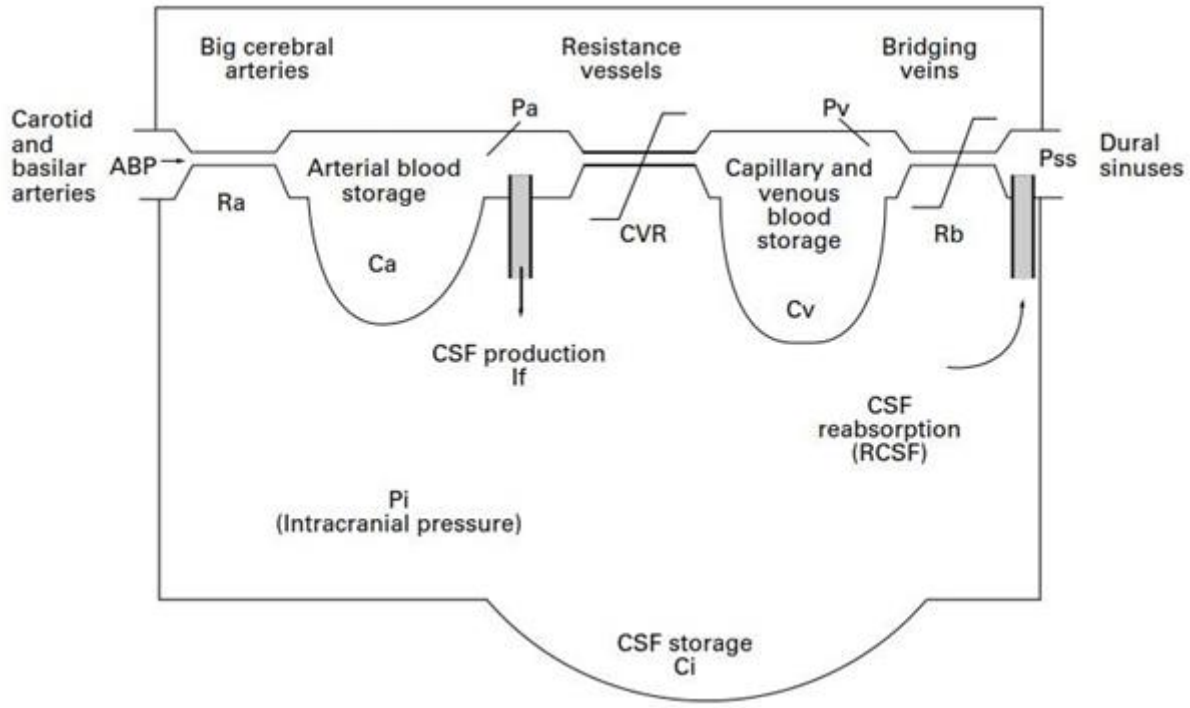

(a)

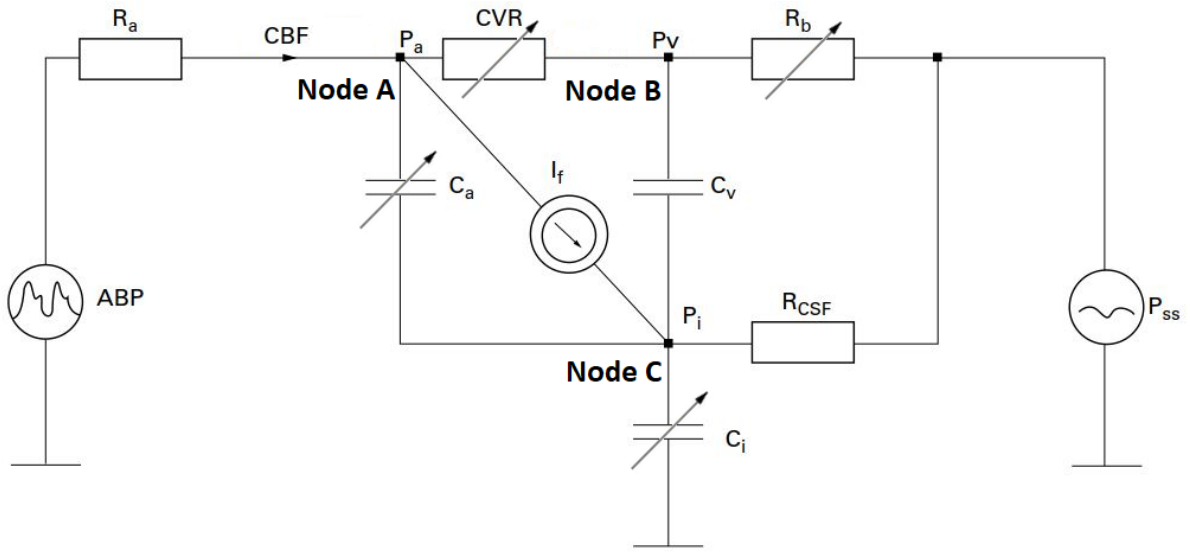

(b)

Figure 6.1. [48] The unilateral hydrodynamic model proposed by Czosnyka (a) and its electrical analogue (b). State equations are derived by considering the flow of current in nodes A, B and C (located in the arterial, venous and CSF compartments respectively).

6.1.1 Characteristics of Model Parameters

This section provides a mathematical description of the resistive and capacitive elements in the model. Anatomical structures represented by these elements were introduced in **Chapter 1**.

6.1.1.1 R_a

Although the resistance at the large cerebral arteries can be increased permanently in pathological conditions such as atherosclerosis and vasospasm [48], its dynamic responses to changes in cerebral perfusion pressure is negligible when compared to the smaller resistive arterioles, and is therefore modelled as a constant.

6.1.1.2 CVR

The cerebrovascular resistance of the resistive arterioles depends on two factors: the active control of myogenic tone due to cerebral autoregulation, and the passive (elastic) response to changes in transmural pressure. To simulate the active dilation and constriction of the vessels in response to cerebral perfusion pressure, the model follows previous studies [39] and uses the inverse of a 6th order polynomial as an effective formula to fit the CPP-CVR relationship observed in clinical data [91].

$$CVR_{active} = CVR_{max} - \frac{CVR_{max} - CVR_{min}}{1 + \left(\frac{CPP_m + CPP_{aoffset}}{CPP_{max} - CPP_{min}}\right)^6} \qquad \textbf{(Equation 6.1)}$$

where

CVR_{max} and CVR_{min} are the active CVR during maximal vasoconstriction and vasodilation,

CPP_{max} and CPP_{min} are the upper and lower limits of autoregulation,

$CPP_{aoffset}$ is a constant translating the active CVR-CPP curve, and

CPP_m is the mean cerebral perfusion pressure, averaging the CPP values in the last 6 seconds to simulate the high pass filter, time lagged, character of the autoregulatory response [131].

When considering the passive component of CVR, a resistive artery can be modelled as an elastic tube with linear relationship between the transmural pressure and its cross-sectional area [132], [133] (i.e. pressure is proportional to the square of its radius). By the Poiseuille's law, the resistance of flow through a tube is inversely proportional to the fourth order of its radius. From these relationships, the passive component of CVR was modelled to be proportional to the inverse of CPP squared:

$$CVR_{passive} = \frac{1}{(CPP_m + CPP_{poffset})^2 \times CVR_{span}} \qquad \textbf{(Equation 6.2)}$$

where

$CPP_{poffset}$ is a constant translating the passive CVR-CPP curve, and

CVR_{span} is a proportionality coefficient describing the sensitivity of passive resistance to CPP changes.

The total CVR is calculated as the sum of its active and passive components. An example of the relationships of CVR_{active}, $CVR_{passive}$, and total CVR with CPP are illustrated in **Figure 6.2**.

$$CVR = CVR_{active} + CVR_{passive} \quad \textbf{(Equation 6.3)}$$

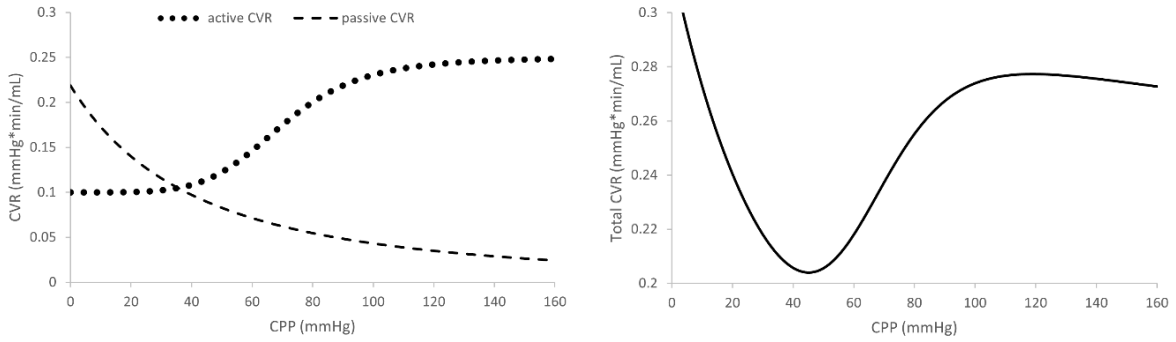

(a) (b)

Figure 6.2. Plots of active and passive components of CVR (a), and total CVR (b) against CPP.

6.1.1.3 C_a

The compliance of the cerebrovascular bed can be described as a non-linear function of either CVR [39] or CPP [134]. As the model seeks to simulate the dependence of compliance on the delayed response of the vascular muscle, the CVR option was chosen:

$$C_a = \frac{C_{aspan}}{CVR_m(CPP_m)/CVR_{min}} + C_{aoffset} \quad \textbf{(Equation 6.4)}$$

where

C_{aspan} is a coefficient reflecting the sensitivity of C_a in response to changes in pressure,

$C_{aoffset}$ is a constant allowing vertical translation of the C_a-CVR curve, and

CVR_{min} is the minimum value of cerebrovascular resistance, during complete vasodilation at the lower limit of autoregulation.

6.1.1.4 C_v

The compliance of the venous compartment is modelled as a constant, as there is no data suggesting its non-linear character [48].

6.1.1.5 R_b

The resistance of venous outflow through the bridging veins is dependent on the pressure gradient P_v-P_i. Due to the small transmural pressure in the venous compartment, the bridging veins are modelled to be collapsible. To simulate the increase in vascular resistance due to a decrease in vascular lumen, the model of 'compression cost' is chosen. This approach is adopted instead of the Starling resistor model, as previous modelling studies [39] were able to generate CBF and ICP signals with more realistic pulsatility when compared to experimental work [135]. The resistance is expressed as the following:

$$R_b = \begin{cases} \frac{R_{b0}}{P_v - P_i} \ for \ P_v > P_i \\ 10000 \ for \ P_v < P_i \end{cases} \qquad \textbf{(Equation 6.5)}$$

where

R_{b0} is a scaling coefficient, and

'10000' is an arbitrary constant term, simulating infinite resistance due to a complete blockage of venous outflow, when ICP exceeds the venous pressure.

6.1.1.6 CSF Circulation

The CSF space is characterised by the intracranial compliance (C_i), rate of CSF formation (I_f), and resistance to CSF outflow (R_{CSF}). Both R_{CSF} and I_f are considered constants, while C_i is related to ICP and the elasticity of CSF space:

$$C_i = \begin{cases} \dfrac{1}{E(P_i - P_0)} & for\ P_i > P_{opt} \\ \dfrac{1}{E\left(P_{opt} - P_0\right)} & for\ P_i < P_{opt} \end{cases} \qquad \textbf{(Equation 6.6)}$$

where

P_{opt} is the pressure breakpoint between linear and non-linear range of cerebrospinal compliance,

P_0 is the pressure corresponding to infinite compliance, which essentially provides an offset to the inverse relationship between compliance and pressure, and

E is the elasticity of the CSF space. Elasticity describes the 'stiffness' of a material, and is used commonly in the field of CSF circulation pathology. It is a constant coefficient in the exponential relationship between volume and pressure, and thus a parameter of the non-linear brain compliance function.

C_i can also be defined as the change in intracranial volume with respect to ICP change. In other words, it is the derivative of the function V(P); its inverse function is commonly plotted as the pressure-volume curve (**Figure 6.3**).

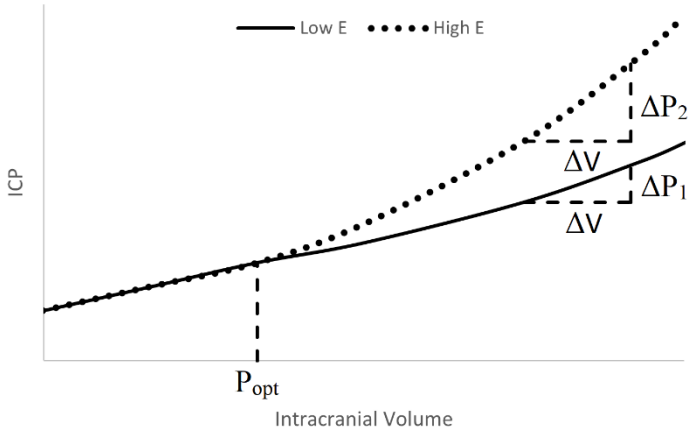

Figure 6.3. The pressure-volume relationship of the CSF space, with C_i equals the reciprocal of its slope. Above the pressure linearity breakpoint (P_{opt}), CSF space with high elasticity has a lower value of C_i than that with low elasticity ($\Delta V/\Delta P_2 < \Delta V/\Delta P_1$).

The variations of C_a and C_i are illustrated in **Figure 6.4** [39], [48] below.

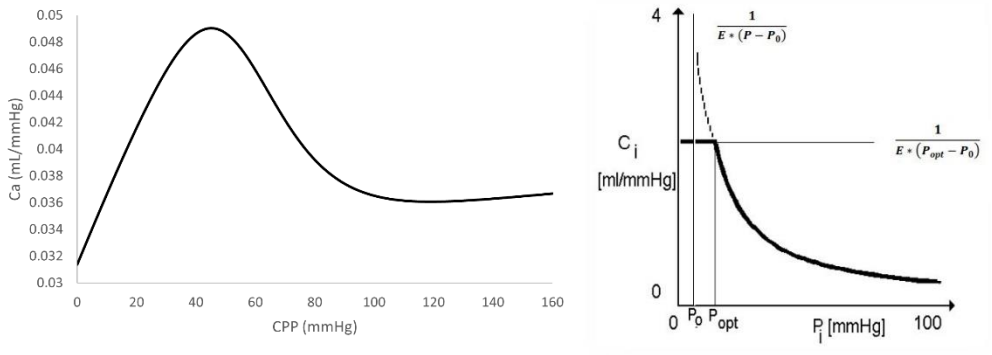

(a) (b)

Figure 6.4. Relationships of C_a (a) with CPP, and C_i with P_i (b).

6.1.1.7 Values of Parameters

As the model is a conceptual simplification of cerebrospinal circulation, some of its parameters can be estimated from physiological measurements: for healthy adults, R_{CSF} has been estimated to be <18 mmHg/mL/min [136], [137], and I_f to be 0.3 – 0.4 mL/min [5]. Other parameters need to be set based on trial-and-error simulations, so that the generated signals do not diverge to infinity (which results in mathematical errors). The ranges of parameters tested to produce non-infinite output signals are listed below:

Table 6.1. Ranges of parameters investigated

Parameter	Range
R_a	0.08 – 0.2 mmHg/mL/min
CVR	0.05 – 0.75 mmHg/mL/min
C_a	0.01 – 0.06 mL/mmHg
C_v	0.5 – 1.5 mL/mmHg
R_b	0.12 – 0.27 mmHg/mL/min
C_i	0.1 – 4 mL/mmHg

While adjusting the values within the above ranges can change the absolute values of the generated signals, it does not alter the model's ability to replicate pathophysiological phenomena of interest, which is the main objective of this study.

6.1.2 Establishing Mathematical Relationships with the Electrical Analogue

The current (flow rate) and voltage (pressure) at different points of the circuit are of interest; they can be described mathematically with 'state equations'. These equations are derived from the electric model with the laws of electric circuits. In the implementation of this model, the Kirchhoff's principle of charge conservation was employed: the algebraic sum of all currents entering a junction is zero.

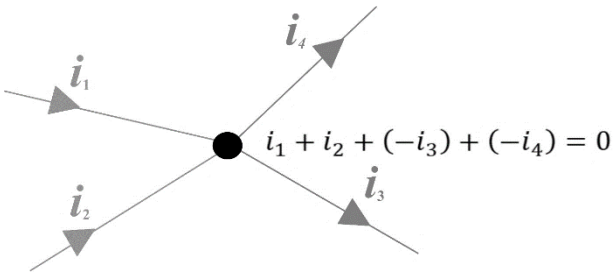

Figure 6.5. Illustration of Kirchhoff's principle of charge conservation ('current law').

Three state equations can be established by considering the current at three nodes of the circuit (**Figure 6.1**):

At node A,

$$\frac{dP_a}{dt} = \frac{dP_i}{dt} + \frac{1}{C_a}\left(\frac{ABP - P_a}{R_a} - \frac{P_a - P_v}{CVR} - I_f\right) \qquad \textbf{(Equation 6.7)}$$

At node B,

$$\frac{dP_v}{dt} = \frac{dP_i}{dt} + \frac{1}{C_v}\left(\frac{P_a - P_v}{CVR} - \frac{P_v - P_{ss}}{R_b}\right) \qquad \textbf{(Equation 6.8)}$$

And at node C,

$$\frac{dP_i}{dt} = \frac{1}{C_i}\left(\frac{ABP - P_a}{R_a} - \frac{P_v - P_{ss}}{R_b} - \frac{P_i - P_{ss}}{R_{CSF}}\right) \qquad \textbf{(Equation 6.9)}$$

where P_a, P_v, and P_i are the cerebral arterial pressure, pial venous pressure, and intracranial pressure respectively.

There are no analytic solutions to this set of first-order differential equations, due to the non-linear dependence of some of its parameters (CVR, C_a, C_i, R_b) on the node pressures. Instead, the solutions were approximated with the 4th order Runge-Kutta method (see **Chapter 5**). After substituting the relationships of the parameters into the three state equations and implementing the RK 4 method, the node pressures P_a, P_v and P_i were evaluated. Also, the cerebral blood flow through the middle cerebral artery (F_a) can be calculated using the Ohm's law:

$$F_a = \frac{ABP - P_a}{R_a} \qquad \textbf{(Equation 6.10)}$$

6.2 Methods

A programme designed to be run on Windows 10 was written in Object Pascal (Embarcadero Delphi 10.2) using the RAD studio (see **Chapter 5**). After importing ABP data from a csv file (details in **section 6.3**), it used the state equations described above to calculate and plot P_a, P_v, P_i, CBF, and CVR against time.

Three pathophysiological phenomena observed in clinical data were simulated by the programme to test the performances of the model:

1. Transient hyperaemic response test (THRT) – a diagnostic test assessing the capacity of cerebral autoregulation. During the test, the common carotid artery was compressed for a few seconds before being released, with a transient increase in cerebral blood flow indicating intact cerebral autoregulation mechanism [138], [139].
2. CSF infusion test – a clinical study used to analyse the dynamics of CSF circulation in patients suspected of normal pressure hydrocephalus (excess buildup of CSF in the brain's ventricles). In a lumbar infusion study, artificial CSF is infused at a constant rate into the CSF space via a lumbar puncture, causing the ICP to rise to a plateau level. [140]–[143]
3. ICP plateau waves – a sudden surge in ICP to a plateau with a duration of 5 to 20 minutes, commonly seen in TBI patients with intact autoregulatory capabilities [144]–[146]. It has been suggested [147] that plateau waves are caused by a vasodilatory cascade (**Figure 6.6**), where the resistive arterioles dilate due to autoregulation in response to an initial, abrupt, drop in ABP. The effect of increasing cerebral blood volume (CBV) is then transmitted to the intracranial compartment and raises the ICP, causing further reduction in CPP. This vicious cycle results in the continuous rise in ICP until the vessels have exhausted their capacity to dilate, and occurs despite blood pressure restoration which may follow the transient drop.

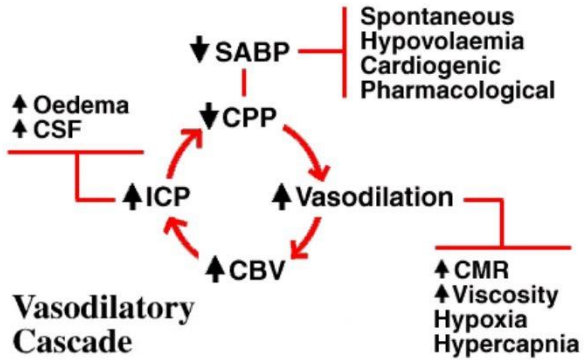

Figure 6.6. [147] Illustration of factors contributing to vasodilatory cascades

Examples of clinical recordings depicting the pathophysiological phenomena mentioned above were included in **Figure 6.7**:

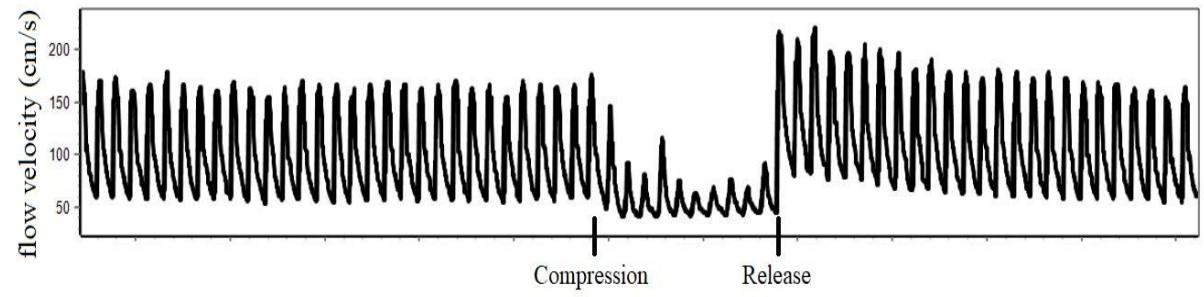

(a)

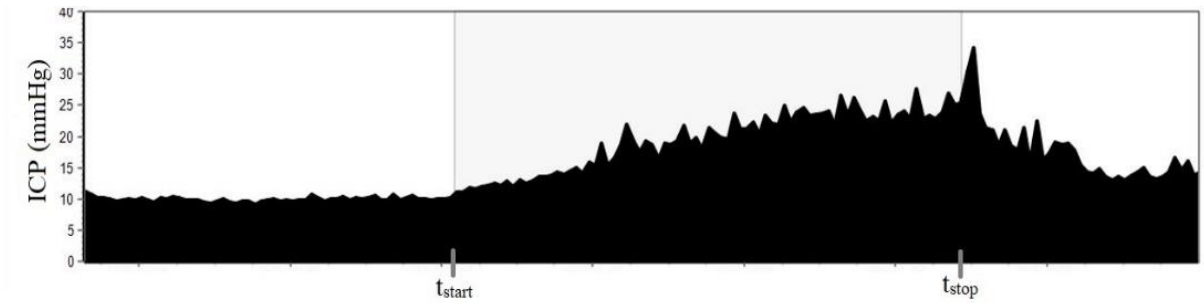

(b)

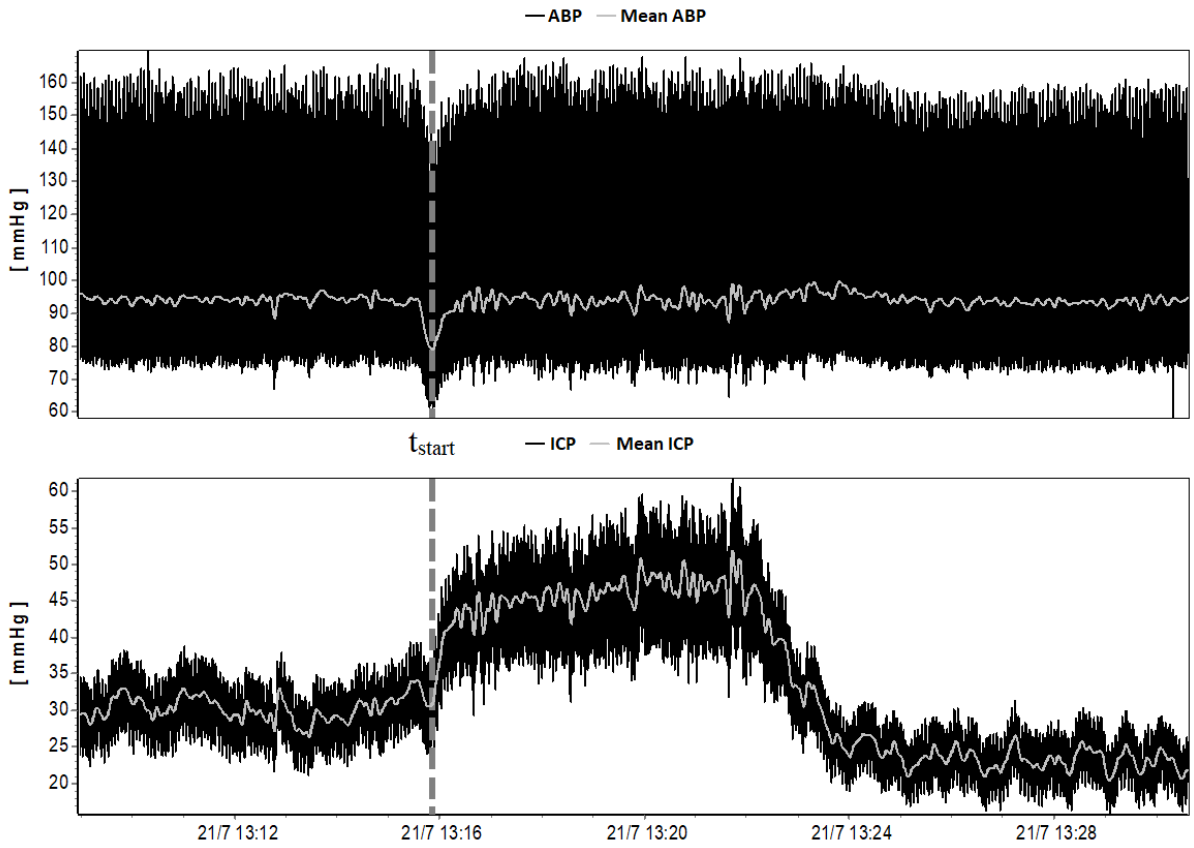

(c)

Figure 6.7. Clinical recordings of the three pathophysiological phenomena to be simulated by the model: (a) transient hyperaemic response test (THRT), (b) CSF infusion test, and (c) ICP plateau waves (where a rapid rise in ICP was triggered by a sudden drop in ABP, beginning from t_{start}).

There are no quantitative definitions for these clinical phenomena, and no previous modelling studies have set any targets to be simulated. The qualitative measure of success of the simulations is the ability to replicate the observed behaviour of the variables (as stated above) measured in human or animal subjects, whereas the quantitative measure is the goodness of fit of data to the measurements. This work mainly focused on the former, as this is the prerequisite of the latter, which will follow in subsequent projects.

6.3 Results

6.3.1 Transient Hyperaemic Response Test

The compression of the common carotid artery was represented by a step drop in ABP, before being restored to its original level (**Figure 6.8** (a)). The responses of CBF and CVR were shown in **Figure 6.8** (b) and (c) respectively.

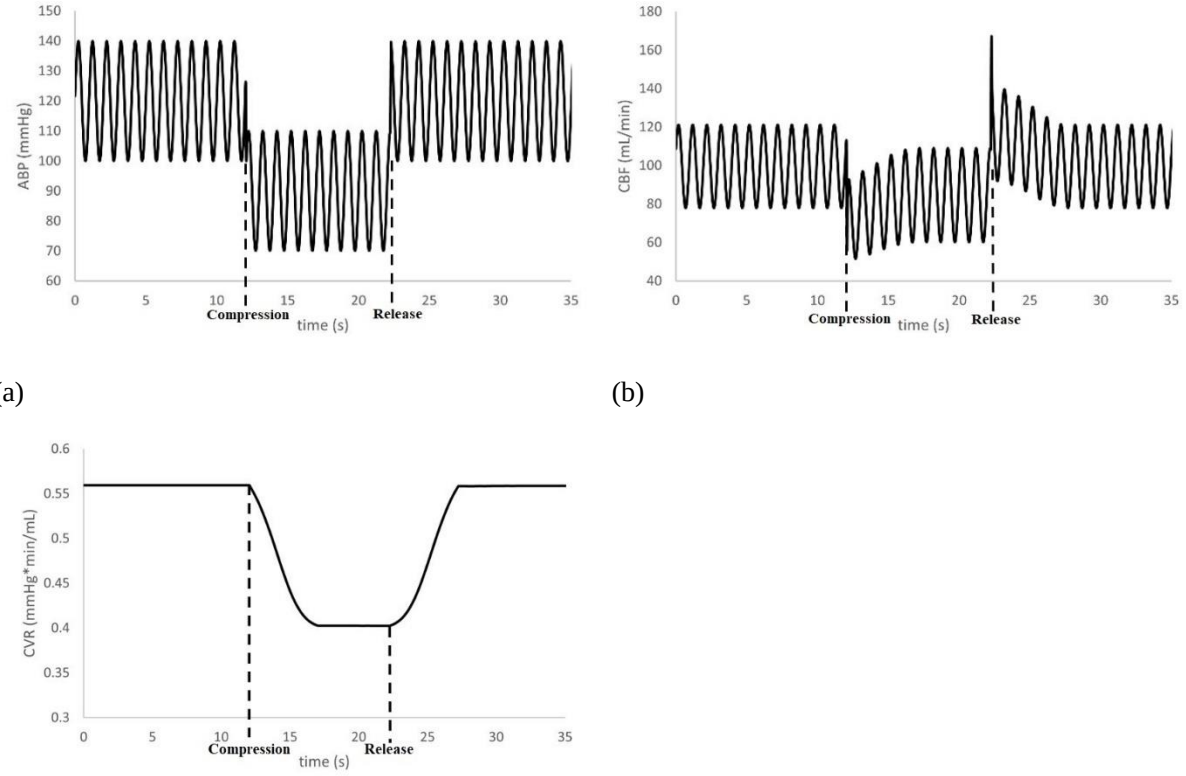

(a) (b)

(c)

Figure 6.8. Simulation of THRT with step changes in ABP between the onset and release of artery compression (a), and the response of CBF (b) and CVR (c) with the model.

The CBF simulated by the model was reduced during the compression, provoking visible compensatory vasodilation (decrease in CVR during the compression). After the compression was released, CBF surged before falling gradually to the level before the compression (as CVR returned to its baseline value due to active vasoconstriction). This showed that the simulation was successful in producing the transient hyperaemic response observed in transcranial Doppler (TCD) ultrasonography recordings [138].

6.3.2 Infusion Test

For the simulations of an infusion stage between t_{start} and t_{stop}, a constant term I_{inf} was added to the rate of CSF formation (I_f) to represent the rate of infusion into the CSF space. The ICP response was plotted in **Figure 6.9**.

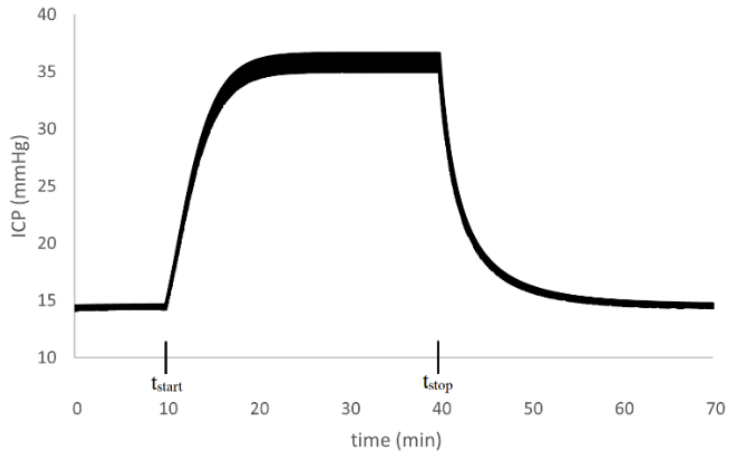

(a)

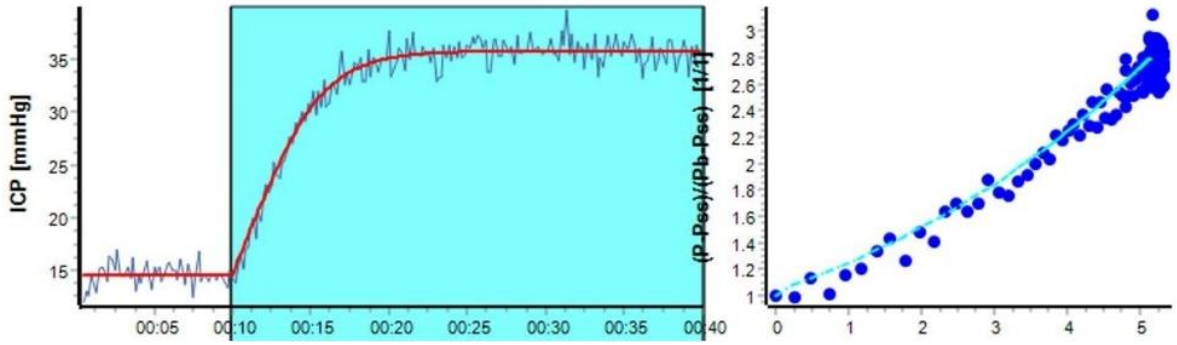

(b)

Figure 6.9. (a) Simulation of ICP response to a constant rate infusion, beginning at t_{start} and terminating at t_{stop} (b) analysis with the ICM+ software, illustrating the model-derived best fit curve (left, ICP [mmHg] vs time [min]), yielding the model parameters and the corresponding pressure-volume curve (right). The latter is plotted by calculating incremental changes in the total CSF volume during the CSF infusion, taking into account simultaneous absorption process, against the corresponding relative pressure change. R_{CSF} was calculated as 13.86 mmHg/mL/min. White noises were added to the generated ICP (in red) for illustrative purposes in the curve-fitting process.

The simulation produced the ICP behaviour commonly seen in real clinical recordings, rising to a plateau during the infusion stage and falling back to the baseline level when the infusion was terminated.

6.3.3 Plateau Wave

ICP plateau waves were simulated by creating a step change in ABP, as a trigger for the vasodilatory cascade (**Figure 6.10** (a)); The ICP response was shown in **Figure 6.10** (b).

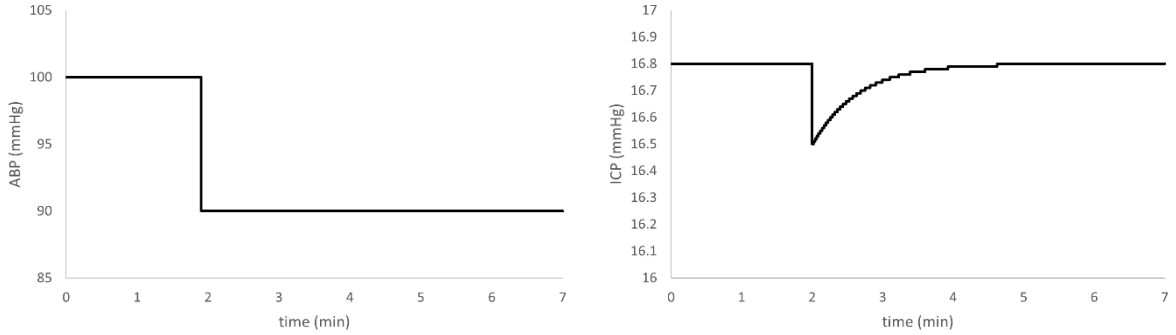

(a) (b)

Figure 6.10. Simulated ICP in response to a step reduction in ABP. No sustained changes in ICP can be observed.

In this case, the model was not able to simulate the onset of a plateau wave: the ICP responded to the step drop in ABP with an immediate decrease, but then gradually restored to its baseline value.

6.4 Discussion

The pressure-flow interactions of each compartment enabled the model to simulate various physiological responses of flow and pressure commonly observed in clinical practice. For instance, the haemodynamic representation has been successful in simulating the behaviours of CBF in response to changes in CPP; this has allowed the demonstration of the effects of cerebral autoregulation: simulations of THRT have created the characteristic transient hyperaemic responses, which is caused by the vasodilation of resistive arterioles in response to

the step drop in ABP. Moreover, the intracranial compartment correctly simulated the response of ICP to constant rate infusion.

However, the sustained effects of vascular constriction and dilation on ICP (such as plateau waves) were not reflected correctly by the model. This can be also seen by analysing the electrical pathways connected to node C of the electrical analogue, which represents the ICP (**Figure 6.11**).

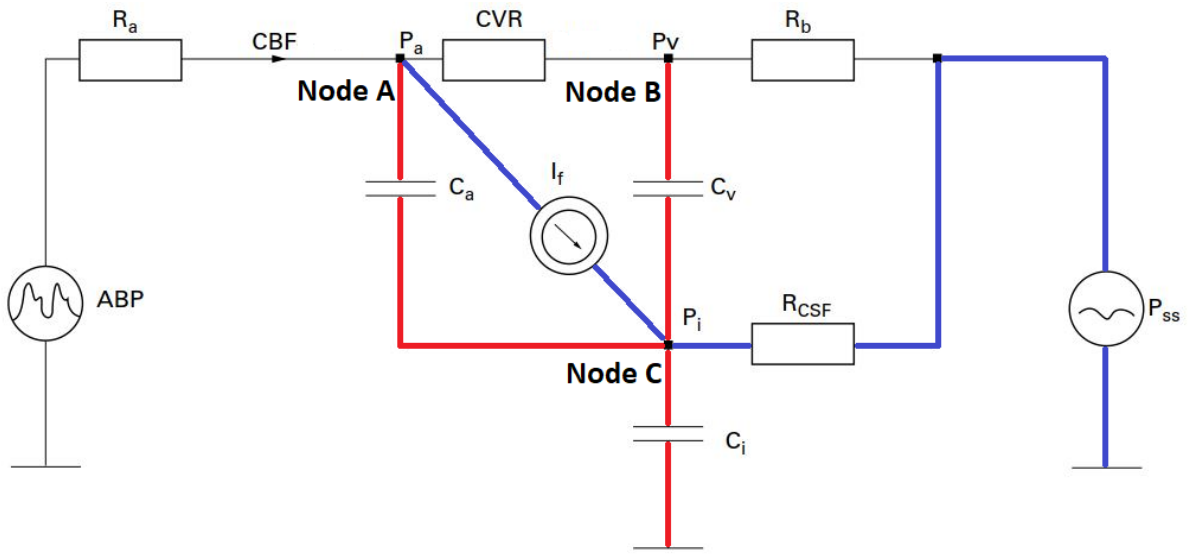

Figure 6.11. The electrical analogue of the model, with 'static' and 'dynamic' pathways connected to node C highlighted in blue and red respectively.

The pathways can be categorised as 'static' and 'dynamic', with the former comprised of current source or resistive elements, and the latter with capacitive elements. As the potential difference of the voltage source changes, current passes through both static and dynamic

pathways. But if the voltage remains constant after a change, the capacitors in the dynamic pathways will eventually become fully charged or discharged, after which no current will pass through. This can be illustrated with a simple circuit consisting of a resistor ('static pathway') and a capacitor ('dynamic pathway') in parallel (**Figure 6.12**).

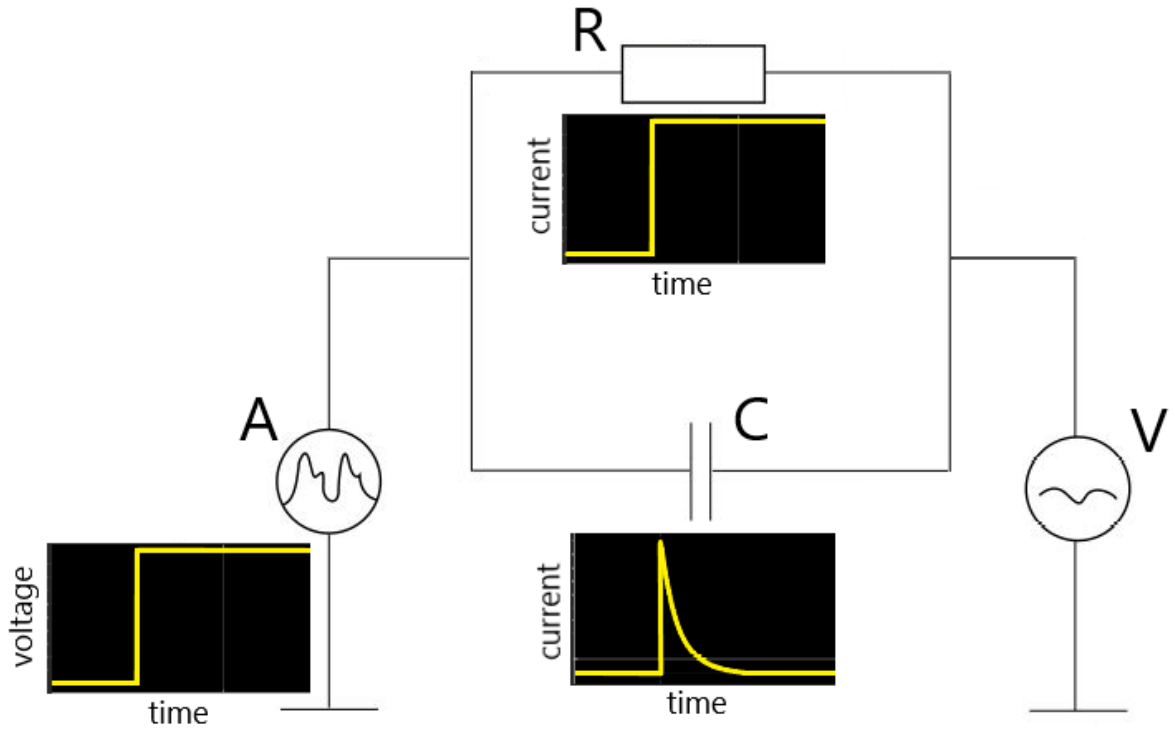

Figure 6.12. A simple circuit with a resistor (R) and capacitor (C) in parallel, illustrating the current passing through the resistor and capacitor in response to a step change in voltage source (A). After the step change, the current persists to flow through the resistor, while the current flowing through the capacitor is gradually reduced to zero.

In a model consisting of only the vascular and CSF compartments, the state equation in a steady state (without current passing through the dynamic pathways) at node C is reduced as

$$I_f = \frac{P_i - P_{ss}}{R_{csf}} \qquad \textbf{(Equation 6.11)}$$

which is the Davson's equation [127]. As I_f, R_{CSF} and P_{ss} are all modelled as constants, P_i (ICP) must also be a constant. This explains why the simulated ICP always returns to a constant value after responding initially to a change in ABP. As a result, the model cannot transmit any long-term volume changes in the vasculature to the intracranial compartment. Without modifications to the model, any clinical phenomena involving prolonged interactions between the two cannot be simulated correctly.

6.5 Conclusions

Electrical-equivalence mathematical models that integrate vascular and CSF compartments perform well in simulations of dynamic cerebrovascular variations and their transient effects on ICP. However, they may be less robust in representing long-term interactions between CBV and ICP. As demonstrated in this study, simulations with such models could be inaccurate when attempting to reflect clinical phenomena caused by prolonged changes in CBV, such as sustained vasodilation. To rectify this, a new static mechanism must be added to link the fluid dynamics in the arterial and intracranial compartments.

Chapter 7

Modifications to the Model and Verification of Its Validity

Part of the work in this chapter formed the basis of the following publication:

K. H. Chu, I. Olakorede, E. Beqiri, M. Czosnyka, and P. Smielewski, "Mathematical modelling of cerebral haemodynamics and their effects on ICP," *Brain and Spine*, vol. 4, January 2024, Art. no. 102772, doi: 10.1016/j.bas.2024.102772.

7.1 Introduction

As discussed in the previous chapter, simulations of cerebral blood flow (CBF) and cerebrospinal fluid (CSF) circulation are made immensely more difficult by the fact that these systems are embedded in the brain, which in turn is confined in the rigid dura and skull structures. This implies that any changes in cerebral blood volume (CBV) would interact with all the compartments of the intracranial space and alter the intracranial pressure (ICP). While current modelling studies are able to simulate the variations of cerebrovascular resistance (CVR) and their transient effects on ICP, pressure changes due to sustained vascular constriction and dilation were modelled much less successfully. In order to capture the effects

of such changes accurately, a robust mechanism allowing the long-term interaction between the arterial and intracranial compartments is required.

In an attempt to represent the intracranial pressure-volume relationships of patients with cerebral oedema, Doron *et al* [148] incorporated into their electrical model volume changes of brain tissue (**Figure 7.1**). In addition to elements representing the subarachnoid space, ventricles and cerebral vasculature, a new compartment was added into the model, depicting the bulk flow of cerebral interstitial fluid (ISF). This compartment was characterised by a resistive element to represent the resistance of ISF circulation through the brain parenchyma into the subarachnoid space. This novel design was based on the theory that cellular swelling reduces the volume of cerebral extracellular space, hence narrowing the channels through which cerebral ISF can flow [149], [150]. With a set of differential equations relating the pressure to volume at each compartment, the model allowed the changes in brain volume to interact with ICP dynamics. Simulations with this approach successfully mimicked various physiological features, in particular the elevated ICP and reduced ventricular volume observed in patients with cerebral oedema and disruption of the blood-brain barrier.

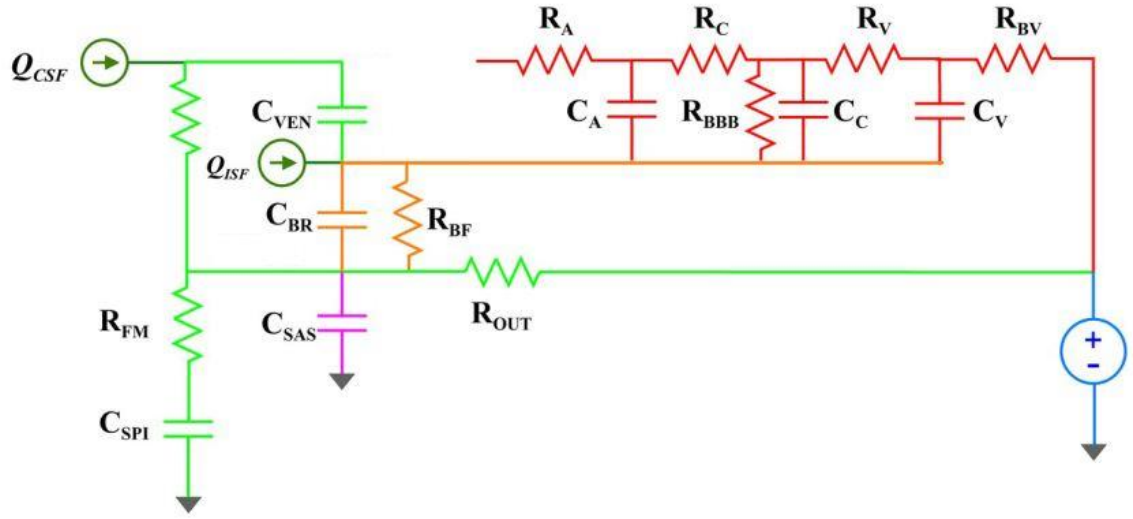

Figure 7.1. [148] Electrical analogue of the four-compartment intracranial space model proposed by Doron *et al*, incorporating compartments representing cerebral vascular circulation (red), ventricles (green), subarachnoid space (purple), and brain tissue (orange). In the vascular compartment, the arterial-arteriolar, capillary and venous compliances are described by capacitors C_A C_C and C_V; R_A, R_C, R_V, R_{BV} and R_{BBB} represent the resistance of flow through the arterioles, capillaries, veins, bridging veins, and the blood-brain barrier. The compliances of the ventricles, subarachnoid space and brain tissue are characterised by capacitors C_{VEN}, C_{SAS} and C_{BR}. CSF flows (with rate Q_{CSF}) through the ventricles with resistance R_{VEN}; it then flows from the intracranial subarachnoid space to the spinal subarachnoid space (C_{SPI}) with resistance R_{FM}, or is absorbed into the superior sagittal sinus (blue) with outflow resistance R_{OUT}. ISF flows (with rate Q_{ISF}) through the brain parenchyma into the subarachnoid space with resistance R_{BF}.

Doron's work provided a modelling mechanism for sustained interactions among the resistances of fluid flow, compartmental volumes and ICP, via the ISF circulation compartment. This is especially important when investigating phenomena involving the interplay between CBV and ICP. A notable example is cerebral autoregulation, a homeostatic mechanism of the

vascular system to stabilise CBF, in spite of variations in cerebral perfusion pressure. Resistive cerebral arterioles react to changes in perfusion pressure or vasoactive stimuli such as carbon dioxide [28], [151] by actively controlling the myogenic tone of the vessel walls, in order to dilate or constrict. This alters the CVR of the vessels and hence the CBV. Intracranial pathologies such as traumatic brain injuries often cause reduction in intracranial compliance, rendering the intracranial compartment susceptible to CBV increase, and resulting in ICP surges, falls in cerebral perfusion pressure (CPP) and consequently in secondary brain insults [152]. It is therefore crucial for models of intracranial hydrodynamics to capture the effects of cerebral haemodynamics on ICP. This study built on a classical model of CBF and CSF circulation, and incorporated a compartment depicting the flow of cerebral ISF. With the modified model, this study attempted to replicate various pathophysiological features observed in clinical data, hence proving its robustness when exploring the influences of model parameters on the performance of cerebrospinal dynamics indices.

7.2 Methods

7.2.1 Modifications to the Model

To provide a mechanism for pressure interactions between the cerebrovascular and intracranial compartments, a representation of ISF circulation was added to the model. In the electrical analogue, it was depicted as a pathway with a resistive, non-linear component (**Figure 7.2**).

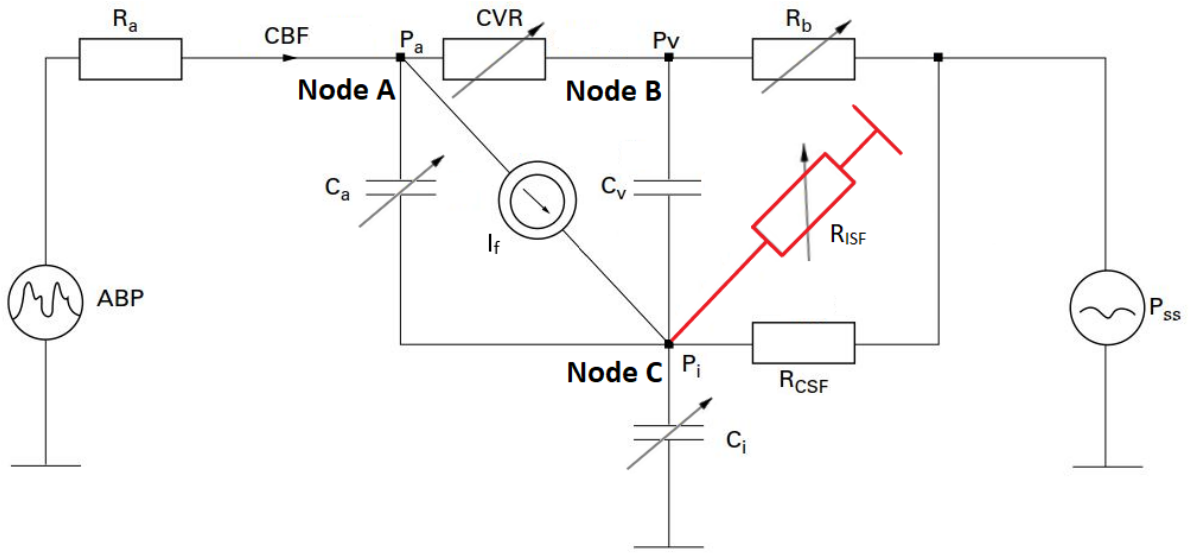

Figure 7.2. The modified hydrodynamic model with ISF compartment (in red), represented by a resistive component (R_{ISF}).

It is postulated that vasodilation (represented as reduction in CVR and increased volume in the arterial bed) reduces the volume of ISF space (depicted as increased R_{ISF}). As there is currently a lack of experimental data quantifying this interaction, R_{ISF} is simply modelled as being reciprocally related to the CVR as the first approximation (further discussed in **section 7.4**).

$$R_{ISF} = \frac{R_{ISFspan}}{CVR} + R_{ISFoffset} \qquad \textbf{(Equation 7.1)}$$

where $R_{ISFspan}$ and $R_{ISFoffset}$ are constants.

With the incorporation of the ISF compartment, the state equation at node C of the new model was modified:

$$\frac{dP_i}{dt} = \frac{1}{C_i}\left(\frac{ABP - P_a}{R_a} - \frac{P_v - P_{ss}}{R_b} - \frac{P_i - P_{ss}}{R_{CSF}} - \frac{P_i}{R_{ISF}}\right) \qquad \textbf{(Equation 7.2)}$$

The state equations at nodes A and B remain the same as in the original model:

At node A,

$$\frac{dP_a}{dt} = \frac{dP_i}{dt} + \frac{1}{C_a}\left(\frac{ABP - P_a}{R_a} - \frac{P_a - P_v}{CVR} - I_f\right) \qquad \textbf{(Equation 7.3)}$$

And at node B,

$$\frac{dP_v}{dt} = \frac{dP_i}{dt} + \frac{1}{C_v}\left(\frac{P_a - P_v}{CVR} - \frac{P_v - P_{ss}}{R_b}\right) \qquad \textbf{(Equation 7.4)}$$

With these modifications, the performance of the new model was tested with a series of experiments (described in the next section); its results were compared to that of the original model. A programme designed to be run on Windows 10 was written in Object Pascal (Embarcadero Delphi 10.2) using the RAD studio (see **Chapter 5**). After importing ABP data (details in **section 7.3**) from a csv file, the programme used the state equations described above to evaluate and plot P_a, P_v, P_i, CBF, and CVR against time.

7.2.2 Experiments

To examine the simulated responses of CBF and ICP to blood pressure, the ABP input was first set to increase at a constant rate. Within the range of cerebral autoregulation, rising ABP leads to active vasoconstriction. According to the pressure-volume relationship, the resulting

decrease in CBV is transmitted to the intracranial space as reduced ICP, which should be reflected in model simulations.

The experiments described in the previous chapter were repeated with the modified model. Briefly, these included:

1. Transient hyperaemic response test (THRT) – with intact cerebral autoregulation, compression of the common carotid artery lowers the CBF due to active vasodilation. Subsequent release of the compression results in a sudden rise in CBF, followed by compensatory vasoconstriction and the restoration of CBF to its baseline level.
2. CSF infusion test – the addition of artificial CSF increases the volume of the intracranial space. With the depletion of the compensatory reserve, ICP rises until it stabilises at a plateau level (determined by a balance of extra fluid infusion and increased pressure-gradient driven CSF outflow).
3. ICP plateau waves – a sudden drop in ABP can trigger a vasodilatory cascade, where the increase in CBV due to active vascular expansion is transmitted to the intracranial space as elevated ICP; this lowers CPP and causes further vasodilation. The rise in ICP may persist even after ABP is restored after its transient reduction, and is only arrested as the vessels are fully dilated.

7.3 Results

7.3.1 Relationships of CVR, CBF, and ICP with CPP

In the first set of experiments, ABP was set to increase at a constant rate. The corresponding CBF, CVR and ICP simulated by the new model were compared to the original model. The results were plotted against CPP in **Figure 7.3** (a), (b) and (c).

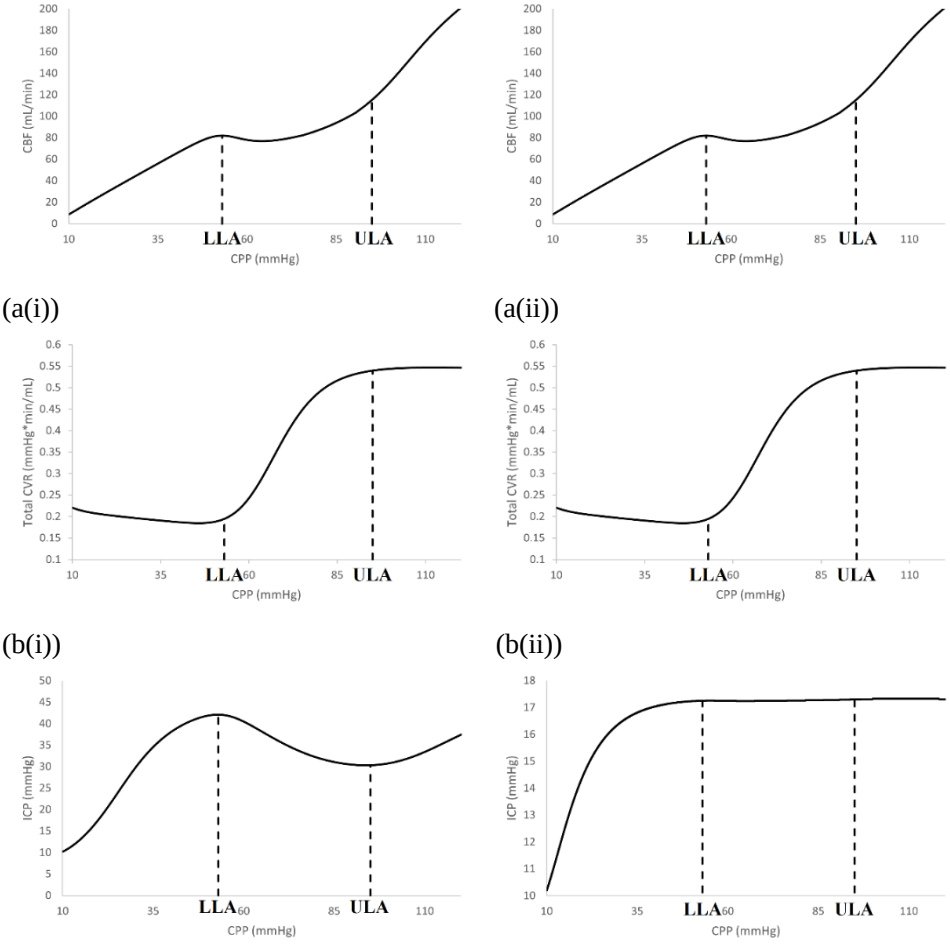

Figure 7.3. Simulations of CBF (a), CVR (b), and ICP (c) with the new (i) and original (ii) models, plotted against CPP, in response to increasing ABP. The lower (LLA) and upper (ULA) limits of autoregulation were marked.

The original and new models produced nearly identical graphs for CBF and CVR. However, the behaviours of ICP were significantly different. As CPP increased, both models showed initial rises in ICP. But the ICP of the original model levelled off at CPP = 80 mmHg, and did not react to further increase in CPP. In contrast, ICP of the new model began to drop in response to rising CPP, before increasing again at CPP = 160 mmHg. This suggests that unlike the old model, the modified model was able to reflect the transmission of CBV changes due to autoregulatory responses as changes in ICP.

7.3.2 Simulations of Physiological Tests and Events

7.3.2.1 Transient Hyperaemic Response Test

The compression of the common carotid artery was represented by a step drop in ABP, before being restored to its original level (**Figure 7.4** (a)). The responses of CBF and CVR are shown in **Figure 7.4** (b) and (c) respectively.

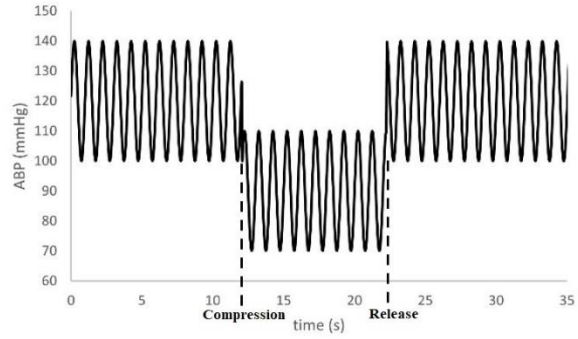

(a)

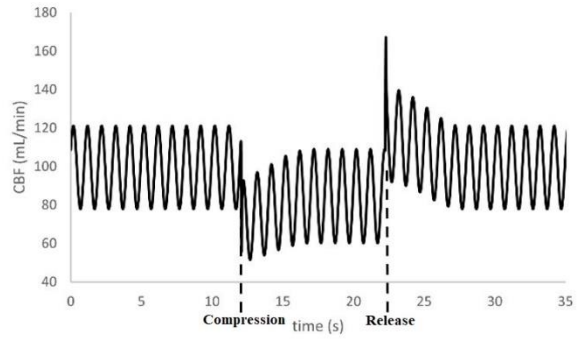

(b(i))

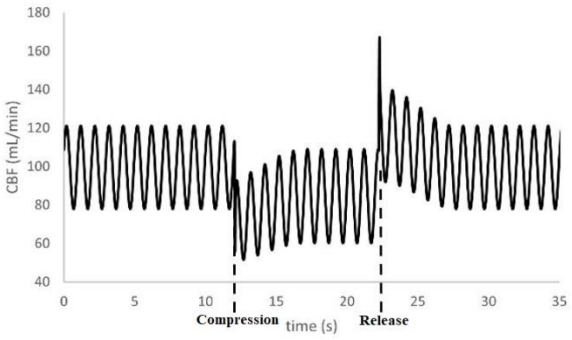

(b(ii))

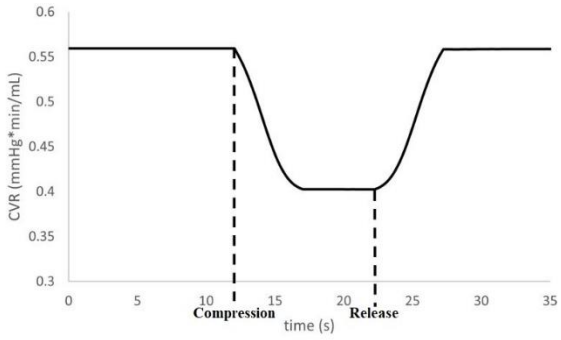

(c(i))

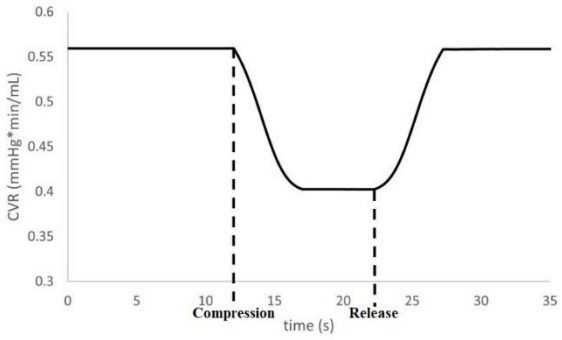

(c(ii))

Figure 7.4. Simulations of THRT with step changes in ABP between the onset and release of artery compression (a), and the responses of CBF (b) and CVR (c) with the new (i) and original (ii) models.

CBF generated by the new model reacted to the step changes in ABP identically as the original model: it was suppressed during the compression, before overshooting and returning to the baseline level as the compression was released. The plots of CVR indicated that both models were successful in simulating active dilation (reduced CVR) of the vessels in response to compression, and the compensatory vasoconstriction (CVR restored to its original level) following the release of compression.

7.3.2.2 Infusion Test

For the simulations of an infusion stage between t_{start} and t_{stop}, a constant term I_{inf} was added to the rate of CSF formation (I_f) to represent the rate of infusion into the CSF space. The ICP responses were plotted in **Figure 7.5** (a), while **Figure 7.5** (b) illustrated the intracranial pressure-volume relationships of the models, evaluated with the ICM+ software.

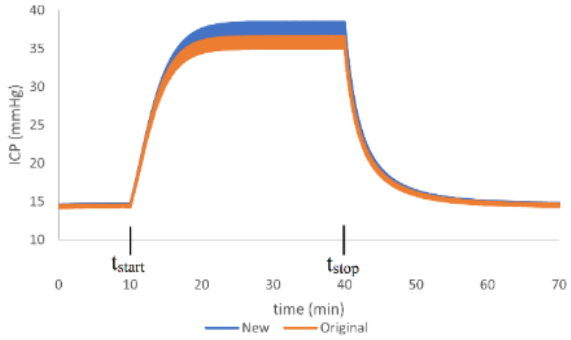

(a)

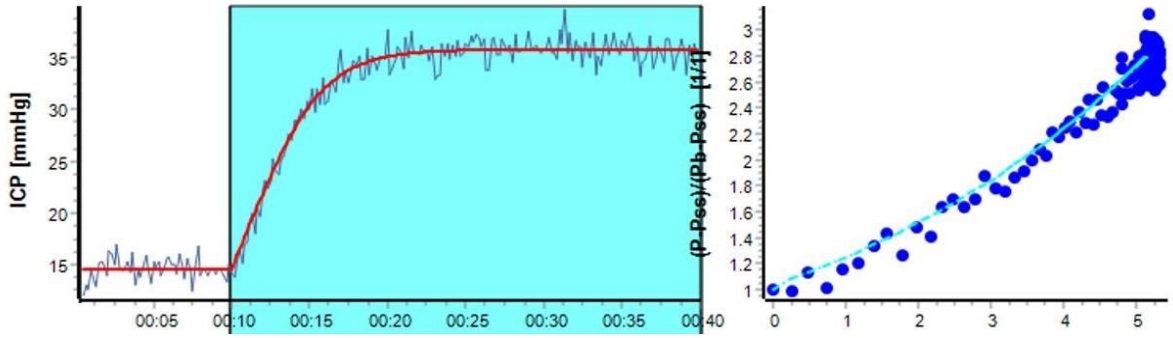

(b(i))

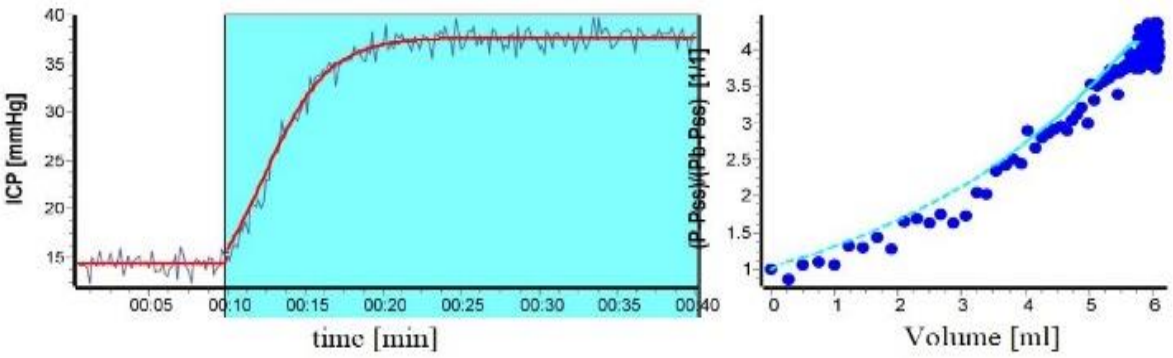

(b(ii))

Figure 7.5. (a) Simulations of the infusion tests (between t_{start} and t_{stop}) with the models; (b) analysis with the ICM+ software, illustrating the pressure-volume relationships represented by the (i) original and (ii) new models; the R_{CSF} were evaluated to be 13.86 and 14.72 mmHg/mL/min respectively. For illustrative purposes in the curve-fitting process, white noises were added to the generated ICP.

Simulations with both models produced the ICP behaviour commonly seen in real clinical recordings, rising to a plateau during the infusion stage and falling back to the baseline level when the infusion was terminated. However, it is worth noting that the ICP generated by the new model rose to a higher level before levelling off; this resulted in a slightly higher value of R_{CSF} produced by the new model. The significance of this is further discussed in **section 7.4**.

7.3.2.3 Plateau Wave

ICP plateau waves were simulated by creating step changes in ABP (**Figure 7.6** (a)). It was reduced by 10 mmHg initially (stage A), before being raised back to its baseline value (stage B). It was then further increased by 10 mmHg (stage C), and again restored to the baseline level (stage D).

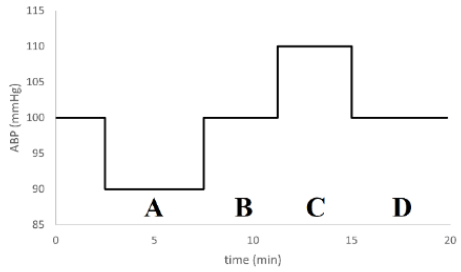

(a)

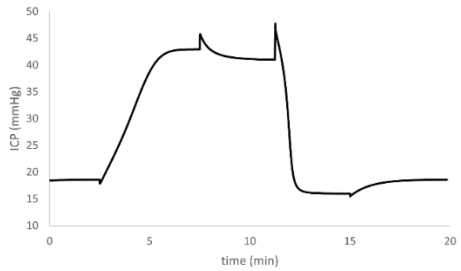

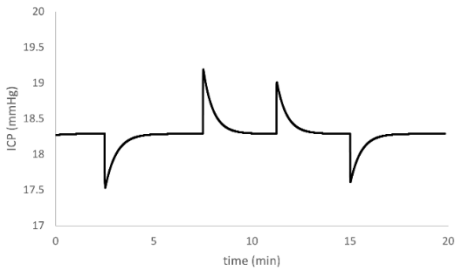

(b(i)) (b(ii))

Figure 7.6. Step changes in ABP (a) and simulated ICP responses for new (b(i)) and original (b(ii)) models.

The models produced very different results. In the new model, a drop in ABP triggered a rise in ICP from its baseline value (18 mmHg) to a plateau level of 43 mmHg within 5 minutes. Raising the ABP back to its initial value caused the ICP to increase momentarily, before stabilising at a slightly lower level (41 mmHg). Further increase in ABP resulted in a rapid drop of ICP until it flattened slightly below the baseline value (16 mmHg). A final restoration of ABP to its initial level brought the ICP back to its baseline. On the other hand, ICP simulated by the original model displayed momentary perturbations in response to each step change in ABP. However, it always returned to its baseline level of 18 mmHg; it was not able to simulate the onset of a plateau wave.

7.4 Discussion

The simulations above highlighted the importance of including the ISF compartment, which provides mechanism explaining sustained haemodynamic influences on ICP. Consideration of such interactions enables accurate simulations of the cerebrovascular effects on ICP (the measure of success was discussed in **sections 6.2** and **7.2.2**). Recent studies have established the physiological bases of cerebral ISF circulation [153], [154] and examined its impairment in intracranial pathologies [155], [156]. These findings inspired the mathematical representation of intracellular swelling as the rise in ISF flow resistance, and the reduction in extracellular space volume [149], [150]. With the incorporation of this mechanism, the

modelling work by Doron *et al* [148] accurately reproduced the elevated ICP due to brain swelling. This study postulated that the dilation of resistive cerebral arterioles can cause the narrowing of the ISF circulation channels, in a similar manner as in cerebral oedema. With the addition of this static pathway, simulated vascular constrictions and dilations can cause persistent changes in ICP. As there is currently a lack of quantitative evidence supporting this hypothesis, CVR and R_{ISF} were assumed to follow a reciprocal relationship in our model; this serves as a simplification to the intracranial pressure-volume interaction in reality. Due to the current incomplete understanding of the dynamics of the ISF pathway, it was assumed in the first approximation that the ISF sink pressure is constant. From the perspective of modelling, given we are at this point not interested in estimating the ISF flow itself, it makes no difference if the pressure in this topology is set as zero or other constant values.

Our modified model has proved to be successful in simulations of responses to various physiological simulations. Notably, with increasing ABP (**Figure 7.3**), the ICP responses produced by the models were markedly different, with the new model accurately reflecting the reduction in ICP with increasing CPP within the range of autoregulation. This is because its inclusion of the ISF compartment allowed the effects of changing CBV in the arterial compartment to be transmitted to the ICP in the intracranial compartment, which the original model failed to represent. When generating plateau waves (**Figure 7.6**), this transmission is

responsible for completing the cycle of vasodilatory cascade, resulting in the rapid rise in ICP as observed in clinical data.

Although it is feasible for the original model to achieve dynamic changes in ICP due to the capacitive elements (C_a, C_v and C_i), the steady-state value of ICP is purely dictated by I_f, R_{CSF} and P_{ss}, which are modelled as constants. A conceptual analysis of the steady state of the circuit elements (**Figure 6.12**) has shown that it is incapable of producing sustained changes in ICP. Moreover, the fact that the original model was unable to produce any plateau waves despite numerous experiments, while it was relatively easy to do so with the new model, provides a robust argument for the necessity of the modification.

A thorough understanding of the interactions between the haemodynamics and ICP is also important to the interpretation of clinical data related to disturbed CSF circulation. A notable example is the treatment of patients with hydrocephalus; their symptoms can be alleviated with the surgical insertion of a shunt, which drains CSF from the brain to the abdominal cavity. A good prognostication of improvement after shunting requires the accurate estimation of key parameters describing the CSF dynamics, one of which is the resistance of CSF outflow (R_{CSF}). This can be achieved through the simulation of an infusion test. The evaluation of R_{CSF} is

conventionally based on a model of CSF circulation [157]; it is calculated with the following formula:

$$R_{CSF} = \frac{P_{plateau} - P_{baseline}}{I_{inf}} \qquad \textbf{(Equation 7.5)}$$

Where $P_{baseline}$ and $P_{plateau}$ are the ICP at baseline and plateau levels respectively at the infusion test, and I_{inf} is the rate of infusion.

Simulations with the new model in this study (**Figure 7.5**) showed that the rise in ICP resulted in vasodilation, which in turn raised the ICP to a higher level than the original model. This suggests that apart from R_{CSF}, the autoregulation capacity can be another factor determining the ICP dynamics in an infusion study. A mathematical model considering only the CSF compartment may neglect the influence of CBV (vasodilation) on ICP, and mistakenly attributing it to R_{CSF}. Theoretically this can result in the overestimation of R_{CSF}. Previous studies have shown that the positive predictive value of R_{CSF} has been clinically acceptable [157], with recommended the R_{CSF} threshold for shunting to be between 13 and 18 mmHg/mL/min [136], [137]. The extra increase in ICP is likely to be small in patients diagnosed for normal pressure hydrocephalus, and thus a small overestimation of R_{CSF} may be on limited clinical significance. Nevertheless, this effect is worth exploring further with concurrent measurements of the strength of cerebral autoregulation during infusion tests.

Admittedly, the fact that the model successfully replicated the clinical phenomena above does not necessarily mean that the model is entirely accurate. Nonetheless, this work has acted as the first of several stages in building and validating a physiological model: ensuring that it can simulate qualitatively situations observed in specific pathophysiological cases, as in the events studied in this project for example. The next step will be to attempt the inverse model problem: identifying model parameters from measurements acquired from bedside monitoring. And even if this is achieved, the level of generalisation will depend on the number of factors considered. Nevertheless, physiological models are far better in generalising than purely data driven models (at least at the moment), since the latter are mainly data interpolators, and their performance for extrapolating is highly dependent on the volume and variety of training data. Thus, physiological models that can reflect behaviours in measured data are already useful in aiding intuitive interpretations of the relationships within the data.

7.5 Conclusions

This study investigated the relationships between cerebral blood volume and ICP with an intracranial hydrodynamic model, which was modified to include a compartment representing the circulation of cerebral ISF and coupled with the cerebrovascular compartment. The modified model was successful in depicting features of intracranial physiology involving the prolonged interplay between CBV and ICP.

Chapter 8

Comparison of the Performance of Autoregulation Indices

8.1 Introduction

As discussed in **Chapter 1**, cerebral autoregulation (CA) is an important mechanism of the brain to stabilise its blood flow in spite of fluctuations in cerebral perfusion pressure (CPP). Retrospective analyses have shown strong association between the state of CA and clinical outcome of patients with traumatic brain injury (TBI) [71]–[76]. This has led to substantial investigations of the feasibility of guiding individualised therapies using information on the patient's autoregulation capacity. Notably, Steiner *et al* [158][82] designed an algorithm allowing identification of CPP levels corresponding to the most intact CA (termed optimal CPP or CPPopt). A subsequent study on the continuous assessment of CPPopt by Aries *et al* enabled its bedside application for TBI patients [83]. Recently, a randomised controlled trial (CPPopt Guided Therapy: Assessment of Target Effectiveness, COGiTATE) has established the safety and practicability of CA-guided CPP management [84]. However, this phase II clinical trial was not designed or powered to study the potential effects of the therapeutic approach on outcome. While this ultimate goal encourages a phase III clinical trial, several considerations (described below) need to be first addressed [159]–[161].

Currently, the adoption of autoregulation-directed management as part of the routine clinical practice is hampered by the incomplete understanding of the mechanisms of CA and methods for its continuous assessment. This is in part due to the lack of concrete clinical data relating the restoration of CA to clinical benefits [85]. Moreover, with the absence of a gold standard measure of CA to validate against, consensus cannot be reached on the accuracy and reliability of any CA assessment methods [162]–[164]. The principles of such methods are introduced in the following section.

8.1.1 Methods of CA Measurement

In order to examine the strength of CA, the response of cerebral blood flow (CBF), and hence the cerebral arterial vasculature, to changes in ABP needs to be measured. Ideally, CA should be assessed by observing / rating CBF responses to a known challenge-provoked variations in ABP; examples include the sudden release of leg cuffs, transient compression of the carotid arteries, and pharmacological interventions [131], [165]. The accuracy of CA assessments through these stimuli are well-established, as the causality between the induced ABP variations and the responses in CBF is certain. Through a Delphi-method based consensus approach, the Seattle International Brain Injury Consensus Conference (SIBICC) has recommended the inclusion of the so-called mean ABP (MAP) Challenge as part of the proposed three-tier protocol of TBI management [68], [166]. However, manipulations in blood pressure may be

detrimental to patients under intensive care, and cannot be performed too frequently. A continuous measure of CA with sufficient accuracy would be much preferred.

For the purpose of continuous CA assessment, the response of CBF to spontaneous changes in ABP can be monitored instead [167]–[169]. The introduction of transcranial Doppler (TCD) ultrasonography has allowed the assessment of dynamic autoregulation; it measures the velocity of cerebral blood flow (CBFV) through the middle cerebral artery (MCA) in response to rapid changes in ABP. Despite its high time resolution, long-term monitoring with it is currently impractical [162]. This is because the process of measurement involves locating the middle cerebral artery, securing the TCD probe at a fixed position (the signal quality is very sensitive to changes in probe position), and the application (and maintenance) of sufficient quantity of ultrasound gel to ensure good propagation of ultrasound waves. These factors make it challenging to acquire continuous measurements with high quality, although recordings of up to several hours are now possible with application of the robotic probes [170]. If a longer monitoring period is required, it may be preferable to use surrogate measures that reflect changes in CBF, such as blood oxygen saturation which can be measured with near-infrared spectroscopy (NIRS) [171], [172]. Alternatively, intracranial pressure (ICP) is also a good indicator for the dynamics of the cerebral vasculature, since the changes in cerebral blood

volume (CBV) due to constrictions and dilations of the resistive vessels alter the pressure within the rigid skull.

Various indices have been proposed for CA assessment through continuous monitoring of the above signals in response to spontaneous ABP fluctuations [79], [169], [173]–[175]. They have also shown strong statistical association with the outcome of patients with head injuries, independent of other measures of injury severity [47], [82], [176]–[178]. This chapter studies the time-correlation methods and the autoregulation index, which are among the most widely used approaches to grading the state of CA.

8.1.1.1 Time Correlation Methods

The time-correlation indices evaluate CA through a moving correlation between the slow changes (0.008 – 0.05 Hz) of the input pressure and the output surrogate flow measures [79]. For example, the mean flow index (Mx) is calculated through the correlation between the fluctuations of mean CPP and mean CBFV; positive Mx indicates impaired CA, while Mx close to 0 or negative implies good autoregulation (this concept is illustrated in **Figure 8.1** [169]). Mxa, a similar index using mean ABP instead of mean CPP, was proposed as an alternative to evaluate CA without invasive ICP measurements.

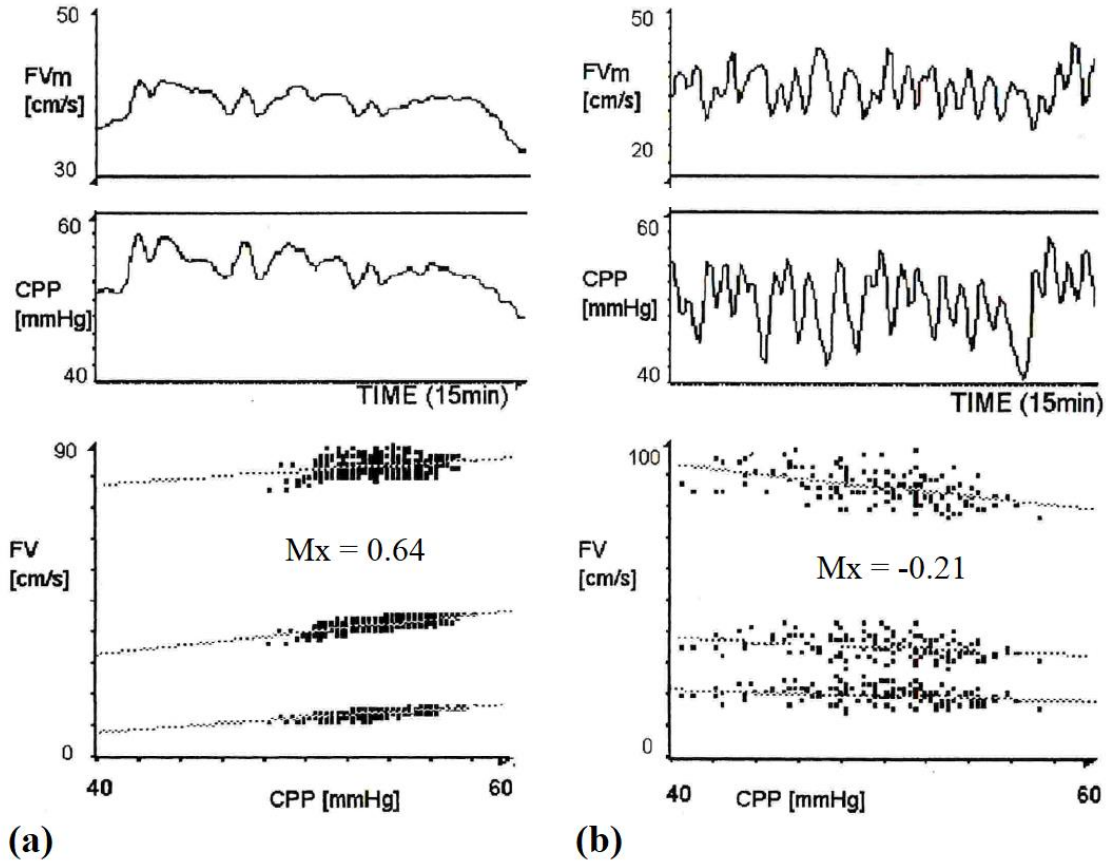

Figure 8.1. [169] Time series of mean CBFV and mean CPP, and scatterplots showing the correlation between them (Mx). A positive value of Mx (a) implies impaired CA, while a negative value (b) indicates intact CA.

On the other hand, the pressure reactivity index (PRx) reflects the association of variation in mean ABP and mean ICP based on the interaction between the cerebral vasculature and the intracranial compartment. This transmission of pressure changes is characterised by the pressure-volume relationship (see the pressure-volume curve in **Figure 6.3**), where an increase in CBV produces a rise in ICP. A higher value of intracranial elasticity (E) corresponds to reduced intracranial compliance (C_i). This creates a steeper pressure-volume curve, meaning

that a change in CBV can cause substantial variations in ICP. With intact CA, the decreasing CBV due to active vasoconstriction in response to rising ABP lowers the ICP, resulting in a negative correlation between them. On the contrary, a positive PRx implies passive vascular response and impaired CA. The concept of PRx is illustrated in **Figure 8.2** [79]:

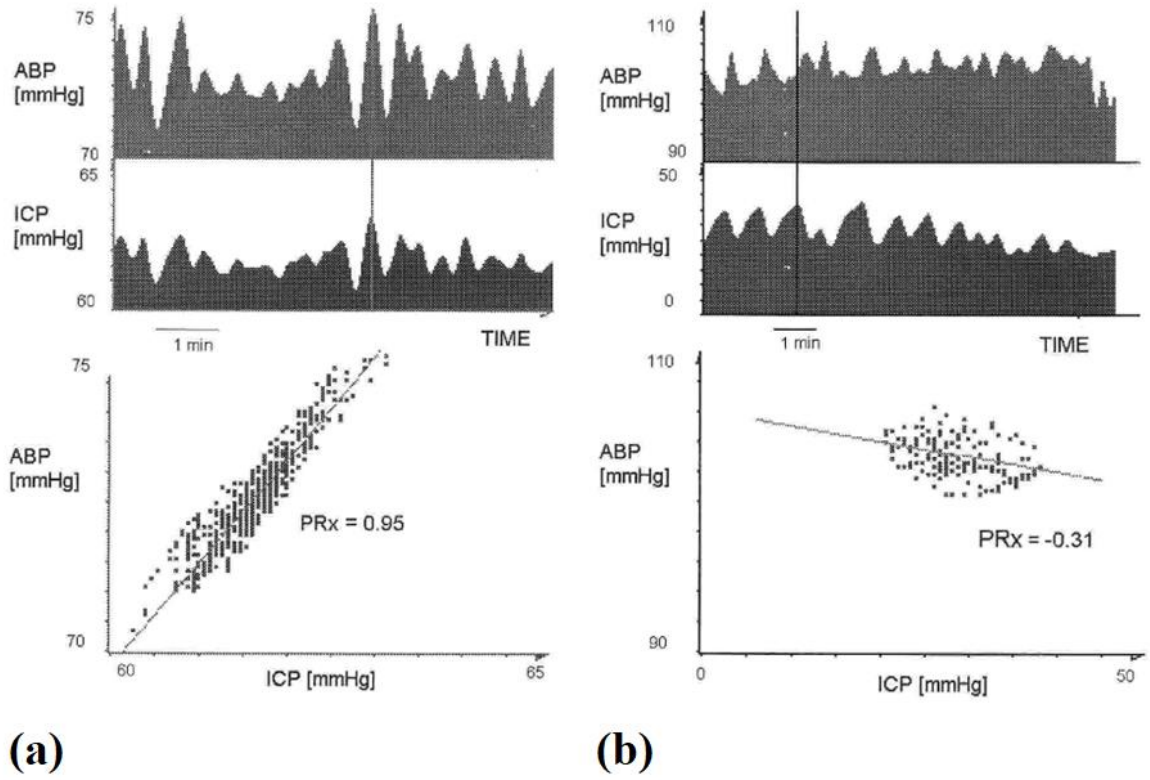

Figure 8.2. [79] Time series of mean ABP and mean ICP, and scatterplots showing the correlation between them (PRx). A positive value of PRx (a) implies impaired CA, while a negative value (b) indicates intact CA.

8.1.1.2 Transfer Function Analysis and Autoregulation Index (ARI)

Another popular method of CA assessment is the transfer function analysis (TFA). This technique decomposes input and output signals as the sum of simple sinusoidal waves with different frequencies, and uses the parameters gain, phase, and coherence to quantify CA. As CA acts to attenuate the pressure-to-flow transmission below a certain frequency, it can be modelled mathematically as a high-pass filter. The phase parameter of TFA is regarded as the most relevant indicator of CA, with larger values indicating increased lag between pressure and flow waves, and hence improved CA [179]. However, analyses of phase produce phase values in a range of frequencies, making it challenging for the results to be directly interpreted as a standardised 'strength of CA'.

On the other hand, a related methodology known as the autoregulation index (ARI) takes advantage of TFA, but is able to provide a standardised evaluation of CA. Developed by Tiecks *et al*, this index was initially used to grade the CBFV response to the sudden deflation of thigh cuffs with a parametric model [173]. The grading system classifies the strength of autoregulation into 10 levels, with 0 describing completely abolished CA and 9 the strongest autoregulatory response (**Figure 8.3** (a)). ARI can also be assessed through monitoring the spontaneous variations in ABP and CBFV, in which case the impulse response (IR) is estimated using TFA (**Figure 8.3** (b)) [180].

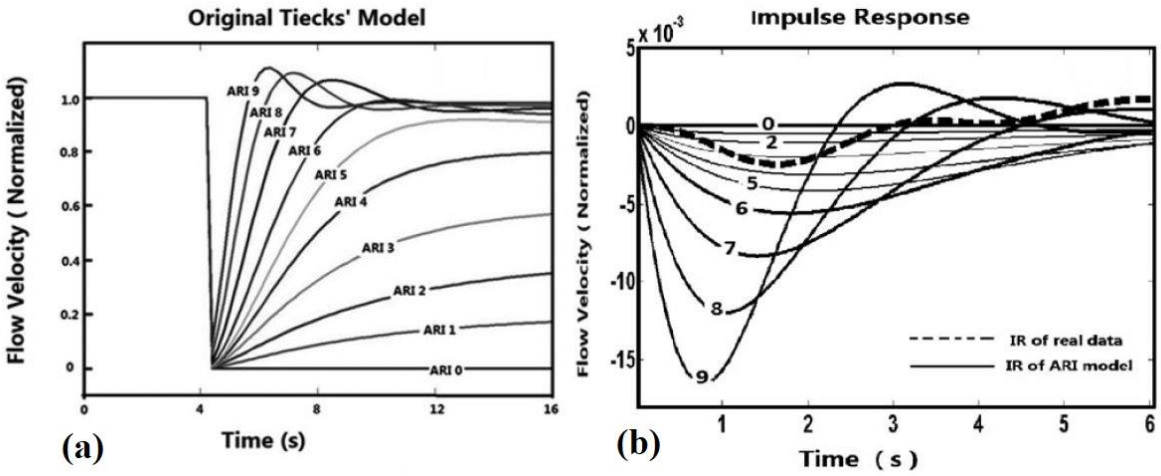

Figure 8.3. [180] Normalised CBFV in response to a step change in ABP (a) and impulse response (b).

The Tiecks' model uses a second-order linear differential equation (implemented as a difference equation in numerical calculations, see Equations 8.1 – 8.4 [180]) to simulate ten possible levels of flow velocities in response to a step change in ABP. Each level of the model is defined by a set of three parameters (**Table 8.1**): the time constant (τ), the damping factor (D), and the autoregulatory dynamic gain (K) [173]. In the original model (**Figure 8.3** (a)), P(n) is the normalised ABP change from its baseline value and V(n) is the CBFV response; for the IR method (**Figure 8.3** (b)) they are defined as the impulse ABP signal (with baseline signal = 0) and its impulse response respectively. The recorded CBFV response is compared to each of the ten levels of the model, with the best fit chosen as its index number.

$$P(n) = \begin{cases} 1 & n \neq 1 \\ 0 & n = 1 \end{cases} \quad \textbf{(Equation 8.1)}$$

$$x_1(n) = x_1(n-1) + \frac{P(n) - x_2(n-1)}{f \cdot \tau} \quad \textbf{(Equation 8.2)}$$

$$x_2(n) = x_2(n-1) + \frac{x_1(n) - 2D \cdot x_2(n-1)}{f \cdot \tau} \quad \textbf{(Equation 8.3)}$$

$$V(n) = P(n) - K \cdot x_2(n) \quad \textbf{(Equation 8.4)}$$

where

f is the sampling frequency of ABP,

c is a constant representing the initial value of ABP, and

x_1 and x_2 are intermediate state variables, initialised as zero during simulations.

Table 8.1. Parameters defining the autoregulation index (ARI)

ARI	τ, s	D	K
0	…	0.00	0
1	2.00	1.60	0.20
2	2.00	1.50	0.40
3	2.00	1.15	0.60
4	2.00	0.90	0.80
5	1.90	0.75	0.90
6	1.60	0.65	0.94
7	1.20	0.55	0.96
8	0.87	0.52	0.97
9	0.65	0.50	0.98

τ: time constant; D: damping factor; K: autoregulatory dynamic gain.

8.1.2 Potential Confounders of CA Indices

The indices described above have been generally used in various clinical scenarios requiring assessment of CA. However, their ability to reflect the true state of autoregulation may be hindered by a number of factors, one of which is the ICP. This is because CBF is regulated by the pressure gradient between upstream and downstream pressures, which is CPP and not ABP alone. Also, changes in ICP (due to ABP challenges or spontaneous variations) will directly alter CPP, thus modifying the state of CA. Although recommendations have been made to standardise the parameters and settings for the evaluation of CBFV-based indices [179], the patients targeted in such studies were expected to have low ICP and normal brain compliance. Therefore, the effects of ICP were approximated as negligible and not taken into account.

The performance of the autoregulation indices also depends on the compliance of the brain (C_i) and the arteries (C_a). This is because ABP waves propagate through the arterial walls and alter CBV (determined by C_a). These changes are then transmitted into the intracranial space, resulting in ICP fluctuations (governed by C_i) and (as described above) effects on CBFV. Hence, changes in either C_i or C_a would modulate the transmission of ABP waves into CBFV.

Previous studies have shown limited reproducibility and high variability of autoregulation indices [83], [181]–[184]. Part of this variability may be related to the influences of ICP and

cerebral compliances, which have not been assessed in detail. A theoretical, *in silico*, exploration of such influences may therefore help interpret the results of CA assessment and their apparent variabilities.

8.1.3 Aims and Objectives

This study compared the performance of the autoregulation indices Mx, Mxa, ARI and PRx in response to changing strength of CA, and investigated the role of ICP and intracranial compliance in CA assessments.

8.2 Methods

8.2.1 Generation of Simulated Signals

The computer programme described in **Chapter 7** was used to simulate the pressures and flow at different compartments of the hydrodynamic model. Artificially generated ABP (illustrated in **Figure 8.4**) was used as the input of the model:

$$ABP = offset + pulse\ wave + slow\ wave \qquad \textbf{(Equation 8.5)}$$

where

- *offset* is the mean ABP,

- *pulse wave* simulates the pulse waveform of ABP due to cardiac cycles (period of 1 second), consisting of a fundamental wave (amplitude of 16 mmHg) with a first harmonic (amplitude of 8 mmHg), and
- *slow wave* simulates the slow sinusoidal fluctuations of ABP, with amplitude of 5 mmHg and period of 1 minute.

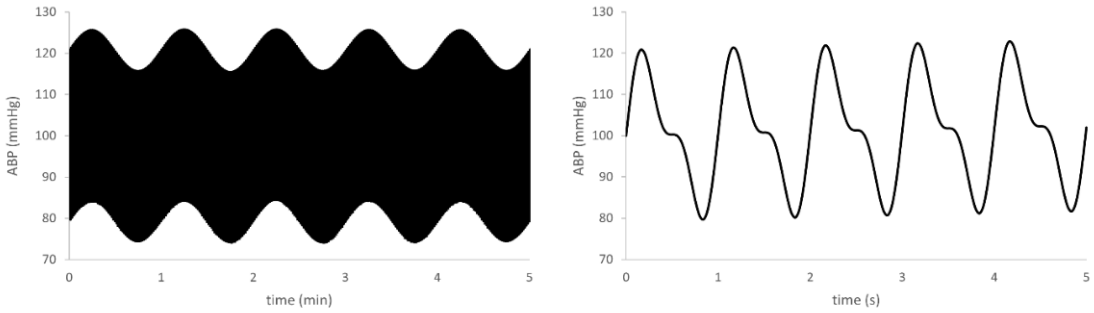

(a) (b)

Figure 8.4. Artificially generated ABP signal (a) and its pulse (b) used as input for model simulations.

The elasticity parameter (E) of the model was first set as 0.3, and the strength of CA was increased from 0 (fully impaired) to 1 (intact). The strength of CA is defined as

$$\frac{\%\ change\ in\ CVR}{\%\ change\ in\ CPP} = \frac{\left(\frac{CVR_{max} - CVR_{min}}{CVR_{min}}\right)}{\left(\frac{CPP_{upper} - CPP_{lower}}{CPP_{lower}}\right)} \qquad \textbf{(Equation 8.6)}$$

Sixty minutes of the generated ICP and flow through the middle cerebral artery (F_a) were recorded for each strength of CA. The experiments were then repeated with lower C_i (E = 0.6 and 0.9) to investigate its influence on autoregulation indices.

8.2.2 Evaluation of Autoregulation Indices

The recorded signals were processed and analysed with the ICM+ software (Cambridge Enterprise Ltd, Cambridge, UK, https://icmplus.neurosurg.cam.ac.uk). To simulate the extraneous physiologic variabilities of CBF and ICP slow waves (further explained in **section 8.4**), coloured noise was added to the calculated CBF (F_a) and ICP (Gaussian white noise filtered with a low pass Butterworth filter (cut-off frequency of 0.2 Hz)). The autoregulation indices ARI, Mx, Mxa, and PRx were evaluated (described below) using the following ICM+ configuration file and averaged over the entire recording at each strength of CA.

8.2.2.1 ARI

A plugin for ICM+ (a built-in function allowing off-line data analysis) was created to calculate ARI by fitting the impulse response (IR) of the generated signals to that of the Tiecks' model (illustrated in **Figure 8.3** (b)). The following steps were involved:

1. Generate CBFV with each level of CA

Ten recordings of CBFV (ARI from 0 to 9) were generated with the second-order linear differential equation (implemented in the programme as a difference equation) described in Equations 8.1 – 8.4.

2. Calculate the IR of CBFV with TFA

ABP and CBFV of each level of CA were normalised and transformed with the Fast Fourier transformation (FFT) algorithm; the auto- and cross-spectra were calculated with the Welch's method, using four segments of data (120 seconds in duration each) and 50% segment overlap. Inverse FFT was then applied to compute the IR in the time domain, with a cutoff frequency of 0.5 Hz. [185], [186]

3. Fitting the IR of the hydrodynamic model to that of the Tiecks' model

Step 2 was repeated for each of the F_a generated by the hydrodynamic model. The IR obtained was then fitted to each of the 10 IR models, and the best fit (chosen with minimum squared error) was selected as the ARI value of that data segment.

ARI was calculated with a 300-second moving window and updated every ten seconds.

8.2.2.2 Mx, Mxa and PRx

Ten-second moving average filter was applied to ABP, ICP, and F_a waveforms, and the resulting time series downsampled to 0.1Hz. Subsequently, the Pearson's correlation coefficient of CPP with F_a (Mx), ABP with F_a (Mxa), and ABP with ICP (PRx) were calculated

using 30 consecutive samples (5 min) moving window [79]. All the calculations were performed within the ICM+ calculation engine pipeline.

8.3 Results

An example of the time trends of the calculated indices is plotted in **Figure 8.5**.

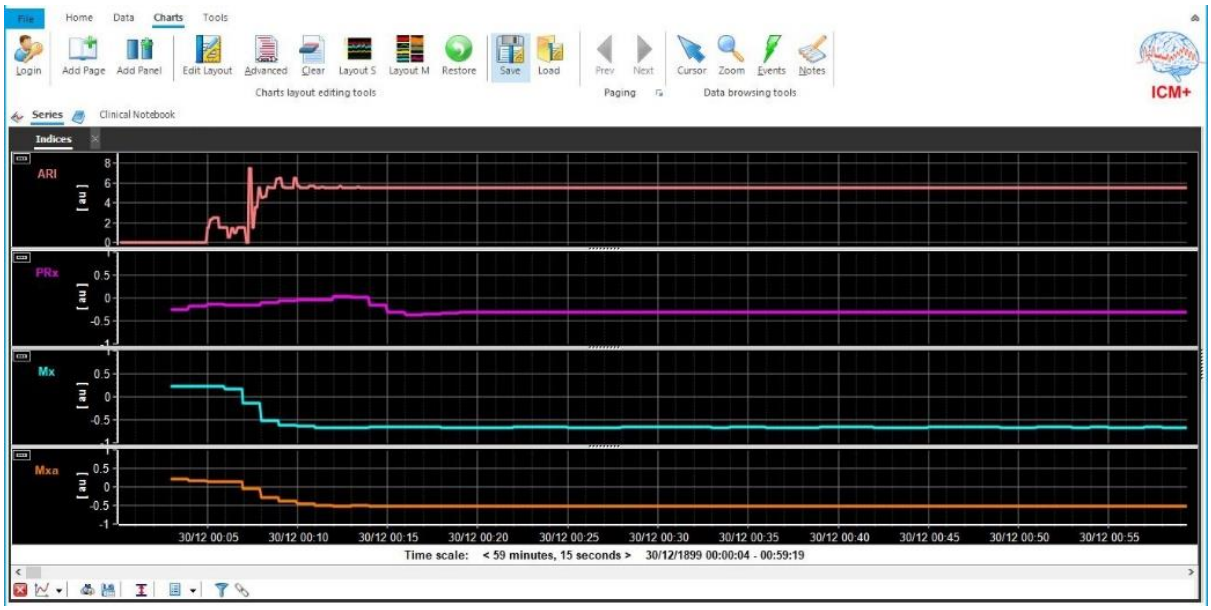

Figure 8.5. An example of the time trends of autoregulation indices (ARI, PRx, Mx, Mxa) calculated with ICM+. The variations at the initial portion of the charts are the result of the burn-in phase of numerical integration (also mentioned in **Chapter 5**).

The autoregulation indices Mx, Mxa, ARI, and PRx of simulations with different C_i (E = 0.3, 0.6, 0.9) and increasing strength of CA were compared in **Figure 8.6**.

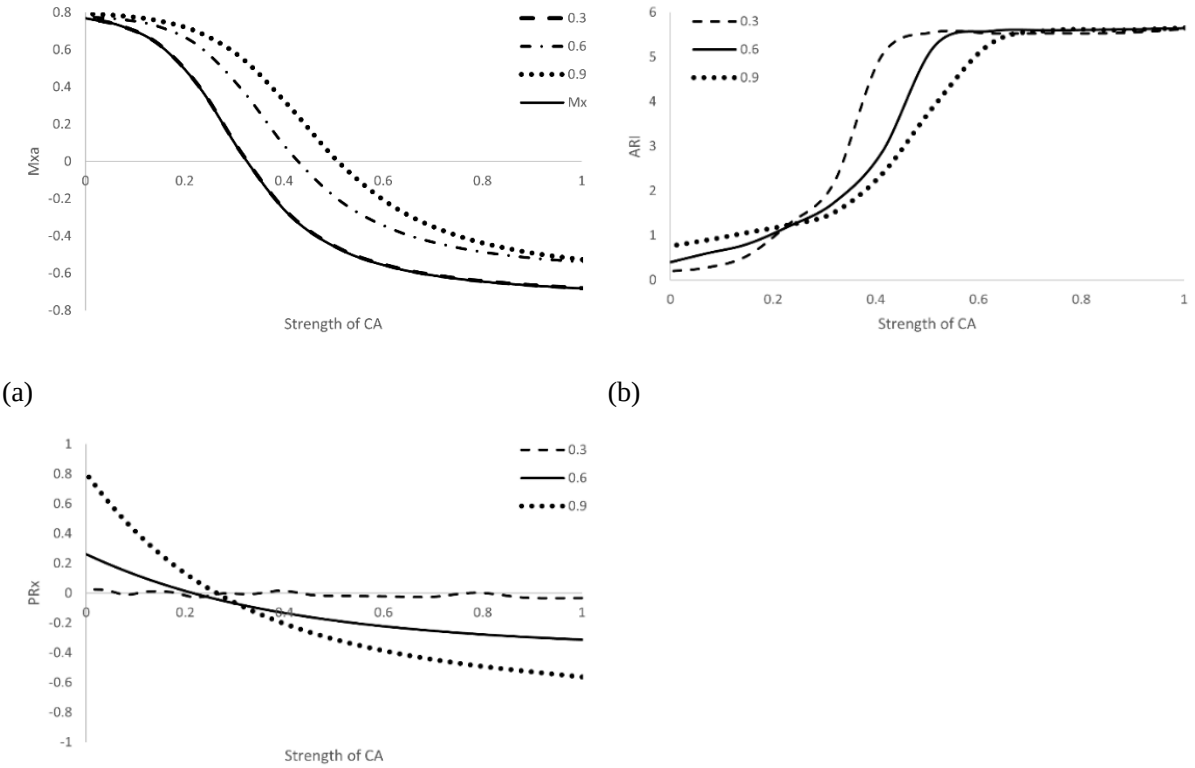

(a) (b)

(c)

Figure 8.6. Mx, Mxa (a), ARI (b) and PRx (c) of simulations with different C_i (E = 0.3, 0.6, 0.9).

Both Mx and Mxa (**Figure 8.6** (a)) decreased from about 0.8 and stabilised at a negative value in response to increasing strength of CA. Mxa was sensitive to E (which is inversely related to C_i): as the strength of CA approached 1, Mxa with high E became significantly higher (-0.53 for E = 0.9) than that with low E (-0.68 for E = 0.3). In contrast, Mx (solid black curve) was independent of E; it appeared identical to Mxa with low E. On the other hand, ARI (**Figure 8.6** (b)) was higher with higher E when autoregulation was impaired. With rising strength of CA the opposite was observed: ARI with lower E increased more rapidly. Eventually ARI of all simulations saturated at about 5.6. Finally, PRx (**Figure 8.6** (c)) at low E (0.3) remained close

to zero and was independent of the strength of CA; with higher E, PRx became more responsive to the strength of CA (decreasing from 0.26 to -0.30 for E = 0.6, and from 0.80 to -0.56 for E = 0.9).

8.4 Discussion

This study has demonstrated that ICP may be a significant confounder to the calculated indices of autoregulation, with consequences for the potential inaccuracies in the interpretation of the strength of CA using such indices. Specifically, changes in ICP due to ABP variations affect CPP (which determines the changes in CBF), and can therefore modulate the evaluated status of CA. The effects of ICP on CA assessment can be observed in clinical studies: for TBI patients with elevated ICP (in particular those with severe brain swelling), the calculated ARI was lower when ICP was used as an input instead of ABP [187].

These effects of ICP on CA indices became apparent through simulations with different intracranial compliances, using the modified model described in **Chapter 7**. With the addition of a compartment of interstitial fluid, it has provided a mechanism allowing the pressure-volume interaction between cerebral vasculature and intracranial compartment. This link is crucial to simulating the effects of ICP on the indices of autoregulation.

8.4.1 Simulated Noise

Artificial noises were added to the generated F_a and ICP to create more physiologically realistic simulations. In clinical recordings extraneous noises can be observed [151], [180], [188], with components in CPP and CBFV that appear unrelated to each other. Such noises could be attributed to the effects of cerebral metabolic processes and neural activities [28]. While previous work [180] have investigated the effects of adding artificial noise on the performance of ARI, this study highlights its importance on the evaluation of the correlation-based indices. Applying correlation analysis to the input and output signals of the model, the correlation coefficient can only reflect the angle of the relationship between them, but it will not be sensitive to the amplitude changes, and thus will not reflect its nature when applied to real measurement, exposed to extraneous influences. The addition of noise allows the indices to better reflect the level of autoregulatory response: as the extent of CBF attenuation due to CA becomes more pronounced, parts of the signal with lower amplitude are 'drown' by the noises, resulting in the gradually reducing time correlation indices.

8.4.2 Mx vs Mxa

The increasing differences between Mx and Mxa with low C_i and improving autoregulation (**Figure 8.6** (a)) can be explained by the effects of ICP. With intact CA, ICP moved in the opposite direction to changes in ABP. This caused CPP to fluctuate more strongly than ABP

(illustrated in **Figure 8.7** (a)), resulting in a more negative correlation with F_a (Mx < Mxa). When autoregulation was impaired (**Figure 8.7** (b)), ICP changes were more in-phase to ABP changes. However, variations in ICP were small compared to that of ABP, and were not sufficient to switch the direction of CPP changes. Therefore Mx and Mxa appeared the same as the strength of CA approached 0. With high C_i (**Figure 8.7** (c), (d)) the effects of ICP diminished, producing identical trends of Mx and Mxa.

The simulated results were in agreement with a clinical study involving TBI patients [176], where Mxa was found to be significantly larger than Mx. Mx also had a much stronger association with patients' outcome than Mxa; this can be explained by the attenuated response of Mxa to changing strength of CA with reduced C_i (as shown in **Figure 8.6** (a)). Due to the potential inaccuracies caused by elevated ICP, other studies [189]–[191] also recommended the use of CPP instead of ABP alone during CA assessments of patients with head injuries.

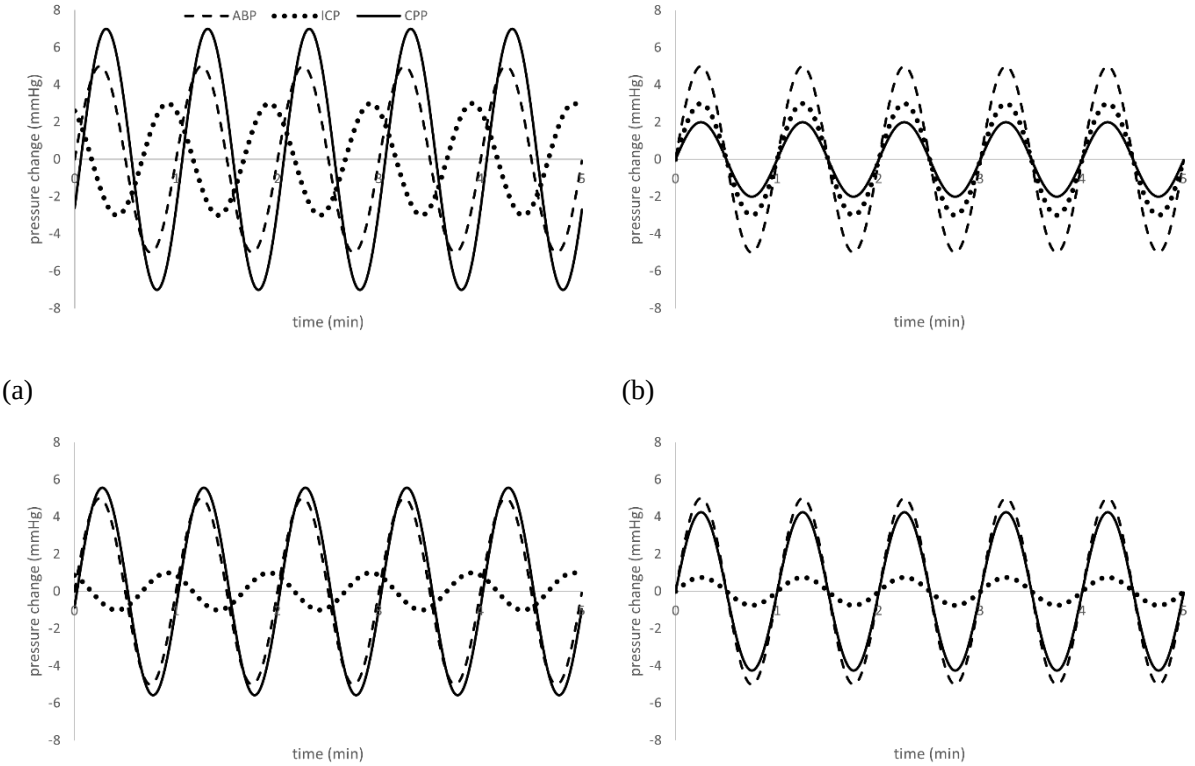

Figure 8.7. Changes of ICP and CPP in response to ABP fluctuations. ABP is out of phase with ICP if CA is intact ((a),(c)), and in-phase with impaired autoregulation ((b),(d)). With low C_i and intact CA (a), ICP varied in opposite direction to ABP, resulting in CPP with higher amplitude. This produced a more negative correlation between the noise-added F_a and CPP (Mx) compared to ABP (Mxa). With impaired autoregulation (b), the in-phase relationship between ABP and ICP resulted in CPP with diminished amplitude. In this case, ICP amplitude was insufficient to switch the direction of CPP changes; Mx and Mxa therefore appeared the same. However, with very low values C_i and high C_a, ICP amplitude may become large enough to cancel out ABP changes, resulting in a seemingly constant CPP. This effect is known as 'false autoregulation'. With high C_i (c), (d) the effects of ICP were diminished, creating identical trends of Mx and Mxa.

8.4.3 ARI

ARI followed a similar pattern as Mx and Mxa with intact CA. But with the strength of CA falling below 0.23, ARI with low C_i rose above that with high C_i. This can likely be attributed to the effect of so-called 'false autoregulation', where ICP responses cancel out (at least partially) changes in CPP due to ABP changes [192]. This reduces fluctuations in F_a, creating a false impression of effective CA. At present, ARI is mainly used in patients with strokes [193] where the effects of ICP are considered negligible. The potential effects of elevated ICP on ARI in TBI patients are yet to be investigated.

8.4.4 Flow vs Volume Indices

The volume index, PRx (**Figure 8.6** (c)) reflects the ABP → CBV → ICP interaction, which is not the same as the autoregulatory effects of ABP → CBF, represented in the model of F_a. The crucial difference is that it relies on good transmission of CBV changes to ICP, which is governed by C_i. Therefore, lower C_i increases the sensitivity of PRx to the strength of CA, and improves its accuracy when assessing autoregulation. In contrast, a flow index such as Mxa (**Figure 8.6** (a)) has shown a higher sensitivity to increasing strength of CA with higher C_i. This is because Mxa only takes CBF into account and neglects the role of ICP. As the effects of ICP became more apparent with reducing C_i, its accuracy of CA evaluation worsened. As a

result, with moderate strengths of autoregulation where Mx showed intact CA, Mxa with low C_i was elevated, indicating impaired CA.

While PRx is a well-validated metric for CA assessments, its accuracy depends on the assumption that the variations in CBV are effectively transmitted to ICP changes; this is only true if the intracranial compliance is low. In cases where C_i is increased artificially through surgical interventions such as decompressive craniectomy (DC), the responses of ICP to spontaneous changes in ABP may not be sufficient to distinguish itself from the extraneous physiological variability of ICP in the slow wave frequency region [151], [194]. Clinical studies have suggested that PRx either worsened [158], [195] or remained uninfluenced [196] after DC. The absence of definitive results is in part due to a lack of robust measure of intracranial compliance, causing C_i in some patients to appear more affected by DC than in others. The use of PRx in such patients is therefore still a matter of debate. Further analyses with multi-modal monitoring are required to validate and determine whether these results represent genuine alterations in cerebrovascular dynamics.

8.4.5 Limitations

The artificial noise added to the generated signals is a gross simplification of the real physiological variabilities of CBF and ICP. The coloured Gaussian noise was chosen mainly

as a demonstration of its importance when evaluating time correlation indices, but it may be an inaccurate representation of the variabilities observed in clinical data. Moreover, this study uses generated F_a to calculate Mx, Mxa and ARI, which is different from clinical studies where CBFV is measured. As it is not entirely certain if the cross-sectional area of middle cerebral artery can be assumed as a constant, simulations of F_a may not be able to accurately represent measured CBFV. Therefore, the possible expansions and contractions of the large cerebral arteries can potentially influence the performance of the flow indices.

8.5 Conclusions

The intracranial compliance is an important factor determining the accuracy of CA assessment. The simulations in this study suggested that PRx may not be able to evaluate autoregulation if C_i became too high. On the contrary, Mxa may also provide inaccurate results with low C_i. While the results of ARI largely resemble those of the time correlation flow indices, it may be prone to the effects of false autoregulation when CA is impaired.

Chapter 9

Assessment of the Performance of Pressure Reactivity Indices

9.1 Introduction

The core of intensive care management for patients with traumatic brain injury (TBI) includes stabilisation of intracranial pressure (ICP) and cerebral perfusion pressure (CPP) at an adequate level, in order to prevent secondary brain injuries due to hyperperfusion or ischaemia. Although the current clinical guidelines still recommended management of TBI patients according to universal perfusion pressures targets [66], [197], it is now understood that fixed thresholds may not lead to the best clinical outcome, due to the evolving severity of injuries and diverse demographics of patients [77], [166], [198], [199].

As discussed in the previous chapter, one plausible concept of individualising CPP targets is to use the information of cerebral autoregulation (CA). Multimodal monitoring in neurocritical care units has facilitated the continuous assessment of CA, as it provides surrogate measures of cerebral blood flow (CBF) / volume (CBV) suitable for use in the assessment of pressure reactivity of the cerebral vasculature, allowing indices of autoregulation to be derived. One of such surrogates is ICP, since the variations in CBV due to constrictions and dilations of the

resistive vessels are transmitted as pressure changes in the intracranial space, which is confined by the rigid cranium. The pressure reactivity index (PRx) proposed by Czosnyka *et al* correlates the slow changes in ABP with ICP [79]. With intact CA a slow drop in ABP increases the CBV due to active vasodilation, resulting in elevated ICP and hence a negative PRx. In contrast, the passive vascular response in cases with impaired CA produces a positive correlation between ABP and ICP. The application of PRx in bedside monitoring allows the individualised optimisation of CPP by maximising the autoregulatory capability of the patient, with the value corresponding to the lowest PRx (CPPopt) chosen as target. [82], [200]

The prognostic value of PRx has been well documented in clinical studies [201]. It is of particular value in cases of intracranial hypertension, which is a major problem in patients with TBI and often leads to fatal outcome. However, there is a problem. Essentially, clinicians have several actions at their disposal to counteract hypertension driven by brain swelling, one of which is decompressive craniectomy (DC) [202], [203]. Used as a last resort, this surgical procedure aims to reduce ICP by removing a large part of the skull and creating an opening of the underlying dura mater. The point is that without the confinement of these rigid structures, the compliance of the intracranial space is raised substantially, which may result in unreliable evaluations of PRx. This is because the performance of this index is based on the premise that

the effects of CBV changes can be transmitted readily into the intracranial space (which depends heavily on the intracranial compliance) in order to elicit a robust ICP response.

In an attempt to overcome this limitation, it has been proposed that the pulse amplitude of ICP (AMP) can be used instead of mean ICP to derive indices for bedside monitoring [175], [204]. This was inspired by observations that in circumstances with low and 'flat' mean ICP trend, slow waves visible in ABP were reflected in coherent waves in AMP. This is because the pulsatile component of ICP can be attributed to the expansions and contractions of cerebral arterial walls due to cardiac pulses in ABP. As the arterial wall motions are transmitted to the intracranial space, changes in CBV can be reflected by AMP. This pulsatile transmission depends heavily on the compliance of the cerebral arteries (C_a), which is related to the cerebrovascular resistance (CVR) and can therefore be altered by the strength of vascular reactivity. As the magnitude of ABP pulse (and thus pulsatile CBV) is much larger than the slow fluctuations of mean ICP, it is thought that even with elevated C_i, the ABP-ICP pulse transmission can still act as a robust mechanism for CA assessment. The index PAx was derived by correlating the slow changes (0.008 – 0.05 Hz) in AMP with ABP [175], with zero or negative values indicating intact autoregulation (due to active smooth muscle relaxation and consequently augmented ABP-to-ICP pulse transmission in response to decreased ABP), and

positive values denoting compromised CA. The mechanism of PAx is compared to that of PRx in a conceptual **Figure 9.1**.

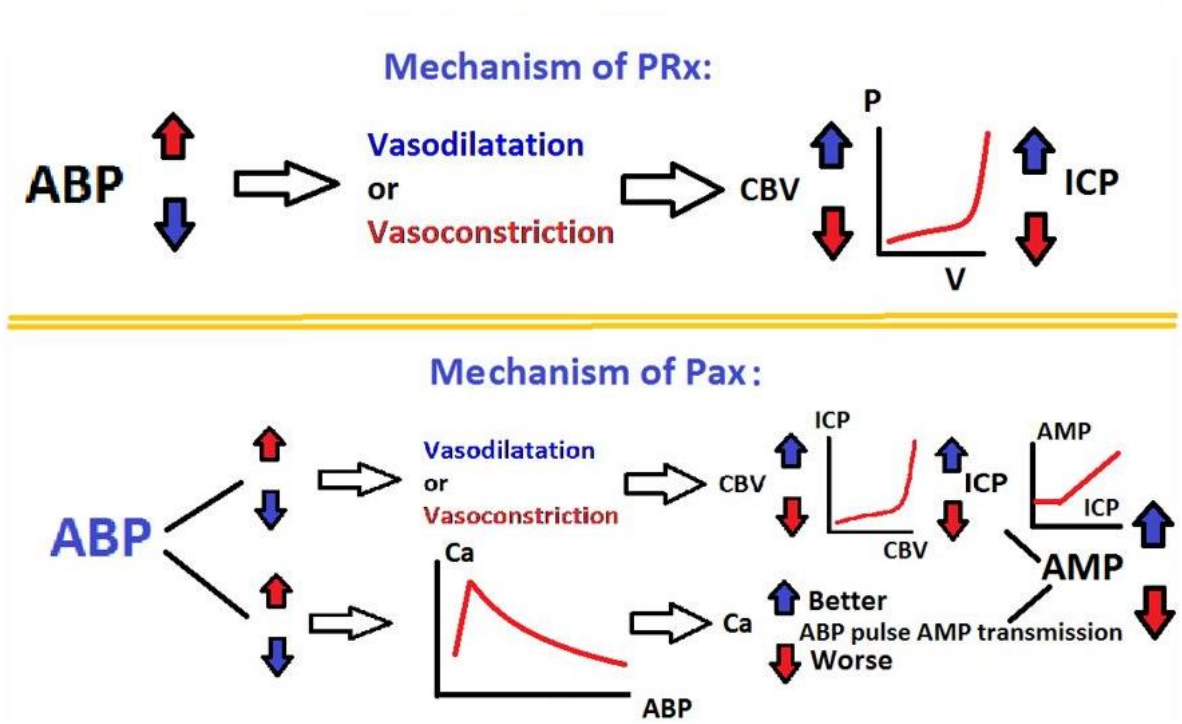

Figure 9.1. A comparison of the mechanisms of PRx and PAx. With high volume compensatory reserve, the transmission of ABP waves is poor, producing unreliable PRx. In contrast, the transmission of pulsatile CBV modulated by ABP compensates for the poor volume-to-pressure transmission, resulting in improved robustness of PAx.

It has been postulated that the monitoring of ICP alone does not provide a full picture of the pathological state of TBI patients, and should be complemented with a measure of cerebral compliance [205]. This is because even at moderate ICP levels, reduced intracranial compliance increases the risk of dangerous hypertensive events such as vasodilatory cascades, which can result in prolonged ICP plateau waves and even refractory intracranial hypertension.

On the other hand, even with moderately elevated ICP, the compensatory capacity of intracranial space with normal compliance is sufficient to buffer ICP fluctuations due to changes in vascular volume. Therefore, monitoring compensatory reserve (CR) has been proposed as a parameter of value alongside ICP. This can be achieved, at least to some extent, using the RAP index (correlation (R) between AMP (A) and ICP (P)), with values close to zero indicating good compensatory reserve, and values approaching +1 meaning exhausted CR [86]. Recently, the two concepts of autoregulatory response (reflected through variations of ICP pulse wave to changes in ABP) and CR (assessed through the relationship of mean ICP with its pulse amplitude) have been integrated into an index RAC [174]; it is thought that this index (correlation (R) between AMP (A) and CPP (C)) can potentially outperform PRx and PAx.

The indices mentioned above seem to agree with each other statistically. However, when exploring in TBI cohort, it is important to understand the factors that contribute to their differences and determine whether it is beneficial to monitor with multiple indices, or simply to choose the most 'robust' one for clinical applications. Therefore, the aim of this study is to explore how the interplay of brain compliances and vascular reactivity affects these indices, thus facilitating the interpretation of clinical observations in TBI patients.

9.2 Methods

9.2.1 Generation of Simulated Signals

A computer programme was used to simulate the pressures and flow at different compartments of the hydrodynamic model described in **Chapter 7**. It was designed to be run on Windows 10 and written in Object Pascal (Embarcadero Delphi 10.2) using the RAD studio (see **Chapter 5**). Artificially generated ABP (illustrated in **Figure 9.2**) was used as the input of the model:

$$ABP = offset + pulse\ wave + slow\ wave \qquad \textbf{(Equation 9.1)}$$

where

- *offset* is the mean ABP,
- *pulse wave* simulates the pulse waveform of ABP due to cardiac cycles (period of 1 second), consisting of a fundamental wave (amplitude of 16 mmHg) with a first harmonic (amplitude of 8 mmHg), and
- *slow wave* simulates the slow sinusoidal fluctuations of ABP, with amplitude of 5 mmHg and period of 1 minute.

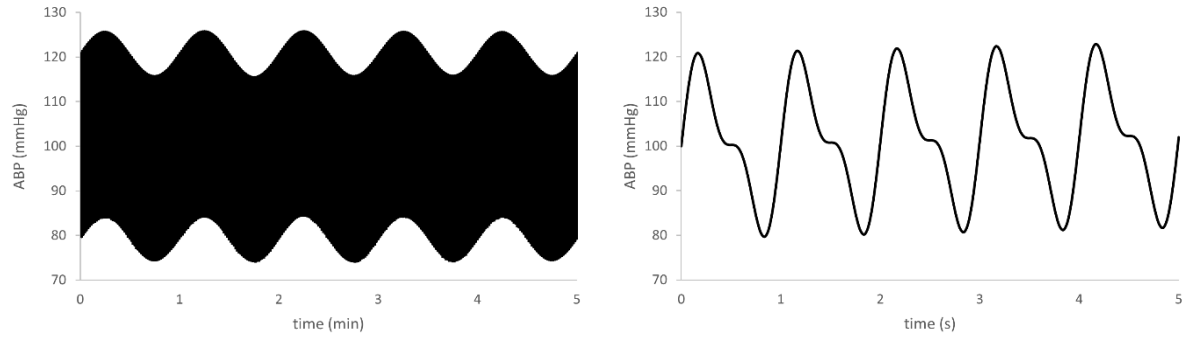

(a) (b)

Figure 9.2. Artificially generated ABP signal (a) and its pulse (b) used as input for model simulations.

After importing the generated ABP data from a csv file, the programme used the state equations derived from the hydrodynamic model described in **Chapter 7** to evaluate and plot ICP and F_a against time. The data were then saved as a csv file for further analyses. An example of the generated signals and imported into ICM+ is shown in **Figure 9.3**:

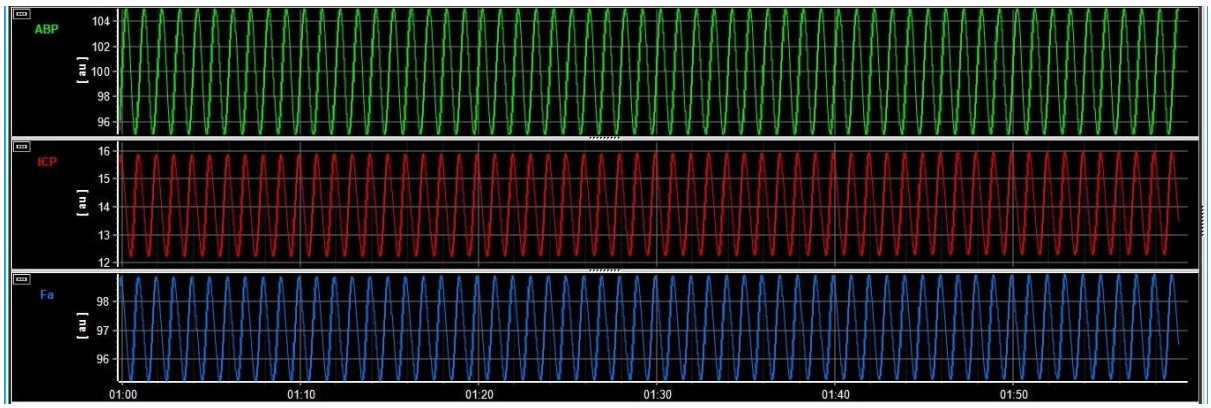

Figure 9.3. Example of artificially generated ABP, and the signals of ICP and F_a generated by the model (the pulse waves were filtered out for clarity).

9.2.2 Experiments

Three sets of experiments were performed using the generated signals:

9.2.2.1 AMP vs C_a

From **Chapter 6**, the model parameter C_a was calculated as

$$C_a = \frac{C_{aspan}}{CVR} + C_{offset} \qquad \textbf{(Equation 9.2)}$$

where

C_{aspan} is a coefficient reflecting the sensitivity of C_a in response to changes in pressure, and

$C_{aoffset}$ is a constant allowing vertical translation of the C_a-CVR curve.

To assess the relationship between C_a and AMP, C_{aspan} was first set as zero, so that the effects of CVR due to cerebral autoregulation were excluded. $C_{aoffset}$ was changed in steps from 0.01 to 0.05, with a step size of 0.01. Sixty minutes of the generated ICP were recorded at each step. AMP was calculated as the fundamental harmonic amplitude of the pulse component in a Fourier transform decomposition of the ICP waveform, with a ten-second window and updated every ten seconds. The experiments were repeated with several elasticity coefficients (E = 0.3, 0.6 and 0.9) to simulate different cerebral compliances C_i; the relationship between E and C_i is given below:

$$C_i = \begin{cases} \dfrac{1}{E(P_i - P_0)} & for\ P_i > P_{opt} \\ \dfrac{1}{E\left(P_{opt} - P_0\right)} & for\ P_i < P_{opt} \end{cases} \qquad \textbf{(Equation 9.3)}$$

where

E is the elasticity of the CSF space,

P_{opt} is the pressure breakpoint between linear and non-linear range of cerebrospinal compliance, and P_0 is the pressure corresponding to infinite compliance, which essentially provides an offset to the inverse relationship between compliance and pressure.

9.2.2.2 Simulations with Increasing CPP

The effect of cerebral autoregulation on intracranial pressure reactivity were then investigated by changing the mean ABP. C_{aspan} was set as 0.002 so that C_a could vary with CVR; $C_{aoffset}$ was initially set as 0.01. Sixty minutes of the generated ICP were recorded for each CPP (from 30 to 150 mmHg, with a step increase of 5 mmHg). The experiments were repeated with different C_i (E = 0.3, 0.6 and 0.9), and then with a higher C_a ($C_{aoffset}$ = 0.04). The parameters were chosen such that the generated signals do not diverge to infinity.

9.2.2.3 Simulations with Increasing ICP

The responses of pressure reactivity indices to ICP changes were evaluated by raising the resistance of interstitial fluid flow (R_{ISF}) at a constant rate, so that ICP increased from 0 to 80 mmHg. $C_{aoffset}$ and E were set at 0.04 and 0.6 respectively. This simulated the effect of progressive brain swelling.

9.2.3 Evaluation of Pressure Reactivity Indices

To simulate the extraneous physiologic variabilities of CBF and ICP slow waves, coloured noise was added to the calculated F_a and ICP (Gaussian white noise filtered with a low pass Butterworth filter (cut-off frequency of 0.2 Hz)). Samples with ten-second averages of ABP, ICP, F_a and AMP signals were taken. The Pearson's correlation coefficient of ABP with ICP (for PRx), CPP with F_a (for Mx), ABP with AMP (for PAx), CPP with AMP (for RAC) and ICP with AMP (for RAP) were calculated with 30 consecutive samples (5 min), and updated every 60 seconds. Each index of a recording was calculated by averaging over the entire time series; this process was then repeated with different recordings.

The recorded signals were processed and analysed with the ICM+ software (Cambridge Enterprise Ltd, Cambridge, UK, https://icmplus.neurosurg.cam.ac.uk): a csv file containing the generated ABP, ICP, and F_a time series was fed to the software, which used a configuration

file to perform calculations of the indices. An example of the evaluated indices is illustrated in **Figure 9.4**. The relationships between model parameters and pressure reactivity indices are illustrated with line plots using Microsoft Excel in the following section.

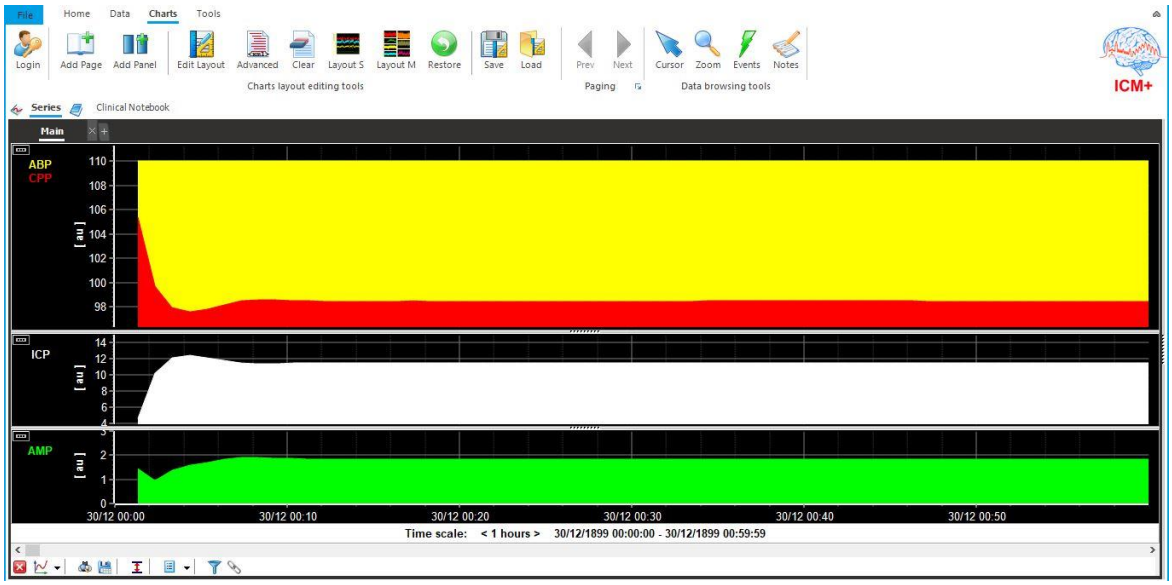

(a)

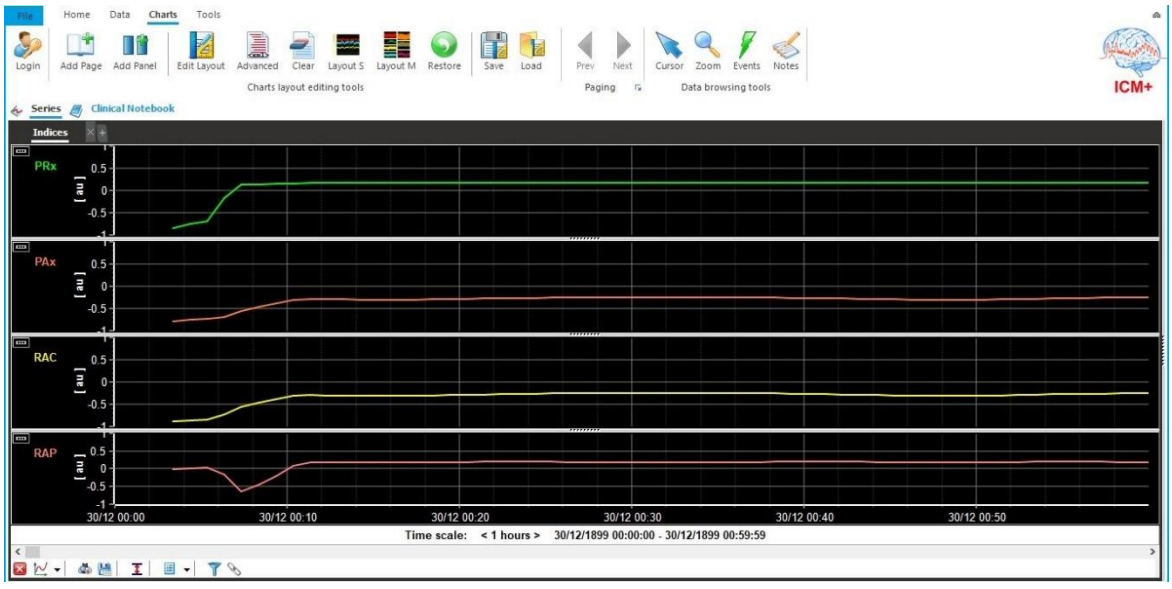

(b)

Figure 9.4. An example of the imported signals (a) and pressure reactivity indices (b) calculated with ICM+. This is a figure for one CPP step; the variations at the initial portion of the charts are the result of the burn-in phase of numerical integration (also mentioned in **Chapter 5**).

9.3 Results

9.3.1 AMP vs C_a

The AMP of simulations with different C_i (E = 0.3, 0.6, 0.9) were plotted against C_a (with an interval of 0.01) in **Figure 9.5**. AMP increased in response to rising C_a for all C_i; with higher C_i it rose more rapidly.

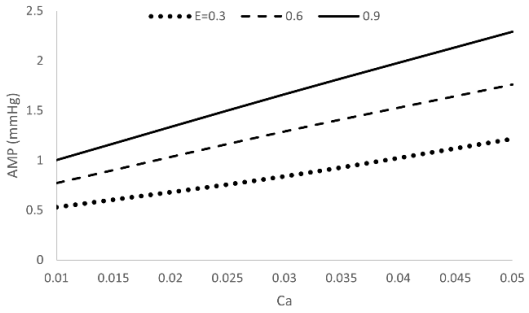

Figure 9.5. AMP vs C_a of simulations with different C_i (E = 0.3, 0.6, 0.9).

9.3.2 Effect of CPP on Pressure Reactivity Indices

Simulations with low and high C_a ($C_{aoffset}$ = 0.01 and 0.04 respectively) were run with different values of CPP (the variations of C_a in response to rising CPP is illustrated in **Figure 9.6**).

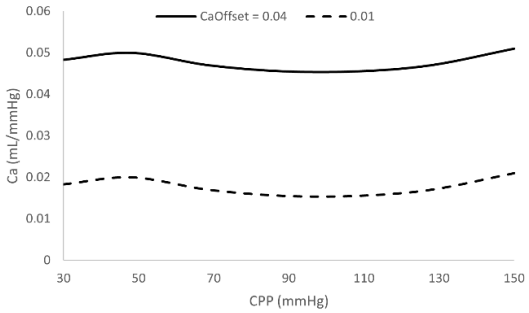

Figure 9.6. Simulations of C_a vs CPP with $C_{aoffset}$ = 0.01 and 0.04. $C_{aoffset}$ is a constant allowing vertical translation of the C_a-CVR curve. In this set of experiments C_{aspan} was set as zero, so that $C_a = C_{aoffset}$.

The effect of C_a on AMP with different C_i are plotted against CPP in **Figure 9.7**.

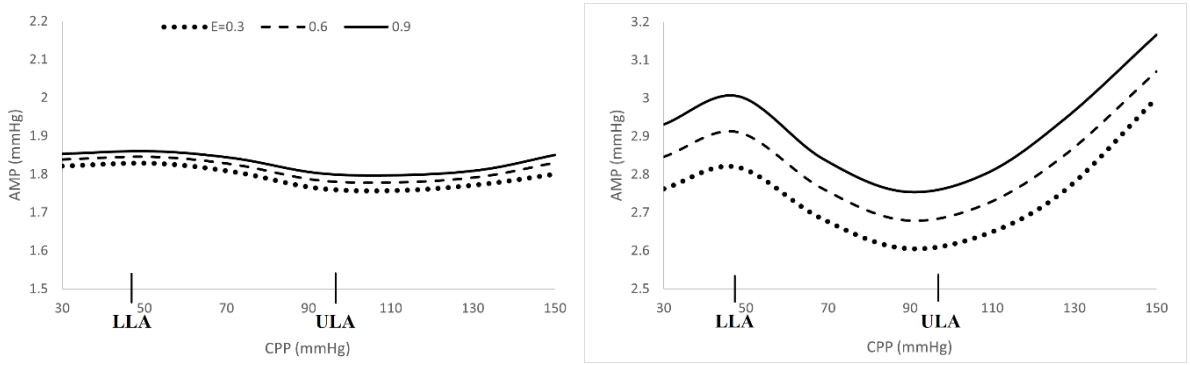

(a) (b)

Figure 9.7. Simulations of AMP vs CPP with low and high C_a ($C_{aoffset}$ = 0.01 in (a), 0.04 in (b)) and different elasticity coefficients (E). The lower (LLA) and upper (ULA) limits of autoregulation are marked.

The AMP of simulations with high C_a (**Figure 9.7** (b)) were significantly higher than those with low C_a (**Figure 9.7** (a)) across the entire range of CPP. On the contrary, simulations with higher C_i (lower E) had AMP lower than those with lower C_i (higher E). Separations between AMP with different C_i were augmented with high C_a. With rising CPP, simulations with both high and low C_a initially increased until reaching the lower limit of autoregulation (LLA), before dropping to a minimum at the upper limit of autoregulation (ULA) and eventually rising again. For all C_i, AMP with high C_a were more responsive to increasing CPP than low C_a.

Figure 9.8 showed the changes in the indices PRx, Mx, PAx, RAC, and RAP of simulations with low and high C_a and different C_i, in response to increasing CPP (with an interval of 5 mmHg).

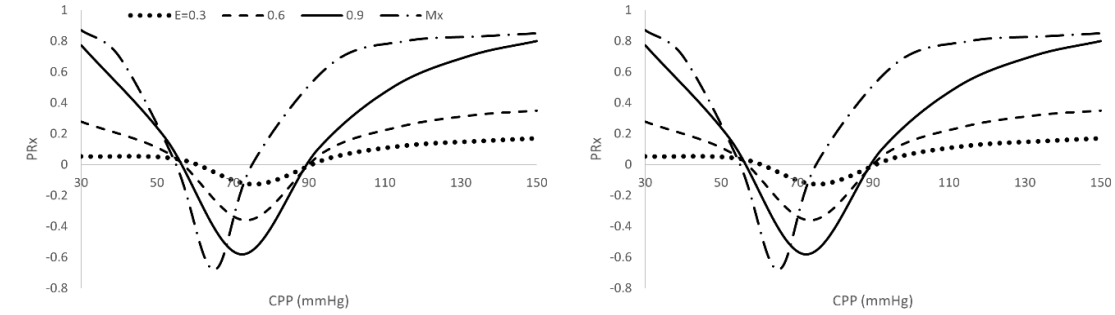

(a(i))

(a(ii))

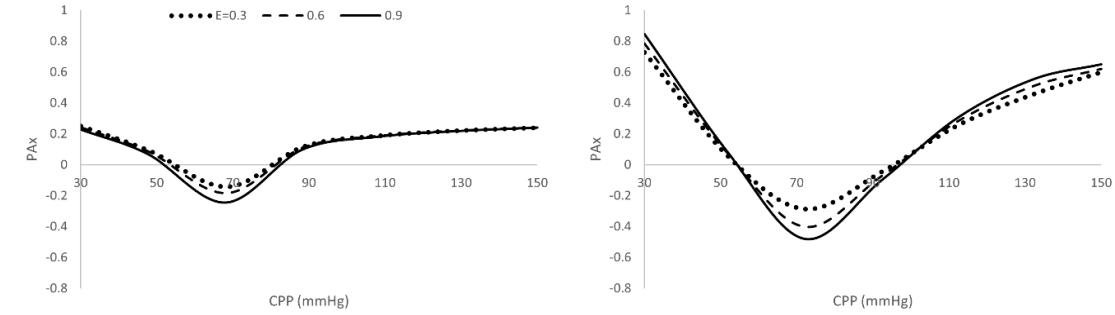

(b(i))

(b(ii))

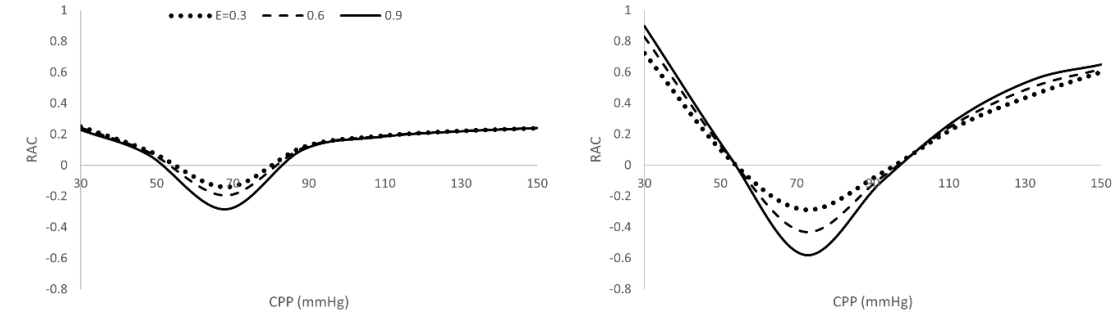

(c(i))

(c(ii))

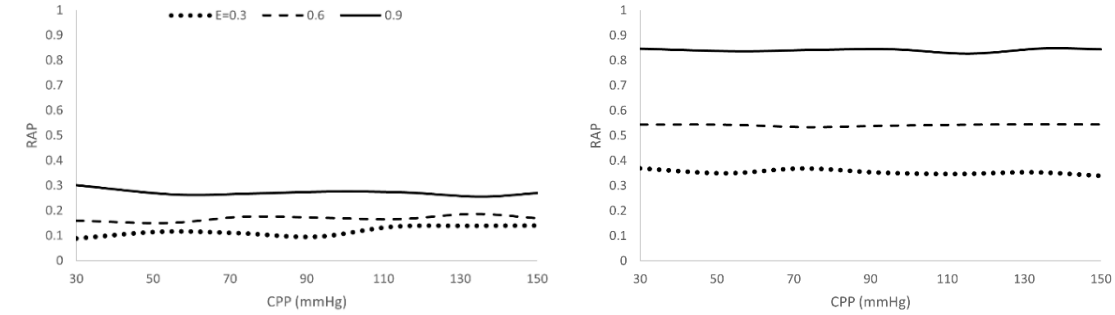

(d(i))

(d(ii))

Figure 9.8. (a) PRx and Mx vs CPP, (b) PAx vs CPP, (c) RAC vs CPP, and (d) RAP vs CPP of simulations with (i) low and (ii) high C_a and different C_i.

Regardless of C_a and C_i, simulations of PRx, Mx (**Figure 9.8** (a)), PAx (**Figure 9.8** (b)), and RAC (**Figure 9.8** (c)) reacted to increasing CPP by reducing to a minimum level before rising again. When compared to PRx, Mx started rising at a lower level of CPP. PRx with low C_a (**Figure 9.8** (a(i))) behaved almost identically to those with high C_a (**Figure 9.8** (a(ii))); it responded much better to CPP with low C_i than with high C_i. In contrast, changing C_i only resulted in relatively small differences in PAx; with low C_a (**Figure 9.8** (b(i))) and low C_i, it fell to a slightly lower minimum than with high C_i. While PAx became much more sensitive with high C_a (**Figure 9.8** (b(ii))), it only varied mildly with changing C_i when compared to PRx.

RAC followed a similar trend to PAx, becoming more responsive to changing CPP with reduced C_i and increased C_a (**Figure 9.8** (c(i)) vs (c(ii))). When comparing RAC to PAx with low C_a (**Figure 9.8** (b(i)) vs (c(i))), the two appeared identical with high C_i, but the former dropped to a slightly lower minimum than the latter as C_i decreased. The same was observed in the case of high C_a (**Figure 9.8** (b(ii)) vs (c(ii))), with the difference between RAC and PAx being more apparent with low C_i. RAP (**Figure 9.8** (d)) appeared to be independent of CPP; it remained constant across the CPP range but increased with reducing C_i. Raising C_a increased the values of RAP with each C_i, as well as the separations between them.

It is worth noting that, despite having a relatively small difference, the value of CPP at which the reactivity is at its best (CPPopt) seems to depend on the intracranial compliance C_i for PRx (slightly reduced with increasing E). Such dependence cannot be observed in the graphs of PAx and RAC; they were shown to be influenced by the arterial compliance C_a instead.

9.3.3 Effect of ICP on Pressure Reactivity Indices

The effects of increasing ICP on the indices PRx, PAx, RAC, and RAP are plotted in **Figure 9.9**.

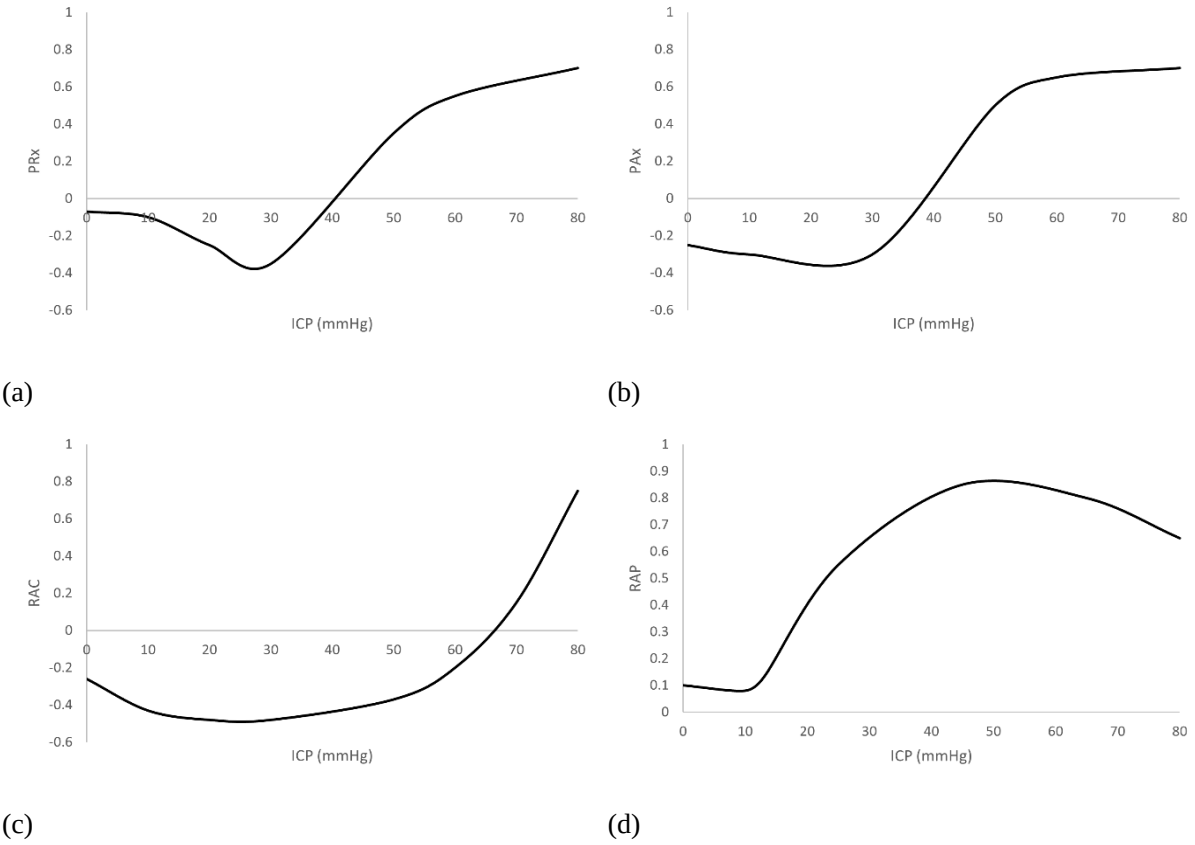

Figure 9.9. Simulations of (a) PRx, (b) PAx, (c) RAC, and (d) RAP vs ICP.

With ICP rising, PRx, PAx and RAC decreased from small negative values to a minimum, before rising to positive values. PRx was closer to zero than PAx at low levels of ICP. In contrast to PRx and PAx, RAC did not rise to zero until ICP was much higher. RAP was initially stable at small positive values, but began to increase as ICP rose above ~10 mmHg; as ICP was further elevated, RAP reached a maximum value before decreasing.

9.4 Discussion

In this project, multiple *in silico* experiments have been run using an enhanced model of cerebrovascular dynamics, in order to explore the relationships of various continuous pressure reactivity indices with CPP, while modulating these relationships via the interplay between the arterial wall and intracranial compliances. The results showed that the pressure reactivity index (PRx) is highly dependent on intracranial compliance. However, this effect can be overcome when the pulse amplitude of ICP is used instead, as in the PAx and RAC indices.

The simulations of ICP in response to slow changes in ABP have revealed the important effects of intracranial compliance and arterial wall compliance on the pulse amplitude of ICP and its derived indices. The differences in their behaviours can be explained by the relationships of AMP with C_a and C_i (**Figure 9.5**). With a higher compliance (reduced stiffness) of the arterial walls, changes in transmural pressure are easily transmitted as changes in CBV. The vascular

response to pressure changes is hence amplified, resulting in an increase of the AMP. On the other hand, reducing the intracranial compliance (tighter brain with poor compensatory reserve) facilitates the transmission of CBV changes to ICP changes, and therefore also raises the AMP. The combined effects of ABP-CBV and CBV-ICP transmissions cause a steeper rise in AMP with low C_i, in response to increasing C_a.

The plots of AMP against CPP (**Figure 9.7**) demonstrates how the pulse amplitude of ICP is affected by the reactivity of the cerebral vessels. At the centre of the graphs, AMP decreases with increasing CPP. This is caused by active vasoconstrictions (and stiffened vessels) due to CA, which reduces C_a and AMP. In contrast, the lower and upper ends of the graphs (below LLA and above ULA) indicate passive dilations of the cerebral arteries in response to increasing CPP (abolished CA), and hence rising C_a and AMP. The dependence of ICP pulse amplitude on autoregulatory capacity is reflected by the characteristic U-shaped curves, when plotting PAx and RAC against CPP (similar to the behaviour of PRx). This suggests that the indices derived from AMP can be used for individualised optimisation of CPP based on CA assessments. The performance of these indices with different C_a and C_i are compared below.

9.4.1 PRx, Mx and PAx

The relationships of PRx and Mx with CPP were both characterised by U-shaped curves (**Figure 9.8** (a)), indicating the presence of cerebral autoregulation. However, it can be observed that Mx began to rise from its minimum value at a lower value of CPP when compared to PRx. This highlights the difference between the range of regulation of cerebral blood flow and vascular reactivity. This discrepancy was also illustrated in the graphs of CBF and ICP vs CPP in **Figure 7.3**, and has been observed in experimental studies which measured the relationships of CBF and arteriole diameters with CPP [14].

While PRx reacted very well to CPP with low C_i, it became much less sensitive when C_i increased (**Figure 9.8** (a)). This result is expected, as a more compliant intracranial space hampered the transmission of CBV-to-ICP changes. The diminished ICP changes were 'drown' in the extraneous variabilities of ICP [151], [206] (simulated as added artificial noise) and cannot be picked up by PRx. However, changing C_a appeared to have no effects on PRx, indicating that the slower CBV-ICP transmission plays a more important role in determining ICP changes than the pulsatile ABP-CBV transmission.

PAx responded to changes in C_a and C_i differently when compared to PRx: with high C_a, PAx was very reactive to CPP (**Figure 9.8** (b(ii))); increasing C_i only resulted in a slight loss in

sensitivity. This is because while a high C_i lowers the AMP, the AMP differences due to changing CPP remained significant; this was illustrated in **Figure 9.7** (b) as the steep AMP variations in response to CPP. In contrast, a lower C_a (**Figure 9.8** (b(i))) worsened the sensitivity of PAx substantially: with extraneous ICP variabilities covering the diminished differences in AMP (**Figure 9.7** (a)), PAx became unresponsive to CPP changes.

Retrospective analyses have compared the performance of PRx and PAx for non-DC TBI patients [175]. Despite a positive correlation between the two indices ($r = 0.63$, $p < 0.001$), PAx (unlike PRx) was able to distinguish fatal vs non-fatal outcome of patients with low ICP (< 15 mmHg). The higher predictive power of outcome of PAx was supported by simulations; this prediction of potential improvement in performance with theoretical modelling helps strengthen the message of retrospective studies, that PAx may be a more reliable and robust index of CA than PRx [207]. However, there currently is a lack of studies targeting patients with increased C_i (e.g. those who underwent DC) or reduced C_a. Further analyses are required to determine whether PAx can outperform PRx in such cases.

9.4.2 PAx and RAC

The use of CPP instead of ABP for AMP-derived indices produced identical results for simulations with high intracranial compliance. However, with reduced C_i the RAC became

slightly more responsive than PAx (**Figure 9.8** (b) vs (c)). This may be attributed to the influence of high ICP, which produced a stronger CPP response than ABP when CA was intact. The effects of ICP can also be observed by comparing the responses of the indices to increasing ICP (**Figure 9.9** (b) vs (c)), with RAC remaining at negative values even when PAx began to turn positive. Combined with the increased AMP due to reduced C_i, the effects of extraneous ICP variabilities were reduced, resulting in a stronger correlation between CPP and AMP. The difference between RAC and PAx with low C_i became more pronounced in the case of high C_a (**Figure 9.8** (c(ii))), where the rise in AMP due to increasing C_i is augmented. As both CPP and C_i have significant influence on RAC, it can be used to reflect changes in states of both CA and CR.

RAC was shown to correlate strongly with PAx ($r = 0.817$, $p < 0.0001$) and PRx ($r = 0.718$, $p < 0.0001$) in a clinical study of TBI patients without DC [174]. The results also indicated increased responsiveness in RAC with high ICP values (> 50 mmHg), suggesting that the index may be able to reflect the exhaustion of compensatory reserve. However, similar to PAx, the performance of RAC has not been assessed with post-DC patients. Moreover, with a relatively small number of data points with high ICP (>30 mmHg) used in the study [174], the conclusions drawn related to RAC require further validation.

Figure 9.8 also showed the mild but observable effects of C_i and C_a on CPPopt. As C_a is a parameter describing vascular properties (inversely related to CVR), its variation inevitably influences the characteristics of autoregulation. It is therefore not surprising that CPPopt alters with C_a. However, **Figure 9.8** (a) suggests that C_i may bias the CPPopt of PRx even when it is not directly related to vascular reactivity; this bias is not observed in the graphs of PAx (**Figure 9.8** (b)). The results indicate that PAx is more accurate than PRx in determining the CPPopt, as it is not influenced by C_i. While the CPPopt of RAC seems to be independent of C_i, the index encapsulates information related to both vascular reactivity and brain compliance, and may therefore be more challenging to interpret.

9.4.3 RAP

RAP also reacted to changing C_i and C_a: with reduced C_i (**Figure 9.8** (d)), AMP increased so that its correlation with ICP became less susceptible to extraneous ICP variabilities, producing higher levels of RAP. However, with reduced C_a the differences between AMP with different intracranial compliance were diminished (**Figure 9.8** (a)). This caused a reduction in separation between RAP with different C_i (**Figure 9.8** (d(i))), indicating a loss in sensitivity to changing CR. The behaviour of RAP in response to increasing ICP (**Figure 9.9** (d)) agreed with clinical results [174], [208], [209]: initially there was little correlation between ICP and its pulse amplitude, and RAP stayed close to zero. However, as ICP was elevated beyond a threshold

value (P_{opt}) CR became exhausted and RAP began to rise. This continued until a very high level of ICP was reached, where CPP fell below the lower limit of autoregulation (~50 mmHg). Further increases in ICP was accompanied with reduction in AMP, causing RAP to drop. From **Figure 9.6**, this is also the CPP level (~50 mmHg) below which C_a began to decrease. The upper breakpoint of the AMP-ICP relationship corresponds to the critical closing pressure, a point where the cerebral vasculature starts to collapse due to insufficient transmural pressure for keeping the arteries open [86], [174], [210], [211].

RAP has been studied in patients with hydrocephalus and TBI [86], [208], [212], [213]. Although the index has been shown to be related to clinical outcome after head injuries [205], its significance was not as high as PRx when predicting a poor prognosis [214]. Moreover, while patients who died always had higher PRx than those with favourable outcome, results of different retrospective studies could not agree on whether RAP was higher or lower for patients with fatal outcome [209], [215]. This can perhaps be explained by the upper breakpoint characteristic of the AMP-ICP relationship, where RAP falls to negative values with very high levels of ICP. In addition, despite the seemingly heavy influence of brain compliances on RAP, the effects of increased C_i and reduced C_a have not been examined in clinical studies. In general, the relationships between brain compliances and AMP-derived indices can potentially be

studied by analysing transcranial Doppler (TCD) flow velocity measurements, from which C_a and C_i can be derived.

9.4.4 Limitations

The relationships of pressure reactivity indices uncovered with model simulations do seem to reflect and explain phenomena observed in clinical data. However, this is a relatively simple model with lumped parameters, and may not necessarily capture the relationships accurately, and the relationships may depend on the actual values of parameters governing the model elements, given the highly nonlinear nature of interactions between its elements. Therefore, our conclusions need to be interpreted with caution. Moreover, the artificial noise was added to the ICP signal to facilitate the evaluation of indices, and only served as a gross simplification of real-life scenarios; its frequency and amplitude may not reflect true ICP variabilities.

9.5 Conclusions

The proposed hydrodynamic model allows to study *in silico* performance of various pressure reactivity indices in different scenarios related to brain compliances, and help to understand findings in clinical research. PRx can be made unreliable by elevated intracranial compliance (as in cases following DC for example), but the indices using AMP (such as PAx and RAC) can help to overcome this limitation.

Chapter 10

Conclusions and Future Directions

10.1 Summary of Main Findings

This thesis explored the relationships between pressure and vascular volume changes inside the cranium using an electrical-equivalence mathematical model, and studied the effects of these relationships on the performance of the common vascular dynamics indices. The main findings are listed below:

1. While an existing model of cerebral fluids circulation performed well in simulations of dynamic cerebrovascular variations and their transient effects on intracranial pressure (ICP), it was not able to reflect accurately the clinical phenomena caused by prolonged changes in cerebral blood volume (CBV), such as sustained vasodilation. This important finding called for the addition of a novel mechanism in the model to link the fluid dynamics in the arterial and intracranial compartments.
2. After the above issue was addressed, the simulations were repeated to verify the modified model. It was successful in depicting features of intracranial physiology involving the long-term interactions between CBV and ICP.

3. The modified model was used to compare the performance of autoregulation indices Mx, Mxa, ARI and PRx. The results have revealed that ICP is a significant confounder to the indices of autoregulation, potentially leading to bias when interpreting the strength of CA using such indices. The intracranial compliance was also shown to be an important factor determining the accuracy of CA assessment.
4. The modified model was also used to explore the influence of CPP on pressure reactivity indices derived from the pulse amplitude of ICP (AMP). The simulated results confirmed findings from previous clinical studies, but importantly, they have also shown that while indices derived from mean ICP can be made unreliable in cases with elevated intracranial compliance, those using AMP can help to overcome this limitation. The model has proved to be a robust tool to study the performance of pressure reactivity indices in different scenarios from the point of view of the compliances, and may facilitate the interpretation of findings in clinical research.

10.2 Future Directions

This study is a step towards the ultimate goal of creating a ‘digital twin’ of cerebral hydrodynamics. Such a tool would facilitate personalisation of treatments in neuro-intensive care, especially in pathologies (such as traumatic brain injury) with a highly dynamic profile

and treatments relying on the continuous monitoring of physiological signals. In order to achieve this, the following points still need to be addressed:

1. **The representation of model elements needs to be improved based on anatomical evidence.**

   While the addition of the ISF pathway has improved the simulation accuracy of the current model, it constitutes a considerable simplification of the modelled mechanism and further clinical evidence is required to justify its mathematical representation. Other ways of incorporating pressure-volume interaction within the rigid skull may require moving away from pure electrical-equivalent model representation. This would likely make the model less intuitive in interpretation but possibly more accurate. Furthermore, depending on the clinical phenomena to be investigated, future model development will need to explore splitting the cerebrovascular pathway to allow for exploration of parallel cerebral circulation paths, following individual arteries branching off the circle of Willis.

2. **The model should be further validated.**

   Other physiological phenomena can also be simulated in addition to those performed in this thesis. Examples include the effects of posture on ICP, the behaviour of CBF and ICP as cerebral perfusion pressure (CPP) falls below the critical closing pressure, and blood flow in the venous compartment during intracranial hypertension. By comparing the

simulated results to clinical findings, the performance of the model can be further validated and the model adjusted if required.

3. **High-performance methods should be considered allowing the evaluation of model parameters with imported signals – the inverse problem.**

   The ultimate goal of developing this model is its integration into intensive care monitoring software such as ICM+, in order to provide real-time estimations of the model parameters based on continuous measurements of physical quantities such as arterial blood pressure (ABP), intracranial pressure (ICP), and cerebral blood flow (CBF) representing the nodes in the model. This work will require exploration of high-performance methods for numerically solving partial differential equations of the models, possibly supported by machine learning approaches like Neural ODEs. Once this is achieved, the resulting 'digital twin' could be used for exploring natural trajectories and treatment predictions in real time.

10.3 Final Remarks

In its current state, the model is only supposed to simulate observed phenomena to explore which parameters, reflecting concrete physiological concepts, need to be modified in order to achieve the responses observed. Failure to do so would trigger a necessity of introducing further elements to the model, or modifying characteristics of the relationships between the existing

ones. Thus, generalisation of the model is iterative, and is the main concern of this thesis. This project has identified phenomena which could not be simulated correctly, and sought to extend the model in order to rectify them. Once the model is qualitatively capable of simulating the entire spectrum of physiological relationships observed in clinical recordings, one can proceed to the next step – the inverse problem – where the model parameters are estimated based on the observed data. From that point one could use the model to 'explore' the model responses to changes in individual parameters, which can be manipulated with different therapies regimes.

At present, the model itself is likely not complex enough to provide clinically meaningful predictions in a dynamic pathology such as TBI. However, it should be capable of aiding clinicians in better understanding of the underlying pathophysiological processes. In particular, it can potentially facilitate the development and validation of cerebral autoregulation indices. These indices are often very noisy, and it is important to understand their uncertainty when interpretating them. This project has proven that the model is able to identify their potential confounders, and can therefore be used to evaluate their reliability and improve the accuracy of clinical decision-making.

Appendix A

"A COMPARISON OF TWO ICP CALCULATION METHODS AND THEIR EFFECTS ON MEAN-ICP AND ICP DOSE"

K.H. Chu, E. Beqiri, M. Czosnyka, P. Smielewski

SUMMARY

This study compared two methods of calculating the intracranial pressure (ICP) of a patient: end-hour ICP and hour-averaged ICP. 1060 patients with traumatic brain injury (TBI) and known clinical outcome were studied. For each patient, the end-hour ICP and hour-averaged ICP were calculated. The mean ICP and ICP dose above 20 mmHg were evaluated using both calculation methods. The results for patients who survived and those who died were compared using the Student's t-test.

The average correlation between end-hour and hour-averaged mean ICP was 0.747, indicating that the end-hour ICP method agrees moderately with the hour-averaged method. However, comparison between survived and dead patients does not present significant difference between ICP values averaged with two different methods. Student's t-test gives similar results for both mean ICP and Dose. The results suggest that the end-hour and hour-averaged methods have similar predicting power for patients' clinical outcome.

Key Words: Traumatic brain injury, intracranial pressure, end-hour ICP, hour-averaged ICP

INTRODUCTION

Traumatic brain injury (TBI) is a common cerebral pathology affecting more than 50 million people every year. An acute head trauma can be followed by swelling of the brain (secondary damage), which causes the pressure within the cranial cavity (intracranial pressure, or ICP) to increase, as the brain is surrounded by a rigid skull. This rise in ICP can cause secondary damages to the brain, partly because it disrupts the cerebral perfusion, resulting in ischaemia and hypoxia [62]. The ICP of a head injured patient is a vital quantity to be monitored. It not only provides means about the secondary damage in the brain, but also provides an indication on the physiological state of the brain (such as compliance and elastance), and clinical decisions can be made based on the ICP level to ensure adequate cerebral perfusion [45]. It is common to have ICP above 20 mmHg after a head trauma, and efforts are made to stabilise it below this level.

It is believed that the clinical outcome of a patient with TBI is significantly influenced by his / her mean ICP and ICP dose. The dose is defined as the area under the curve (AUC) where an ICP-time graph exceeds a certain threshold (20 mmHg in this study); it is considered to be a

more informative parameter than mean ICP when describing secondary brain damages, as it describes both the extent and duration of an insult [216].

Commonly, in a critical care unit, ICP is recorded on hourly basis, even when the electronic record systems are used. Two methods can be used to report such hourly values: hour-averaged ICP, only available when using electronic record systems, configured to return these values, and, more often (possibly because of legacy paper-based nursing charts), end-hour ICP. The former averages the ICP of the whole hour, while the latter reports point measurement of mean ICP at the end of each hour. The end-hour ICP is naturally a more practical option when using manual entry of bedside monitoring values into nursing charts [217]. However, the significance of the under-sampling true ICP variability with the end-hour reporting, missing entirely an hour worth of variability of ICP at each reporting time point, is not fully examined. Previously, Zanier *et al* compared digital hour-averaged ICP measurements with manually recorded end-hour ICP, including the number of episodes of high ICP (HICP, where ICP is above 20 mmHg) and the percentage of time of HICP [217]. This study, on the other hand, investigates the mean ICP and dose obtained using hour-averaged ICP and digital end-hour ICP (which averages the ICP in the final minute of every hour), and thus the difference in predictive power of a patient's mortality.

METHODS

A retrospective data analysis was conducted using high-frequency monitoring ICP data. The raw ICP data were obtained from the ICM+ software (Cambridge Enterprise Ltd., Cambridge, UK); they were recorded with digital data transfer or digitized by A/D converters (DT9801; Data Translation, Marlboro, MA), and sampled at frequency of at least 50 Hz [174]. The age, gender, severity of the injury (as Glasgow Coma Scale), and status upon discharge (as Glasgow Outcome Scale) were also included for each recording; the data were fully anonymised. This study examined the ICP data of 1060 TBI patients admitted to the Neurocritical Care Unit (NCCU) of Addenbrooke's Hospital (Cambridge, UK) during the period from 1993 to 2017.

Data Processing

Using the 'batch export' function of ICM+, the end-hour ICP and hour-averaged ICP time series of each patient were created automatically. The mean ICP and ICP dose of each patient were calculated using both methods; the ICP dose was estimated using the trapezoidal method, which modelled the AUC as a series of rectangles and summed up their areas.

Statistical Analysis

The patients were first dichotomised by mortality (with 244 patients dead), and the average mean ICP and average dose of each group were calculated. The correlation coefficient (r)

between end-hour and hour-averaged mean ICP was then evaluated for each patient, and the average correlation of all patients was obtained. After that, the coefficient of determination (r^2) for each patient between the methods was calculated, and the estimate of the average proportion of variance unexplained (i.e. missed) by end-hour values (calculated as $1- r^2$) of all patients were hence found. The student's t-test was used to compare mean ICP and ICP dose for both calculation methods between the patient group that survived and the group that died. In addition, the t-test was also performed between the two methods within each group. The Bland-Altman Method was also used to illustrate the difference between the two methods.

RESULTS

The mean age of the patients was 38±17.2 years (range 3-89), and there were 827 males (78.0%). The Glasgow Coma Scale ranged from 3 to 15, and the Glasgow Outcome Scale ranged from 1 to 5. The average correlation between end-hour and hour-averaged mean ICP was 0.747, and the average, relative, ICP variance missed by end-of-hour measurement was 40.49%. Both mean ICP and ICP dose averaged with the two calculation methods do not differ significantly. Student's t-test gives similar results, but it also suggests that in both calculation methods, the mean-ICP and ICP dose are significantly higher in the group of patients that died. The t-test performed on ICP dose between the two methods within the group that survived showed that $t = 1.82$, which narrowly missed significance, at $p < 0.07$. **Table A1** lists the mean

ICP and ICP dose averaged for both patient groups and both calculation methods, and the results of the student's t-test. **Figure A1** shows the Bland-Altman Plots for mean ICP (a) and ICP dose (b). For mean ICP, the mean difference (solid line) is 0.015 mmHg, while the limits of agreement (dotted lines) are 1.10 and -1.07. For ICP dose, the mean difference is 21.52 mmHg • hr, and the limits of agreement are 102.04 and -59.00.

DISCUSSIONS

As expected, both the mean ICP and dose are significantly higher for patients who died than those who survived. In the Bland-Altman Plots, the narrower limits of agreement for mean ICP implies a smaller uncertainty, and hence a more reliable analysis than in case of ICP dose. The mean ICP calculated using end-hour and hour-averaged methods are moderately correlated. Despite that the end-hour method has missed a substantial amount (40.49%) of dynamic variabilities in ICP, statistically the relationships with the outcomes of the two methods do not differ significantly from each other. This may suggest that the end-hour ICP is a suitable method to assess the clinical outcome of TBI patients. However, this analysis was performed by averaging the measurements of patients, so the individual differences between the methods could be smoothed out. In particular, the relatively low p-value in the t-test performed on ICP dose within the group that survived, means that the end-hour method is almost significantly different from the hour-averaged method. Therefore, the results do not indicate that one can

make clinical decisions with confidence based on individual end-hour mean ICP or ICP dose measurements during the management of TBI patients.

TABLES

Table A1. Mean ICP and ICP dose (with standard error) for both patient groups and both calculation methods, and the results of the Student's t-test between patient groups.

		Mean-ICP			Dose		
		Mean (mmHg)	**t**	**p<**	**Mean (mmHg•Hr)**	**t**	**p<**
End-hour	**Died**	20.9 ± 0.9	6.92	1×10^{-10}	352 ± 36	5.93	1×10^{-8}
	Survived	14.2 ± 0.2			132 ± 9		
Hour-avg	**Died**	20.8 ± 0.9	6.89	1×10^{-10}	335 ± 35	6.18	1×10^{-8}
	Survived	14.3 ± 0.2			109 ± 9		

FIGURES

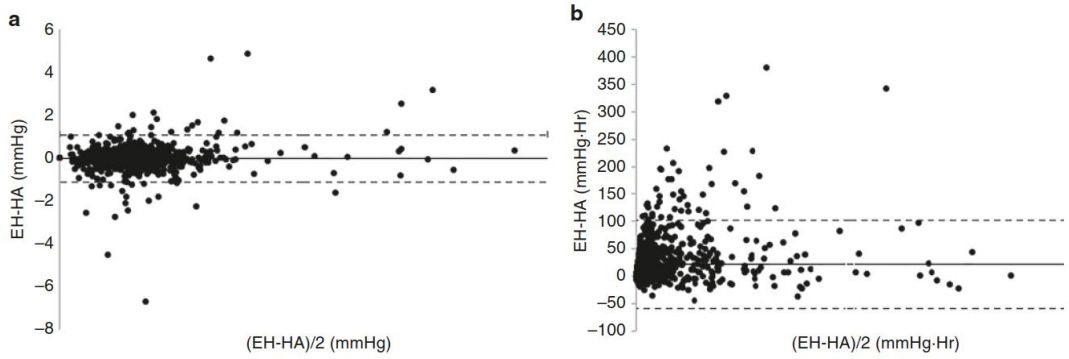

Figure A1. Bland-Altman Plots for (a) mean ICP and (b) ICP dose (EH: end-hour method, HA: hour-averaged method).

ACKNOWLEDGEMENT

MC is supported by the National Institute for Health Research (NIHR), Cambridge Biomedical Research Centre.

CONFLICT OF INTEREST STATEMENT

PS and MC has financial interest in a part of licensing fee of ICM+ software (https://icmplus.neurosurg.cam.ac.uk)

Appendix B

Mathematical Modelling of Cerebral Haemodynamics and Their Effects on ICP

Ka Hing Chu, Ihsane Olakorede, Erta Beqiri, Marek Czosnyka, and Peter Smielewski

Highlights

- Sustained haemodynamic effects on ICP are not well reflected in electrical models.
- We included a compartment representing the bulk flow of interstitial fluid.
- The new compartment allows to simulate prolonged haemodynamic influences on ICP.

Abstract (248, max 250)

Introduction Electrical-equivalence mathematical models that integrate vascular and cerebrospinal fluid (CSF) compartments perform well in simulations of dynamic cerebrovascular variations and their transient effects on intracranial pressure (ICP). However, ICP changes due to sustained vascular diameter changes have not been comprehensively examined. We hypothesise that changes in cerebrovascular resistance (CVR) alter the resistance of the bulk flow of interstitial fluid (ISF).

Research Question

We hypothesise that changes in CVR alter the resistance of the bulk flow of ISF, thus allowing simulations of ICP in response to sustained vascular diameter changes.

Material and Methods A lumped parameter model with vascular and CSF compartments was constructed and converted into an electrical analogue. The flow and pressure responses to transient hyperaemic response test (THRT) and CSF infusion test (IT) were observed. Arterial blood pressure (ABP) was manipulated to simulate ICP plateau waves. The experiments were repeated with a modified model that included the ISF compartment.

Results Simulations of the THRT produced identical cerebral blood flow (CBF) responses. ICP generated by the new model reacted in a similar manner as the original model during ITs. Plateau pressure reached during ITs was however higher in the ISF model. Only the latter was successful in simulating the onset of ICP plateau waves in response to selective blood pressure manipulations.

Discussion and Conclusion Our simulations highlighted the importance of including the ISF compartment, which provides mechanism explaining sustained haemodynamic influences on

ICP. Consideration of such interactions enables accurate simulations of the cerebrovascular effects on ICP.

Keywords

Mathematical modelling, intracranial pressure, cerebral hemodynamics, interstitial fluid

Abbreviations

ABP – arterial blood pressure

ICP – intracranial pressure

CPP – cerebral perfusion pressure

TBI – traumatic brain injury

ISF – interstitial fluid

CSF – cerebrospinal fluid

CVR – cerebrovascular resistance

CBF – cerebral blood flow

CBV – cerebral blood volume

THRT – transient hyperaemic response test

IT – infusion test

1. Introduction

Intracranial pressure (ICP) is a vital quantity to be monitored for clinical decisions in neurointensive care, and substantial effort has been made to investigate its dynamics with mathematical modelling. Works by Monro and Kellie [43], [44] described the volume conservation of fluids and brain matter within the skull due to the unique intracranial structure: the systems of cerebral blood flow (CBF) and cerebrospinal fluid (CSF) circulation are embedded in the brain tissue, which in turn is constrained by the rigid dura and cranium. This indicates that the changes in fluid flow at different time scales contribute to ICP variations in different ways. Subsequent studies have explored the transient and sustained effects of CSF flow on ICP. Notably, Davson [127] attributed the steady-state changes in ICP to the formation rate of CSF, the resistance of CSF outflow through the skull, and the pressure at the sagittal sinus where CSF absorption occurs. On the other hand, Marmarou [90], [128] introduced the concept of intracranial compliance in his modelling studies, and demonstrated its role on the dynamic aspects of ICP.

The interactions between cerebral haemodynamics and ICP is of much interest, particularly in scenarios like traumatic brain injury. Importantly, Ursino [98], [100], [129], [130] included in his model a representation of cerebrovascular circulation; this enabled the simulations of physiological phenomena involving vascular dilation and constriction such as cerebral

autoregulation. However, it is common for modelling studies to integrate compartments of CBF and CSF circulation to explore their combined effects on ICP. While these models are highly successful in illustrating the dynamic effects of fluid flow, they may be less robust in representing long-term interactions between cerebral blood volume (CBV) and ICP. Simulations with such models could therefore be inaccurate when attempting to reflect clinical phenomena caused by prolonged changes in CBV, such as sustained vasodilation.

In an attempt to represent the intracranial pressure-volume relationships of patients with cerebral oedema, Doron et al. [148] incorporated into their electrical model volume changes of brain tissue. In addition to elements representing the subarachnoid space, ventricles and cerebral vasculature, a new compartment was added into the model, depicting the bulk flow of cerebral interstitial fluid (ISF). This compartment was characterised by a resistive element to represent the resistance of ISF circulation through the brain parenchyma into the subarachnoid space. This novel design was based on the theory that cellular swelling reduces the volume of cerebral extracellular space, hence narrowing the channels through which cerebral ISF can flow [149], [150]. With a set of differential equations relating the pressure to volume at each compartment, the model allowed the changes in brain volume to interact with ICP dynamics. Simulations with this approach successfully mimicked various physiological features, in

particular the elevated ICP and reduced ventricular volume observed in patients with cerebral oedema and disruption of the blood-brain barrier.

Doron's work provided a modelling mechanism for sustained interactions among the resistances of fluid flow, compartmental volumes and ICP, via the ISF circulation compartment. This is especially important when investigating phenomena involving the interplay between CBV and ICP. A notable example is cerebral autoregulation, a homeostatic mechanism of the vascular system to stabilise the cerebral blood flow (CBF), in spite of variations in cerebral perfusion pressure. Resistive cerebral arterioles react to changes in perfusion pressure or vasoactive stimuli such as carbon dioxide [28], [151] by actively controlling the myogenic tone of the vessel walls, in order to dilate or constrict. This alters the cerebrovascular resistance (CVR) of the vessels and hence the CBV. Intracranial pathologies such as traumatic brain injuries often cause reduction in intracranial compliance, rendering the intracranial compartment susceptible to CBV increase, and resulting in ICP surges, falls in cerebral perfusion pressure (CPP) and consequently in secondary brain insults [152]. It is therefore crucial for models of intracranial hydrodynamics to capture the effects of cerebral haemodynamics on ICP. In this study, we built on a classical model of CBF and CSF circulation, and incorporated a compartment depicting the flow of cerebral ISF. With this model we attempted to replicate various pathophysiological features observed in clinical data.

2. Material and Methods

2.1. Construction of the Electric Analogue Model

This study initially replicated the unilateral hydrodynamic model proposed by Czosnyka [48] (**Figure B1** (a)). The electrical analogue of the model (**Figure B1** (b)) consists of four resistive (R_a, CVR, R_b, and R_{CSF}) and three capacitive (C_a, C_v, and C_i) components, the meaning of which will be described in detail below. It also includes two input voltage sources ABP and P_{ss}, representing the systemic arterial blood pressure and the venous pressure in the dural sinuses respectively.

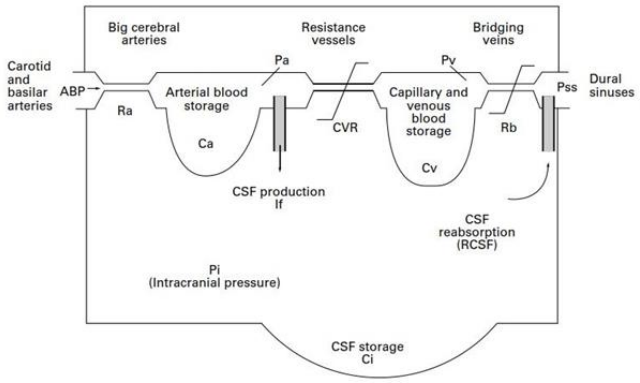

(a)

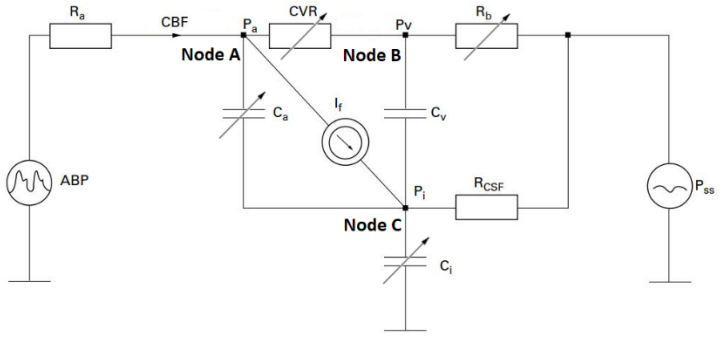

(b)

Figure B1. [48] The unilateral hydrodynamic model proposed by Czosnyka (a) and its electrical analogue (b). State equations are derived by considering the flow of current in nodes A, B and C (located in the arterial, venous and CSF compartments respectively).

A mathematical description of the resistive and capacitive elements in the model is provided in the Appendix section.

2.2. Modifications to the Model

To provide a mechanism for pressure interactions between the cerebrovascular and intracranial compartments, a representation of ISF circulation was added to the model. In the electrical analogue, it was depicted as a pathway with a resistive component (**Figure B2**).

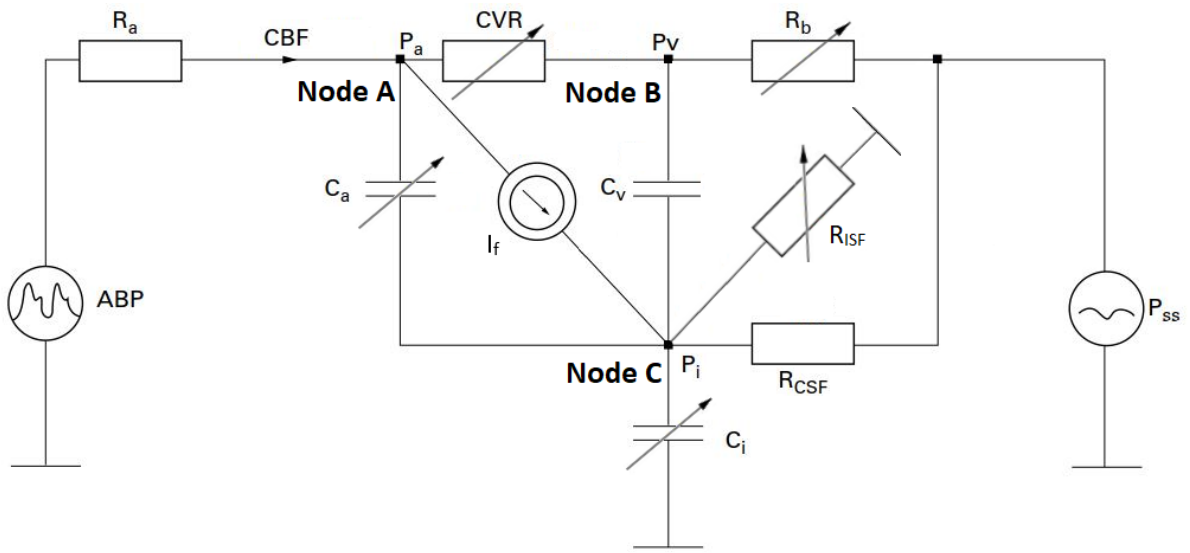

Figure B2. The modified unilateral model with added ISF compartment, represented by a resistive component (RISF).

It is postulated that vasodilation (represented as reduction in CVR and increased volume in the arterial bed) would cause reduction in ISF space volume (depicted as increased R_{ISF}). As there

is currently a lack of experimental data quantifying this interaction, we have simply modelled R_{ISF} as being reciprocally related to the CVR as the first approximation.

$$R_{ISF} = \frac{R_{ISFspan}}{CVR} + R_{ISFoffset}$$

where $R_{ISFspan}$ and $R_{ISFoffset}$ are constants.

2.3. Experiments

A programme designed to be run on Windows 10 was written in Object Pascal (Embarcadero Delphi 10.2) using the RAD studio. After selecting either the original or the new model and importing ABP data from a csv file, the programme used a set of equations (described in the Appendix section) to evaluate and plot P_a, P_v, P_i, and CBF against time.

Three pathophysiological phenomena observed in clinical data were simulated by the programme to test and compare the performances of the models:

1. Transient hyperaemic response test (THRT) – a diagnostic test assessing the capacity of cerebral autoregulation. During the test, the common carotid artery was compressed for a few seconds before being released, with a transient increase in cerebral blood flow indicating intact cerebral autoregulation mechanism [138], [139].
2. CSF infusion test – a clinical study used to analyse the dynamics of CSF circulation in

patients suspected of normal pressure hydrocephalus. In a lumbar infusion study, artificial CSF is infused at a constant rate into the CSF space via a lumbar puncture, causing the ICP to rise to a plateau level (determined by a balance of extra fluid infusion and increased pressure-gradient driven CSF outflow). [127], [140]–[143], [218]

3. ICP plateau waves – a sudden surge in ICP to a plateau with a duration of 5 to 20 minutes, commonly seen in TBI patients with intact autoregulatory capabilities [144]–[146]. It has been suggested [147] that plateau waves are caused by a vasodilatory cascade (**Figure B3**), where the resistive arterioles dilate due to autoregulation in response to an initial, abrupt, drop in ABP. The effect of increasing cerebral blood volume (CBV) is then transmitted to the intracranial compartment and raises the ICP, causing further reduction in CPP. This vicious cycle results in the continuous rise in ICP until the vessels have exhausted their capacity to dilate, and occurs despite blood pressure restoration which may follow the transient drop.

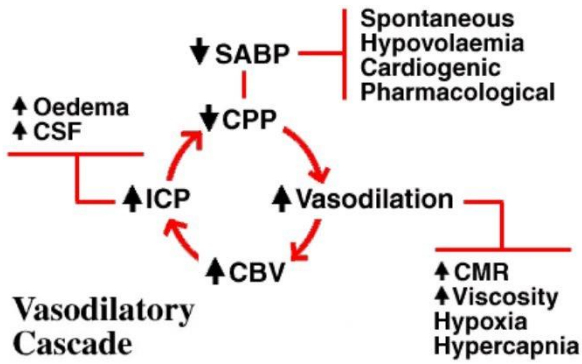

Figure B3. [147] Illustration of factors contributing to vasodilatory cascades

Appendix B

Examples of clinical recordings depicting the pathophysiological phenomena mentioned above were included in **Figure B4**:

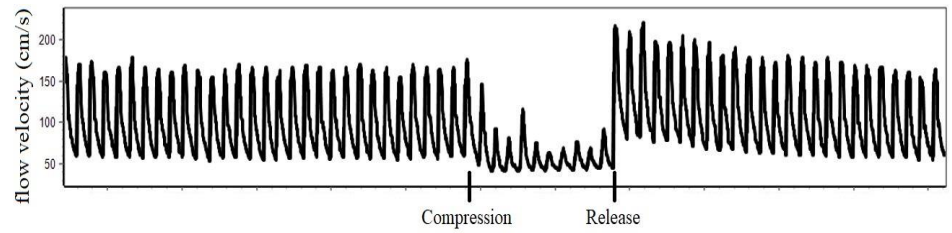

(a)

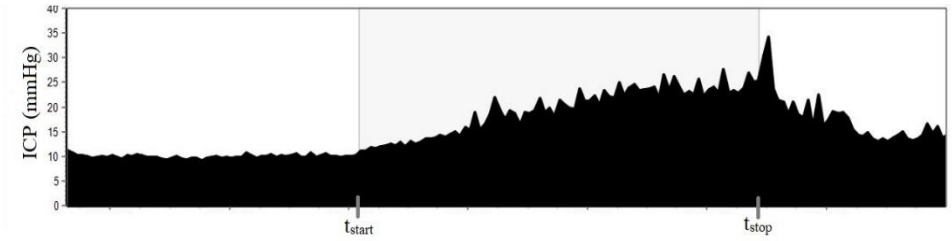

(b)

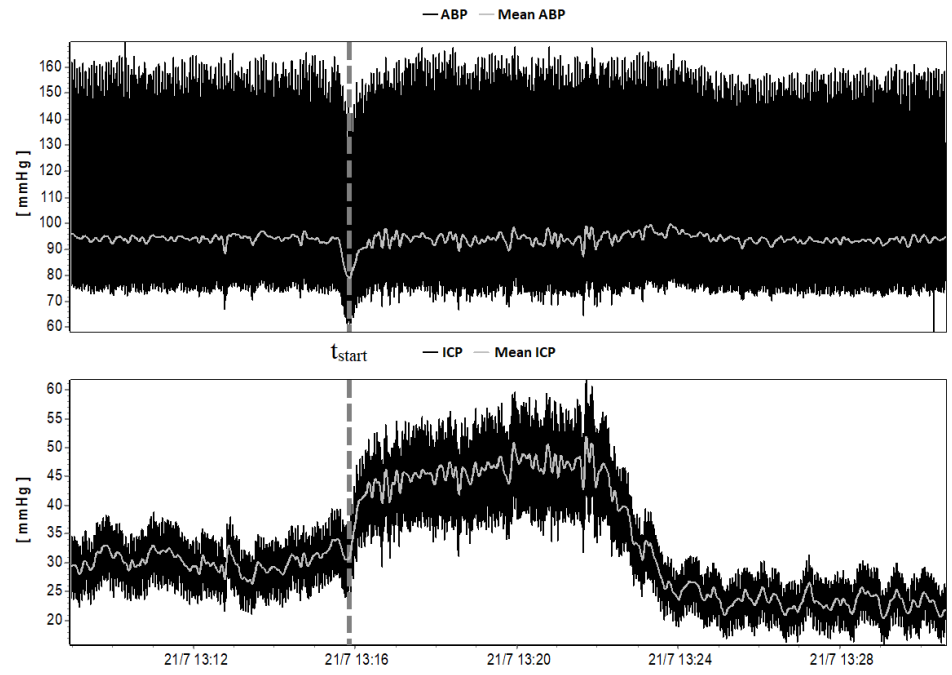

(c)

Figure B4. Clinical recordings of the three pathophysiological phenomena to be simulated by the model: (a) transient hyperaemic response test (THRT), (b) CSF infusion test, and (c) ICP plateau waves (where a rapid rise in ICP was triggered by a sudden drop in ABP, beginning from t_{start}).

3. Results

3.1. Transient hyperaemic response test

The compression of the common carotid artery was represented by a step drop in ABP, before being restored to its original level (**Figure B5** (a)). The responses of CBF and CVR are shown in **Figure B5** (b) and (c) respectively.

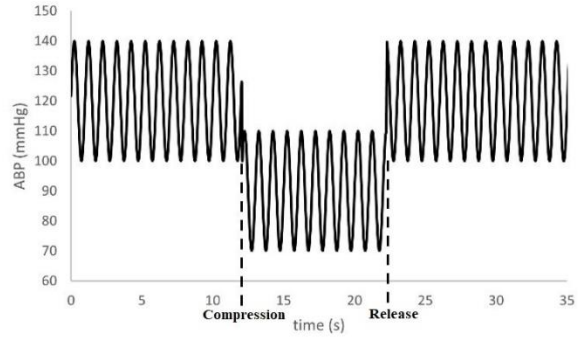

(a)

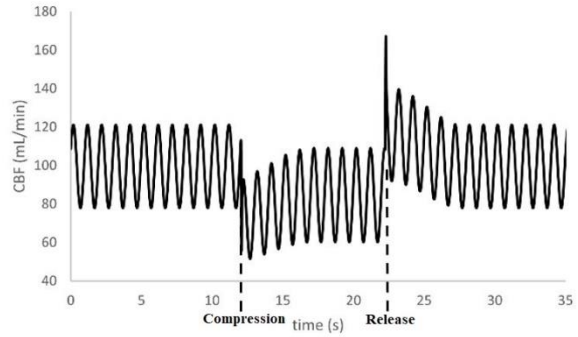

(b)

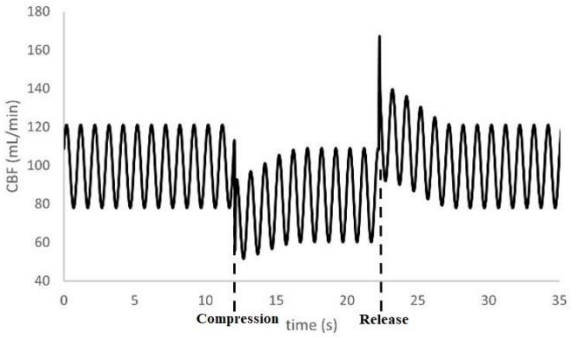

(c)

Figure B5. Simulations of THRT with step changes in ABP between the onset and release of artery compression (a), and the CBF responses with the new (b) and original (c) models.

The CBF simulated by the original was reduced during the compression, provoking visible compensatory vasodilation (decrease in CVR during the compression). After the compression was released, CBF surged before falling gradually to the level before the compression (as CVR returned to its baseline value due to active vasoconstriction). CBF generated by the new model reacted to the step changes in ABP identically: it was suppressed during the compression, before overshooting and returning to the baseline level as the compression was released. This shows that the simulations with both models were able to produce the transient hyperaemic response observed in transcranial Doppler (TCD) ultrasonography recordings [138].

3.2. Infusion test

For the simulations of an infusion stage between t_{start} and t_{stop}, a constant term I_{inf} was added to the rate of CSF formation (I_f) to represent the rate of infusion into the CSF space. The ICP responses are plotted in **Figure B6** (a), while **Figure B6** (b) and (c) illustrate the intracranial pressure-volume relationships of the models, evaluated with the ICM+® software.

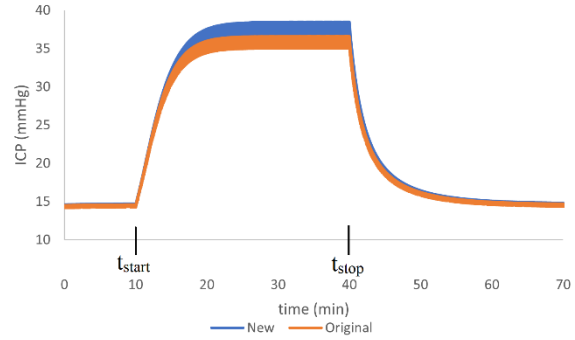

(a)

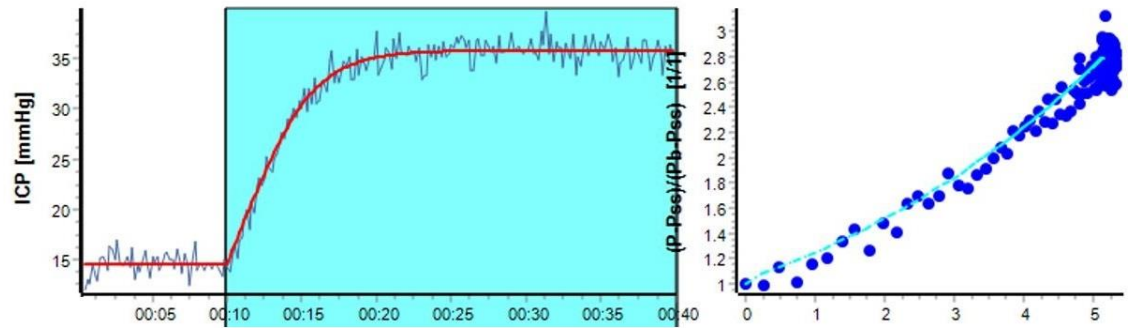

(b)

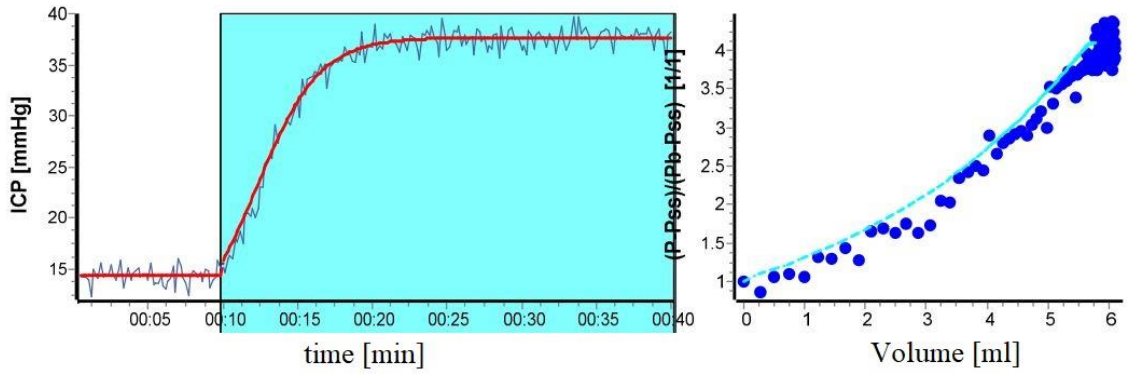

(c)

Figure B6. Simulations of the infusion tests (between t_{start} and t_{stop}) with the models (a); and the analysis with the ICM+® software, illustrating the pressure-volume relationships represented by the original (b) and new (c) models; the R_{CSF} were evaluated to be 13.86 and 14.72 mmHg/mL/min respectively. For illustrative purposes in the curve-fitting process, white noises were added to the generated ICP.

Simulations with both models produced the ICP behaviour commonly seen in real clinical recordings, rising to a plateau during the infusion stage and falling back to the baseline level when the infusion was terminated. However it is worth noting that the ICP generated by the new model rose to a higher level before levelling off; this resulted in a slightly higher value of R_{CSF} produced by the new model.

3.3. Plateau wave

ICP plateau waves were simulated by creating step changes in ABP (**Figure B7** (a)). It was reduced by 10 mmHg initially (stage A), before being raised back to its baseline value (stage B). It was then further increased by 10 mmHg (stage C), and again restored to the baseline level (stage D). In order to produce a significant rise in ICP, the elasticity parameter (E) was set as 0.25, as opposed to 0.05 as in the two previous experiments.

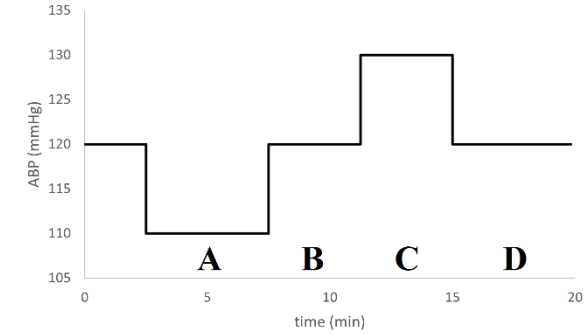

(a)

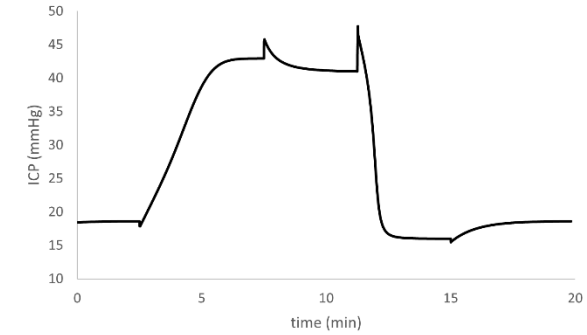

(b)

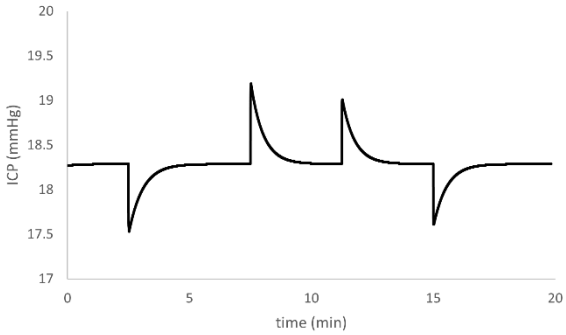

(c)

Figure B7. Simulated ICP for the new (b) and original (c) models, in response to step changes in ABP (a).

The models produced very different results. In the new model, a drop in ABP triggered a rise in ICP from its baseline value (18 mmHg) to a plateau level of 43 mmHg within 5 minutes. Raising the ABP back to its initial value caused the ICP to increase momentarily, before stabilising at a slightly lower level (41 mmHg). Further increase in ABP resulted in a rapid drop of ICP until it flattened slightly below the baseline value (16 mmHg). A final restoration of ABP to its initial level brought the ICP back to its baseline. On the other hand, ICP simulated by the original model displayed momentary perturbations in response to each step change in

ABP. However, it always returned to its baseline level of 18 mmHg; it was not able to simulate the onset of a plateau wave.

4. Discussion

The pressure-flow interactions of each compartment enabled the original model to simulate various physiological responses of flow and pressure commonly observed in clinical practice. For instance, the haemodynamic representation has been successful in simulating the behaviours of CBF in response to changes in CPP; this has allowed the demonstration of the effects of cerebral autoregulation: simulations of THRT have created the characteristic transient hyperaemic responses, which is caused by the vasodilation of resistive arterioles in response to the step drop in ABP. Moreover, the intracranial compartment correctly simulated the response of ICP to constant rate infusion.

However, the sustained effects of vascular constriction and dilation on ICP (such as plateau waves) could not be reflected correctly by the model: in a model consisting of only the vascular and CSF compartments, the state equation in a steady state (without current passing through the dynamic pathways) at node C is reduced as

$$I_f = \frac{P_i - P_{ss}}{R_{csf}}$$

which is the Davson's equation. As I_f, R_{CSF} and P_{ss} are all modelled as constants, P_i (ICP) must also be a constant. This explains why the simulated ICP always returns to a constant value after responding initially to a change in ABP. As a result, the original model cannot transmit any long-term volume changes in the vasculature to the intracranial compartment. Without modifications to the model, any clinical phenomena involving prolonged interactions between the two cannot be simulated correctly. To rectify this, a new static mechanism must be added to link the fluid dynamics in the arterial and intracranial compartments.

Recent studies have established the physiological bases of cerebral ISF circulation [153], [154] and examined its impairment in intracranial pathologies [155], [156]. These findings allowed the mathematical representation of intracellular swelling as the rise in ISF flow resistance, and the reduction in extracellular space volume [149], [150]. With the incorporation of this mechanism, the modelling work by Doron et al. [148] accurately reproduced the elevated ICP due to brain swelling. This study postulated that the dilation of resistive cerebral arterioles can cause the narrowing of the ISF circulation channels, in a similar manner as in cerebral oedema. With the addition of this static pathway, simulated vascular constrictions and dilations can cause persistent changes in ICP. As there is currently a lack of quantitative evidence supporting this hypothesis, the CVR and R_{ISF} were assumed to follow a reciprocal relationship; this serves as a simplification to the intracranial pressure-volume interaction in reality. Due to the current

incomplete understanding of the dynamics of the ISF pathway, it was assumed in the first approximation that the ISF sink pressure is constant. From the perspective of modelling, given we are at this point not interested in estimating the ISF flow itself, it makes no difference if the pressure in this topology is set as zero or other constant values.

Our modified model has proved to be successful in simulations of responses to various physiological simulations. Notably, with increasing ABP (**Figure B7**), the ICP responses produced by the models were markedly different, with the new model accurately reflecting the reduction in ICP with increasing CPP within the range of autoregulation. This is because its inclusion of the ISF compartment allowed the effects of changing CBV in the arterial compartment to be transmitted to the ICP in the intracranial compartment, which the original model failed to represent. When generating plateau waves (**Figure B7**), this transmission is responsible for completing the cycle of vasodilatory cascade, resulting in the rapid rise in ICP as observed in clinical data.

Previous work by Ursino and Giammarco [98] also attempted to generate the plateau waves. Compared to their study, our approach aims to describe the phenomena of cerebrovascular dynamics with a model that is as simple as possible, which only requires a minimal number of parameters. Our ultimate goal is to estimate these parameters from multimodal neuro-

monitoring time series data. Examples of such estimations using our model can be found in the works studying C_a, C_i, CVR and critical closing pressure based on Transcranial Doppler Ultrasonography [48], [219], and R_{CSF} and C_i using infusion tests [220]. Thus, the model has proven itself as a practical base for interpretation of the neuro-monitoring data. With a slight modification to the model, it became possible to demonstrate the intracranial pressure-volume interactions through the generation of plateau waves, and thereby improving the reliability of parameter estimations.

A thorough understanding of the interactions between the haemodynamics and ICP is also important to the interpretation of clinical data related to disturbed CSF circulation. A notable example is the treatment of patients with hydrocephalus; their symptoms can be alleviated with the surgical insertion of a shunt, which drains CSF from the brain to the abdominal cavity. A good prognostication of improvement after shunting requires the accurate estimation of key parameters describing the CSF dynamics, one of which is the resistance of CSF outflow (R_{CSF}). This can be achieved through the simulation of a post-shunting infusion test. The evaluation of R_{CSF} is conventionally based on a model of CSF circulation [157]; it is calculated with the following formula:

$$R_{CSF} = \frac{P_{plateau} - P_{baseline}}{I_{inf}}$$

Where $P_{baseline}$ and $P_{plateau}$ are the ICP at baseline and plateau levels respectively at the infusion test.

Simulations with the new model in this study (**Figure B6**) showed that the rise in ICP resulted in vasodilation, which in turn raised the ICP to a higher level than the original model. This suggests that apart from R_{CSF}, the autoregulation capacity can be another factor determining the ICP dynamics in an infusion study. A mathematical model considering only the CSF compartment may neglect the influence of CBV on ICP, and mistakenly attributing it to R_{CSF}. Theoretically this can result in the overestimation of R_{CSF}. Previous studies have shown that the positive predictive power of R_{CSF} has been clinically acceptable [157], with recommended the R_{CSF} threshold for shunting to be between 13 and 18 mmHg/ml/min [136], [137]. The extra increase in ICP is likely to be small in patients diagnosed for normal pressure hydrocephalus, and thus a small overestimation of R_{CSF} may be on limited clinical significance. Nevertheless, this effect is worth exploring further with concurrent measurements of the strength of cerebral autoregulation during infusion tests.

5. Conclusions

This study investigated the relationships between cerebral blood volume and ICP with an intracranial hydrodynamic model, which was modified to include a compartment representing

the circulation of cerebral ISF and coupled with the cerebrovascular compartment. The modified model was successful in depicting features of intracranial physiology involving the prolonged interplay between CBV and ICP.

Acknowledgements

Funding

Erta Beqiri is supported by the Medical Research Council (grant no.: MR N013433-1) and by the Gates Cambridge Scholarship.

Conflict of Interest

Peter Smielewski and Marek Czosnyka receive part of the licensing fees for ICM+® software, licensed by Cambridge Enterprise Ltd, University of Cambridge, Cambridge.

References

[1] A. Parent, “Regional Anatomy of the Brain,” in *Carpenter’s Human Neuroanatomy*, 9th ed., Baltimore: Williams & Wilkins, 1996, pp. 25–64.

[2] K. P. Cosgrove, C. M. Mazure, and J. K. Staley, “Evolving Knowledge of Sex Differences in Brain Structure, Function and Chemistry,” *Biol. Psychiatry*, vol. 62, no. 8, p. 847, Oct. 2007, doi: 10.1016/J.BIOPSYCH.2007.03.001.

[3] J. Brust, “Circulation of the Brain, The Blood-Brain Barrier, Choroid Plexus, and Cerebrospinal Fluid,” in *Principles of Neural Science*, 5th ed., New York: McGraw-Hill, 2012, pp. 1550–1580.

[4] N. A. LASSEN and O. MUNCK, “The cerebral blood flow in man determined by the use of radioactive krypton,” *Acta Physiol. Scand.*, vol. 33, no. 1, pp. 30–49, 1955, doi: 10.1111/J.1748-1716.1955.TB01191.X.

[5] L. Sakka, G. Coll, and J. Chazal, “Anatomy and physiology of cerebrospinal fluid,” *Eur. Ann. Otorhinolaryngol. Head Neck Dis.*, vol. 128, no. 6, pp. 309–316, 2011, doi: 10.1016/J.ANORL.2011.03.002.

[6] T. Champney, “Blood vessels, meninges, and ventricles,” in *Essential clinical neuroanatomy*, 1st ed., Wiley Blackwell, 2016, pp. 20–38.

[7] J. D. Martin, “Vasculature of the Central Nervous System and the Cerebrosptnal Fluid,” in *Neuroanatomy: Text and Atlas*, 5th ed., McGraw Hill, 2021, pp. 53–75.

[8] M. J. Cipolla, “Anatomy and Ultrastructure,” in *The Cerebral Circulation.*, Morgan & Claypool Life Sciences, 2010.

[9] Hall, “Lipid Metabolism,” in *Guyton and Hall Textbook of Medical Physiology*, 14th ed., 2016, pp. 853–864.

[10] L. A. Martinez-Lemus, “The dynamic structure of arterioles,” *Basic Clin. Pharmacol.*

Toxicol., vol. 110, no. 1, pp. 5–11, Jan. 2012, doi: 10.1111/J.1742-7843.2011.00813.X.

[11] R. Carroll, "Vascular Segments," in *Elsevier's Integrated Physiology*, Elsevier, 2007, pp. 77–89.

[12] E. Shardlow and A. Jackson, "Cerebral blood flow and intracranial pressure," *Anaesth. Intensive Care Med.*, vol. 9, no. 5, pp. 222–225, May 2008, doi: 10.1016/J.MPAIC.2008.03.009.

[13] N. A. LASSEN, "Cerebral Blood Flow and Oxygen Consumption in Man," *https://doi.org/10.1152/physrev.1959.39.2.183*, vol. 39, no. 2, pp. 183–238, Apr. 1959, doi: 10.1152/PHYSREV.1959.39.2.183.

[14] S. P. Klein, V. De Sloovere, G. Meyfroidt, and B. Depreitere, "Differential Hemodynamic Response of Pial Arterioles Contributes to a Quadriphasic Cerebral Autoregulation Physiology," *J. Am. Heart Assoc.*, vol. 11, no. 1, p. 22943, Jan. 2022, doi: 10.1161/JAHA.121.022943.

[15] S. J. Phillips and J. P. Whisnant, "Hypertension and the Brain," *Arch. Intern. Med.*, vol. 152, no. 5, pp. 938–945, May 1992, doi: 10.1001/ARCHINTE.1992.00400170028006.

[16] N. A. Lassen, "Normal average value of cerebral blood flow in younger adults is 50 ml/100 g/min," *J. Cereb. Blood Flow Metab.*, vol. 5, no. 3, pp. 347–349, 1985, doi: 10.1038/JCBFM.1985.48.

[17] K. Hoedt-Rasmussen, E. Sveinsdottir, and N. A. Lassen, "Regional cerebral blood flow in man determined by intra-arterial injection of radioactive inert gas," *Circ. Res.*, vol. 18, no. 3, pp. 237–247, 1966, doi: 10.1161/01.RES.18.3.237.

[18] D. H. Ingvar, S. Cronqvist, R. Ekberg, J. Risberg, and K. Høedt-Rasmussen, "Normal values of regional cerebral blood flow in man, including flow and weight estimates of gray and white matter. A preliminary summary," *Acta Neurol. Scand. Suppl.*, vol. 14, no. 14 S, pp. 72–78, 1965, doi: 10.1111/J.1600-0404.1965.TB01958.X.

[19] J. E. Rees, J. W. D. Bull, G. H. DU Boulay, J. Marshall, R. W. Ross russell, and L. Symon, "The Comparative Analysis of Isotope Clearance Curves in Normal and Ischemic Brain," *Stroke*, vol. 2, no. 5, pp. 444–451, 1971, doi: 10.1161/01.STR.2.5.444.

[20] E. Sveinsdottir, P. Torlöf, J. Risberg, D. H. Ingvar, and N. A. Lassen, "Monitoring regional cerebral blood flow in normal man with a computer-controlled 32-dector system," *Eur. Neurol.*, vol. 6, no. 1, pp. 228–233, 1971, doi: 10.1159/000114498.

[21] S. Strandgaard, J. V. Jones, E. T. MacKenzie, and A. M. Harper, "Upper limit of cerebral blood flow autoregulation in experimental renovascular hypertension in the baboon," *Circ. Res.*, vol. 37, no. 2, pp. 164–167, 1975, doi: 10.1161/01.RES.37.2.164.

[22] A. J. Peixoto, "Acute Severe Hypertension," *N. Engl. J. Med.*, vol. 381, no. 19, pp. 1843–1852, Nov. 2019, doi: 10.1056/NEJMCP1901117/SUPPL_FILE/NEJMCP1901117_DISCLOSURES.PDF.

[23] I. Gonzalez-Marrero, L. G. Hernández-Abad, L. Castañeyra-Ruiz, E. M. Carmona-Calero, and A. Castañeyra-Perdomo, "Variaciones de los plexos coroideos y las barreras cerebrales en la hipertensión arterial y el envejecimiento," *Neurología*, vol. 37, no. 5, pp. 371–382, Jun. 2022, doi: 10.1016/J.NRL.2018.06.001.

[24] B. Ekström-Jodal, E. Häggendal, L. E. Linder, and N. J. Nilsson, "Cerebral blood flow autoregulation at high arterial pressures and different levels of carbon dioxide tension in dogs," *Eur. Neurol.*, vol. 6, no. 1, pp. 6–10, 1971, doi: 10.1159/000114457.

[25] H. K. Kimelberg, "Current concepts of brain edema. Review of laboratory investigations," *J. Neurosurg.*, vol. 83, no. 6, pp. 1051–1059, 1995, doi: 10.3171/JNS.1995.83.6.1051.

[26] A. W. Unterberg, J. Stover, B. Kress, and K. L. Kiening, "Edema and brain trauma," *Neuroscience*, vol. 129, no. 4, pp. 1019–1027, 2004, doi: 10.1016/J.NEUROSCIENCE.2004.06.046.

[27] H. K. Kimelberg, “Water homeostasis in the brain: basic concepts,” *Neuroscience*, vol. 129, no. 4, pp. 851–860, 2004, doi: 10.1016/J.NEUROSCIENCE.2004.07.033.

[28] J. A. H. R. Claassen, D. H. J. Thijssen, R. B. Panerai, and F. M. Faraci, “Regulation of cerebral blood flowin humans: Physiology and clinical implications of autoregulation,” *Physiol. Rev.*, vol. 101, no. 4, pp. 1487–1559, 2021, doi: 10.1152/physrev.00022.2020.

[29] R. L. Hoiland, A. R. Bain, M. G. Rieger, D. M. Bailey, and P. N. Ainslie, “Hypoxemia, oxygen content, and the regulation of cerebral blood flow,” *Am. J. Physiol. Regul. Integr. Comp. Physiol.*, vol. 310, no. 5, pp. R398–R413, Mar. 2016, doi: 10.1152/AJPREGU.00270.2015.

[30] S. S. Kety and C. F. Schmidt, “THE EFFECTS OF ALTERED ARTERIAL TENSIONS OF CARBON DIOXIDE AND OXYGEN ON CEREBRAL BLOOD FLOW AND CEREBRAL OXYGEN CONSUMPTION OF NORMAL YOUNG MEN,” *J. Clin. Invest.*, vol. 27, no. 4, p. 484, Jul. 1948, doi: 10.1172/JCI101995.

[31] C. K. Willie *et al.*, “Regional brain blood flow in man during acute changes in arterial blood gases,” *J. Physiol.*, vol. 590, no. 14, pp. 3261–3275, Jul. 2012, doi: 10.1113/JPHYSIOL.2012.228551.

[32] A. G. Schneider *et al.*, “Arterial carbon dioxide tension and outcome in patients admitted to the intensive care unit after cardiac arrest,” *Resuscitation*, vol. 84, no. 7, pp. 927–934, Jul. 2013, doi: 10.1016/J.RESUSCITATION.2013.02.014.

[33] R. L. Hoiland, C. Robba, D. K. Menon, G. Citerio, C. Sandroni, and M. S. Sekhon, “Clinical targeting of the cerebral oxygen cascade to improve brain oxygenation in patients with hypoxic-ischaemic brain injury after cardiac arrest,” *Intensive Care Med.*, vol. 49, no. 9, pp. 1062–1078, Sep. 2023, doi: 10.1007/S00134-023-07165-X.

[34] N. Radhakrishnan, “Etiology of varicose veins,” in *Genesis, Pathophysiology and Management of Venous and Lymphatic Disorders*, Elsevier, 2022, pp. 139–144.

[35] T. Kiliç and A. Akakin, “Anatomy of cerebral veins and sinuses,” *Front. Neurol.*

Neurosci., vol. 23, pp. 4–15, 2008, doi: 10.1159/000111256.

[36] S. Piechnik, “The venous cerebrovascular bed and venous outflow from the brain,” in *A Mathematical and Biophysical Modelling of Cerebral Blood Flow and Cerebrospinal Fluid Dynamics.*, 1st ed., Cambridge University Press., 2000, pp. 22–25.

[37] M. Chopp, H. D. Portnoy, and C. Branch, “Hydraulic model of the cerebrovascular bed: an aid to understanding the volume-pressure test,” *Neurosurgery*, vol. 13, no. 1, pp. 5–11, 1983, doi: 10.1227/00006123-198307000-00002.

[38] R. De Simone, A. Ranieri, and V. Bonavita, “Starling resistors, autoregulation of cerebral perfusion and the pathogenesis of idiopathic intracranial hypertension,” *Panminerva Med.*, vol. 59, no. 1, pp. 76–89, Mar. 2017, doi: 10.23736/S0031-0808.16.03248-1.

[39] S. Piechnik, “A Mathematical and Biophysical Modelling of Cerebral Blood Flow and Cerebrospinal Fluid Dynamics,” University of Cambridge, 2000.

[40] D. Orešković and M. Klarica, “The formation of cerebrospinal fluid: nearly a hundred years of interpretations and misinterpretations,” *Brain Res. Rev.*, vol. 64, no. 2, pp. 241–262, Sep. 2010, doi: 10.1016/J.BRAINRESREV.2010.04.006.

[41] J. Buishas, I. G. Gould, and A. A. Linninger, “A computational model of cerebrospinal fluid production and reabsorption driven by Starling forces,” *Croat. Med. J.*, vol. 55, no. 5, p. 481, 2014, doi: 10.3325/CMJ.2014.55.481.

[42] N. A. Jessen, A. S. F. Munk, I. Lundgaard, and M. Nedergaard, “The Glymphatic System – A Beginner’s Guide,” *Neurochem. Res.*, vol. 40, no. 12, p. 2583, Dec. 2015, doi: 10.1007/S11064-015-1581-6.

[43] A. Monro, “Observations on the Structure and Functions of the Nervous System,” *london Med. J.*, vol. 4, no. 2, pp. 113–135, 1783.

[44] G. Kellie, “An Account of the Appearances Observed in the Dissection of Two of

Three Individuals Presumed to Have Perished in the Storm of the 3d, and Whose Bodies Were Discovered in the Vicinity of Leith on the Morning of the 4th, November 1821; with Some Reflection," *Trans. Medico-Chirurgical Soc. Edinburgh*, vol. 1, pp. 84–122, 1824, [Online]. Available: http://www.ncbi.nlm.nih.gov/pubmed/29583621%0Ahttp://www.pubmedcentral.nih.gov/articlerender.fcgi?artid=PMC5405298.

[45] A. J. Wells, P. Smielewski, R. A. Trivedi, and P. J. Hutchinson, "Intracranial Pressure Monitoring in Head Injury," in *Traumatic Brain Injury: A Multidisciplinary Approach*, 1st ed., Cambridge: Cambridge University Press, 2020, pp. 110–131.

[46] L. A. Steiner and P. J. D. Andrews, "Monitoring the injured brain: ICP and CBF," *Br. J. Anaesth.*, vol. 97, no. 1, pp. 26–38, 2006, doi: 10.1093/bja/ael110.

[47] M. Czosnyka and J. D. Pickard, "Monitoring and interpretation of intracranial pressure," *J. Neurol. Neurosurg. Psychiatry*, vol. 75, no. 6, pp. 813–821, Jun. 2004, doi: 10.1136/JNNP.2003.033126.

[48] M. Czosnyka, S. Piechnik, H. K. Richards, P. Kirkpatrick, P. Smielewski, and J. D. Pickard, "Contribution of mathematical modelling to the interpretation of bedside tests of cerebrovascular autoregulation," *J. Neurol. Neurosurg. Psychiatry*, vol. 63, no. 6, pp. 721–731, 1997, doi: 10.1136/jnnp.63.6.721.

[49] J. Szewczykowski, S. Sliwka, A. Kunicki, P. Dytko, and J. Korsak-Sliwka, "A fast method of estimating the elastance of the intracranial system," *J. Neurosurg.*, vol. 47, no. 1, pp. 19–26, 1977, doi: 10.3171/JNS.1977.47.1.0019.

[50] N. Alperin, R. Burman, and S. H. Lee, "Role of the spinal canal compliance in regulating posture-related cerebrospinal fluid hydrodynamics in humans," *J. Magn. Reson. Imaging*, vol. 54, no. 1, pp. 206–214, 2021, doi: 10.1002/jmri.27505.

[51] H. D. Portnoy, M. Chopp, C. Branch, and M. B. Shannon, "Cerebrospinal fluid pulse waveform as an indicator of cerebral autoregulation," *J. Neurosurg.*, vol. 56, no. 5, pp.

666–678, 1982, doi: 10.3171/JNS.1982.56.5.0666.

[52] I. R. Piper, J. D. Miller, N. M. Dearden, J. R. S. Leggate, and I. Robertson, "Systems analysis of cerebrovascular pressure transmission: an observational study in head-injured patients," *J. Neurosurg.*, vol. 73, no. 6, pp. 871–880, 1990, doi: 10.3171/JNS.1990.73.6.0871.

[53] R. C. Dewey, H. P. Pieper, and W. E. Hunt, "Experimental cerebral hemodynamics. Vasomotor tone, critical closing pressure, and vascular bed resistance," *J. Neurosurg.*, vol. 41, no. 5, pp. 597–606, 1974, doi: 10.3171/JNS.1974.41.5.0597.

[54] N. Capra, "Anatomic and physiologic aspects of venous system," in *Cerebral Blood Flow, Physiologic and Clinical Aspects*, New York: McGraw-Hill, 1987, pp. 37–58.

[55] L. J. Carroll, J. D. Cassidy, L. Holm, J. Kraus, and V. G. Coronado, "Methodological issues and research recommendations for mild traumatic brain injury: the WHO Collaborating Centre Task Force on Mild Traumatic Brain Injury," *J. Rehabil. Med.*, no. 43 Suppl, pp. 113–125, Feb. 2004, doi: 10.1080/16501960410023877.

[56] D. K. Menon, K. Schwab, D. W. Wright, and A. I. Maas, "Position statement: definition of traumatic brain injury," *Arch. Phys. Med. Rehabil.*, vol. 91, no. 11, pp. 1637–1640, 2010, doi: 10.1016/J.APMR.2010.05.017.

[57] V. L. Feigin *et al.*, "Incidence of traumatic brain injury in New Zealand: a population-based study," *Lancet. Neurol.*, vol. 12, no. 1, pp. 53–64, Jan. 2013, doi: 10.1016/S1474-4422(12)70262-4.

[58] A. I. Maas, N. Stocchetti, and R. Bullock, "Moderate and severe traumatic brain injury in adults," *Lancet. Neurol.*, vol. 7, no. 8, pp. 728–741, Aug. 2008, doi: 10.1016/S1474-4422(08)70164-9.

[59] A. Brazinova *et al.*, "Epidemiology of Traumatic Brain Injury in Europe: A Living Systematic Review," *J. Neurotrauma*, vol. 38, no. 10, pp. 1411–1440, May 2021, doi: 10.1089/NEU.2015.4126.

[60] J. V. Rosenfeld, A. I. Maas, P. Bragge, M. C. Morganti-Kossmann, G. T. Manley, and R. L. Gruen, "Early management of severe traumatic brain injury," *Lancet (London, England)*, vol. 380, no. 9847, pp. 1088–1098, 2012, doi: 10.1016/S0140-6736(12)60864-2.

[61] G. Teasdale and B. Jennett, "Assessment of coma and impaired consciousness. A practical scale," *Lancet (London, England)*, vol. 2, no. 7872, pp. 81–84, Jul. 1974, doi: 10.1016/S0140-6736(74)91639-0.

[62] A. I. R. Maas *et al.*, "Traumatic brain injury: integrated approaches to improve prevention, clinical care, and research," *Lancet. Neurol.*, vol. 16, no. 12, pp. 987–1048, Dec. 2017, doi: 10.1016/S1474-4422(17)30371-X.

[63] L. Wilson *et al.*, "The chronic and evolving neurological consequences of traumatic brain injury," *Lancet. Neurol.*, vol. 16, no. 10, pp. 813–825, Oct. 2017, doi: 10.1016/S1474-4422(17)30279-X.

[64] J. van der Naalt *et al.*, "Early predictors of outcome after mild traumatic brain injury (UPFRONT): an observational cohort study," *Lancet. Neurol.*, vol. 16, no. 7, pp. 532–540, Jul. 2017, doi: 10.1016/S1474-4422(17)30117-5.

[65] Munakomi, "Brain Herniation," in *StatPearls*, StatPearls Publishing, 2023.

[66] N. Carney *et al.*, "Guidelines for the Management of Severe Traumatic Brain Injury, Fourth Edition," *Neurosurgery*, vol. 80, no. 1, pp. 6–15, Jan. 2017, doi: 10.1227/NEU.0000000000001432.

[67] T. Svedung Wettervik *et al.*, "Brain tissue oxygen monitoring in traumatic brain injury-part II: isolated and combined insults in relation to outcome," *Crit. Care*, vol. 27, no. 1, Dec. 2023, doi: 10.1186/S13054-023-04659-4.

[68] G. W. J. Hawryluk *et al.*, "A management algorithm for patients with intracranial pressure monitoring: the Seattle International Severe Traumatic Brain Injury Consensus Conference (SIBICC)," *Intensive Care Med.*, vol. 45, no. 12, p. 1783, Dec.

2019, doi: 10.1007/S00134-019-05805-9.

[69] R. M. Chesnut, “Intracranial pressure monitoring: Headstone or a new head start. the BEST TRIP trial in perspective,” *Intensive Care Med.*, vol. 39, no. 4, pp. 771–774, Apr. 2013, doi: 10.1007/S00134-013-2852-9/METRICS.

[70] J. F. Payen *et al.*, “Intracranial pressure monitoring with and without brain tissue oxygen pressure monitoring for severe traumatic brain injury in France (OXY-TC): an open-label, randomised controlled superiority trial,” *Lancet. Neurol.*, vol. 22, no. 11, pp. 1005–1014, Nov. 2023, doi: 10.1016/S1474-4422(23)00290-9.

[71] G. E. Sviri, R. Aaslid, C. M. Douville, A. Moore, and D. W. Newell, “Time course for autoregulation recovery following severe traumatic brain injury,” *J. Neurosurg.*, vol. 111, no. 4, pp. 695–700, 2009, doi: 10.3171/2008.10.17686.

[72] G. J. Bouma, J. P. Muizelaar, W. A. Stringer, S. C. Choi, P. Fatouros, and H. F. Young, “Ultra-early evaluation of regional cerebral blood flow in severely head-injured patients using xenon-enhanced computerized tomography,” *J. Neurosurg.*, vol. 77, no. 3, pp. 360–368, 1992, doi: 10.3171/JNS.1992.77.3.0360.

[73] A. Ter Minassian, L. Dubé, A. M. Guilleux, N. Wehrmann, M. Ursino, and L. Beydon, “Changes in intracranial pressure and cerebral autoregulation in patients with severe traumatic brain injury,” *Crit. Care Med.*, vol. 30, no. 7, pp. 1616–1622, 2002, doi: 10.1097/00003246-200207000-00036.

[74] E. W. Lang and R. M. Chesnut, “A bedside method for investigating the integrity and critical thresholds of cerebral pressure autoregulation in severe traumatic brain injury patients,” *Br. J. Neurosurg.*, vol. 14, no. 2, pp. 117–126, 2000, doi: 10.1080/02688690050004534.

[75] T. Howells, “Pressure reactivity as a guide in the treatment of cerebral perfusion pressure in patients with brain trauma,” *J. Neurosurg.*, vol. 102, no. 2, pp. 311–313, Apr. 2005, doi: 10.3171/JNS.2005.102.2.0311.

[76] R. Hlatky, A. B. Valadka, and C. S. Robertson, "Intracranial pressure response to induced hypertension: role of dynamic pressure autoregulation," *Neurosurgery*, vol. 57, no. 5, pp. 917–922, Nov. 2005, doi: 10.1227/01.NEU.0000180025.43747.FC.

[77] E. Beqiri *et al.*, "Feasibility of individualised severe traumatic brain injury management using an automated assessment of optimal cerebral perfusion pressure: the COGiTATE phase II study protocol," *BMJ Open*, vol. 9, no. 9, 2019, doi: 10.1136/BMJOPEN-2019-030727.

[78] M. Czosnyka *et al.*, "Intracranial pressure: more than a number," *Neurosurg. Focus*, vol. 22, no. 5, 2007, doi: 10.3171/FOC.2007.22.5.11.

[79] M. Czosnyka, P. Smielewski, P. Kirkpatrick, R. J. Laing, D. Menon, and J. D. Pickard, "Continuous assessment of the cerebral vasomotor reactivity in head injury," *Neurosurgery*, vol. 41, no. 1, pp. 11–19, Jul. 1997, doi: 10.1097/00006123-199707000-00005.

[80] M. Balestreri *et al.*, "Impact of intracranial pressure and cerebral perfusion pressure on severe disability and mortality after head injury," *Neurocrit. Care*, vol. 4, no. 1, pp. 008–013, 2006, doi: 10.1385/NCC:4:1:008.

[81] M. Balestreri *et al.*, "Association between outcome, cerebral pressure reactivity and slow ICP waves following head injury," *Acta Neurochir. Suppl.*, vol. 95, no. 95, pp. 25–28, 2005, doi: 10.1007/3-211-32318-X_6.

[82] L. A. Steiner *et al.*, "Continuous monitoring of cerebrovascular pressure reactivity allows determination of optimal cerebral perfusion pressure in patients with traumatic brain injury," *Crit. Care Med.*, vol. 30, no. 4, pp. 733–738, 2002, doi: 10.1097/00003246-200204000-00002.

[83] M. J. H. Aries *et al.*, "Continuous determination of optimal cerebral perfusion pressure in traumatic brain injury," *Crit. Care Med.*, vol. 40, no. 8, pp. 2456–2463, Aug. 2012, doi: 10.1097/CCM.0B013E3182514EB6.

[84] J. Tas *et al.*, "Targeting Autoregulation-Guided Cerebral Perfusion Pressure after Traumatic Brain Injury (COGiTATE): A Feasibility Randomized Controlled Clinical Trial," *J. Neurotrauma*, vol. 38, no. 20, pp. 2790–2800, Oct. 2021, doi: 10.1089/NEU.2021.0197/SUPPL_FILE/SUPP_APPS1.PDF.

[85] A. Sarwal, C. Robba, C. Venegas, W. Ziai, M. Czosnyka, and D. Sharma, "Are We Ready for Clinical Therapy based on Cerebral Autoregulation? A Pro-con Debate," *Neurocrit. Care*, 2023, doi: 10.1007/s12028-023-01741-1.

[86] M. Czosnyka *et al.*, "Significance of intracranial pressure waveform analysis after head injury," *Acta Neurochir. (Wien).*, vol. 138, no. 5, pp. 531–542, 1996, doi: 10.1007/BF01411173.

[87] G. C. Agarwal, B. M. Berman, and L. Stark, "A lumped parameter model of the cerebrospinal fluid system," *IEEE Trans. Biomed. Eng.*, vol. 16, no. 1, pp. 45–53, 1969, doi: 10.1109/TBME.1969.4502602.

[88] R. Tym, S. Lichtenstein, and J. Leutheusser, "The Munro-Kellie Doctrine and the Intracranial Venous Space at the 'Limit' of Raised Intracranial Pressure — an Hydrodynamic Experimental Approach," *Intracranial Press.*, pp. 139–143, 1972, doi: 10.1007/978-3-642-65486-2_23.

[89] S. Hakim, J. G. Venegas, and J. D. Burton, "The physics of the cranial cavity, hydrocephalus and normal pressure hydrocephalus: mechanical interpretation and mathematical model.," *Surg. Neurol.*, vol. 5, no. 3, pp. 187–210, Mar. 1976, Accessed: Feb. 04, 2024. [Online]. Available: https://europepmc.org/article/MED/1257894.

[90] A. Marmarou, K. Shulman, and R. M. Rosende, "A nonlinear analysis of the cerebrospinal fluid system and intracranial pressure dynamics," *J. Neurosurg.*, vol. 48, no. 3, pp. 332–344, 1978, doi: 10.3171/JNS.1978.48.3.0332.

[91] O. Hoffmann, "Biomathematics of intracranial CSF and haemodynamics. Simulation and analysis with the aid of a mathematical model.," *Acta Neurochir. Suppl. (Wien).*,

vol. 40, pp. 117–130, 1987, doi: 10.1007/978-3-7091-8941-2_6/COVER.

[92] O. Hoffmann and J. T. Zierski, “Analysis of the ICP pulse-pressure relationship as a function of arterial blood pressure. Clinical validation of a mathematical model,” *Acta Neurochir. (Wien).*, vol. 66, no. 1–2, pp. 1–21, Mar. 1982, doi: 10.1007/BF01809300.

[93] T. Takemae, Y. Kosugi, J. Ikebe, Y. Kumagai, K. Matsuyama, and H. Saito, “A simulation study of intracranial pressure increment using an electrical circuit model of cerebral circulation,” *IEEE Trans. Biomed. Eng.*, vol. 34, no. 12, pp. 958–962, 1987, doi: 10.1109/TBME.1987.325935.

[94] H. L. Rekate, “The usefulness of mathematical modeling in hydrocephalus research,” *Child’s Nerv. Syst.*, vol. 10, no. 1, pp. 13–18, Jan. 1994, doi: 10.1007/BF00313579/METRICS.

[95] H. L. Rekate, J. A. Brodkey, H. J. Chizeck, W. El Sakka, and W. H. Ko, “Ventricular volume regulation: a mathematical model and computer simulation,” *Pediatr. Neurosci.*, vol. 14, no. 2, pp. 77–84, 1988, doi: 10.1159/000120367.

[96] S. Sorek, J. Bear, and Z. Karni, “Resistances and compliances of a compartmental model of the cerebrovascular system,” *Ann. Biomed. Eng.*, vol. 17, no. 1, pp. 1–12, 1989, doi: 10.1007/BF02364270.

[97] H. Nishimura and N. Yasui, “A Simulation Study of Wave Transformation Using a Nonlinear Model of Artery and a Physical Model of Intracranial Vascular Bed,” *Intracranial Press. VIII*, pp. 390–393, 1993, doi: 10.1007/978-3-642-77789-9_83.

[98] M. Ursino and P. Di Giammarco, “A mathematical model of the relationship between cerebral blood volume and intracranial pressure changes: The generation of plateau waves,” *Ann. Biomed. Eng.*, vol. 19, no. 1, pp. 15–42, 1991, doi: 10.1007/BF02368459.

[99] M. Ursino, C. A. Lodi, S. Rossi, and N. Stocchetti, “Intracranial pressure dynamics in patients with acute brain damage,” *J. Appl. Physiol.*, vol. 82, no. 4, pp. 1270–1282,

1997, doi: 10.1152/jappl.1997.82.4.1270.

[100] M. Ursino and C. A. Lodi, “A simple mathematical model of the interaction between intracranial pressure and cerebral hemodynamics,” *J. Appl. Physiol.*, vol. 82, no. 4, pp. 1256–1269, 1997, doi: 10.1152/JAPPL.1997.82.4.1256.

[101] W. J. Thoman, S. Lampotang, D. Gravenstein, and J. Van Der Aa, “A computer model of intracranial dynamics integrated to a full-scale patient simulator,” *Comput. Biomed. Res.*, vol. 31, no. 1, pp. 32–46, 1998, doi: 10.1006/cbmr.1997.1463.

[102] C. A. Lodi, A. Ter Minassian, L. Beydon, and M. Ursino, “Modeling cerebral autoregulation and CO2 reactivity in patients with severe head injury,” *Am. J. Physiol. - Hear. Circ. Physiol.*, vol. 274, no. 5 43-5, pp. 1729–1741, 1998, doi: 10.1152/ajpheart.1998.274.5.h1729.

[103] M. Ursino, C. A. Lodi, C. Alberto, and L. Interaction, “and Intracranial Pressure : a Mathematical Model,” *Am J Physiol Hear. Circ Physiol*, vol. 274, no. 51, pp. 1715–1728, 1998, [Online]. Available: http://ajpheart.physiology.org/content/274/5/H1715.short.

[104] R. B. Panerai, S. L. Dawson, and J. F. Potter, “Linear and nonlinear analysis of human dynamic cerebral autoregulation,” *Am. J. Physiol. - Hear. Circ. Physiol.*, vol. 277, no. 3 46-3, pp. 1089–1099, 1999, doi: 10.1152/ajpheart.1999.277.3.h1089.

[105] S. K. Kirkham, R. E. Craine, and A. A. Birch, “A new mathematical model of dynamic cerebral autoregulation based on a flow dependent feedback mechanism,” *Physiol. Meas.*, vol. 22, no. 3, pp. 461–473, 2001, doi: 10.1088/0967-3334/22/3/305.

[106] S. K. Piechnik, M. Czosnyka, H. K. Richards, P. C. Whitfield, and J. D. Pickard, “Cerebral venous blood outflow: A theoretical model based on laboratory simulation,” *Neurosurgery*, vol. 49, no. 5, pp. 1214–1223, 2001, doi: 10.1097/00006123-200111000-00034.

[107] M. S. Olufsen, A. Nadim, and L. A. Lipsitz, “Dynamics of cerebral blood flow

regulation explained using a lumped parameter model," *Am. J. Physiol. - Regul. Integr. Comp. Physiol.*, vol. 282, no. 2 51-2, pp. 611–622, 2002, doi: 10.1152/ajpregu.00285.2001.

[108] J. Yang, J. W. Clark, R. M. Bryan, and C. S. Robertson, "The myogenic response in isolated rat cerebrovascular arteries: Vessel model," *Med. Eng. Phys.*, vol. 25, no. 8, pp. 711–717, 2003, doi: 10.1016/S1350-4533(03)00101-2.

[109] S. K. Piechnik, M. Czosnyka, N. G. Harris, P. S. Minhas, and J. D. Pickard, "A model of the cerebral and cerebrospinal fluid circulations to examine asymmetry in cerebrovascular reactivity," *J. Cereb. Blood Flow Metab.*, vol. 21, no. 2, pp. 182–192, 2001, doi: 10.1097/00004647-200102000-00010.

[110] T. David, M. Brown, and A. Ferrandez, "Auto-regulation and blood flow in the cerebral circulation," *Int. J. Numer. Methods Fluids*, vol. 43, no. 6–7, pp. 701–713, 2003, doi: 10.1002/fld.495.

[111] M. Banaji, I. Tachtsidis, D. Delpy, and S. Baigent, "A physiological model of cerebral blood flow control," *Math. Biosci.*, vol. 194, no. 2, pp. 125–173, 2005, doi: 10.1016/j.mbs.2004.10.005.

[112] S. J. Payne, H. J. Morris, and A. B. Rowley, "A combined haemodynamic and biochemical model of cerebral autoregulation," *Annu. Int. Conf. IEEE Eng. Med. Biol. - Proc.*, vol. 7 VOLS, pp. 2295–2298, 2005, doi: 10.1109/iembs.2005.1616923.

[113] J. Alastruey, S. M. Moore, K. H. Parker, T. David, J. Peiró, and S. J. Sherwin, "Reduced modelling of blood flow in the cerebral circulation: Coupling 1-D, 0-D and cerebral auto-regulation models," *Int. J. Numer. Methods Fluids*, vol. 56, no. 8, pp. 1061–1067, Mar. 2008, doi: 10.1002/FLD.1606.

[114] S. K. Piechnik, P. A. Chiarelli, and P. Jezzard, "Modelling vascular reactivity to investigate the basis of the relationship between cerebral blood volume and flow under CO2 manipulation," *Neuroimage*, vol. 39, no. 1, pp. 107–118, 2008, doi:

10.1016/j.neuroimage.2007.08.022.

[115] M. Giannessi, M. Ursino, and W. B. Murray, “The design of a digital cerebrovascular simulation model for teaching and research,” *Anesth. Analg.*, vol. 107, no. 6, pp. 1997–2008, 2008, doi: 10.1213/ane.0b013e318187b987.

[116] Y. Zheng and J. Mayhew, “A time-invariant visco-elastic windkessel model relating blood flow and blood volume,” *Neuroimage*, vol. 47, no. 4, pp. 1371–1380, Oct. 2009, doi: 10.1016/J.NEUROIMAGE.2009.04.022.

[117] S. R. Pope, L. M. Ellwein, C. L. Zapata, V. Novak, C. T. Kelley, and M. S. Olufsen, “Estimation and identification of parameters in a lumped cerebrovascular model,” *Math. Biosci. Eng.*, vol. 6, no. 1, pp. 93–115, 2009, doi: 10.3934/mbe.2009.6.93.

[118] G. S. H. Chan *et al.*, “Contribution of arterial Windkessel in low-frequency cerebral hemodynamics during transient changes in blood pressure,” *J. Appl. Physiol.*, vol. 110, no. 4, pp. 917–925, 2011, doi: 10.1152/japplphysiol.01407.2010.

[119] F. M. Kashif, G. C. Verghese, V. Novak, M. Czosnyka, and T. Heldt, “Model-based noninvasive estimation of intracranial pressure from cerebral blood flow velocity and arterial pressure,” *Sci. Transl. Med.*, vol. 4, no. 129, 2012, doi: 10.1126/scitranslmed.3003249.

[120] V. Z. Marmarelis, “Linear and Nonlinear Modeling of Cerebral Flow Autoregulation Using Principal Dynamic Modes,” *Open Biomed. Eng. J.*, vol. 6, no. 1, pp. 42–55, 2012, doi: 10.2174/1874230001206010042.

[121] B. Spronck, E. G. H. J. Martens, E. D. Gommer, and F. N. van de Vosse, “A lumped parameter model of cerebral blood flow control combining cerebral autoregulation and neurovascular coupling,” *Am. J. Physiol. - Hear. Circ. Physiol.*, vol. 303, no. 9, 2012, doi: 10.1152/ajpheart.00303.2012.

[122] G. Mader, M. Olufsen, and A. Mahdi, “Modeling Cerebral Blood Flow Velocity During Orthostatic Stress,” *Ann. Biomed. Eng.*, vol. 43, no. 8, pp. 1748–1758, 2015,

doi: 10.1007/s10439-014-1220-4.

[123] R. Lampe, N. Botkin, V. Turova, T. Blumenstein, and A. Alves-Pinto, "Mathematical modelling of cerebral blood circulation and cerebral autoregulation: Towards preventing intracranial hemorrhages in preterm newborns," *Comput. Math. Methods Med.*, vol. 2014, no. July, 2014, doi: 10.1155/2014/965275.

[124] S. Panunzi, L. D'Orsi, D. Iacoviello, and A. De Gaetano, "A stochastic delay differential model of cerebral autoregulation," *PLoS One*, vol. 10, no. 4, pp. 1–21, 2015, doi: 10.1371/journal.pone.0118456.

[125] B. C. Henley, D. C. Shin, R. Zhang, and V. Z. Marmarelis, "Compartmental and Data-Based Modeling of Cerebral Hemodynamics: Nonlinear Analysis," *IEEE Trans. Biomed. Eng.*, vol. 64, no. 5, pp. 1078–1088, 2017, doi: 10.1109/TBME.2016.2588438.

[126] B. C. Henley, D. C. Shin, R. Zhang, and V. Z. Marmarelis, "Compartmental and Data-Based Modeling of Cerebral Hemodynamics: Linear Analysis," *IEEE access Pract. Innov. open Solut.*, vol. 3, pp. 2317–2332, 2015, doi: 10.1109/ACCESS.2015.2492945.

[127] H. Davson, G. Hollingsworth, and M. B. Segal, "The mechanism of drainage of the cerebrospinal fluid," *Brain*, vol. 93, no. 4, pp. 665–678, 1970, doi: 10.1093/BRAIN/93.4.665.

[128] A. Marmarou, K. Shulman, and J. LaMorgese, "Compartmental analysis of compliance and outflow resistance of the cerebrospinal fluid system," *J. Neurosurg.*, vol. 43, no. 5, pp. 523–534, 1975, doi: 10.3171/JNS.1975.43.5.0523.

[129] M. Ursino, "A mathematical study of human intracranial hydrodynamics. Part 1--The cerebrospinal fluid pulse pressure," *Ann. Biomed. Eng.*, vol. 16, no. 4, pp. 379–401, Jul. 1988, doi: 10.1007/BF02364625.

[130] M. Ursino, "A mathematical study of human intracranial hydrodynamics. Part 2--Simulation of clinical tests," *Ann. Biomed. Eng.*, vol. 16, no. 4, pp. 403–416, Jul. 1988,

doi: 10.1007/BF02364626.

[131] R. Aaslid, K. F. Lindegaard, W. Sorteberg, and H. Nornes, “Cerebral autoregulation dynamics in humans,” *Stroke*, vol. 20, no. 1, pp. 45–52, 1989, doi: 10.1161/01.STR.20.1.45.

[132] R. Absi, “Revisiting the pressure-area relation for the flow in elastic tubes: Application to arterial vessels,” *Ser. Biomech.*, vol. 32, no. 1, pp. 47–59, 2018.

[133] K. Rammos, G. Koullias, T. Pappou, A. Bakas, P. Panagopoulos, and S. Tsangaris, “A computer model for the prediction of left epicardial coronary blood flow in normal, stenotic and bypassed coronary arteries, by single or sequential grafting,” *Cardiovasc. Surg.*, vol. 6, no. 6, pp. 635–648, Dec. 1998, doi: 10.1016/S0967-2109(98)00088-X.

[134] G. Drzewiecki *et al.*, “modeling in physiology Vessel growth and collapsible pressure-area relationship,” *Am. J. Physiol. Heart Circ. Physiol.*, vol. 273, pp. H2030–H2043, 1997.

[135] B. G. H. Schoser, N. Riemenschneider, and H. C. Hansen, “The impact of raised intracranial pressure on cerebral venous hemodynamics: a prospective venous transcranial Doppler ultrasonography study,” *J. Neurosurg.*, vol. 91, no. 5, pp. 744–749, Nov. 1999, doi: 10.3171/JNS.1999.91.5.0744.

[136] A. J. W. Boon *et al.*, “Dutch normal-pressure hydrocephalus study: prediction of outcome after shunting by resistance to outflow of cerebrospinal fluid,” *J. Neurosurg.*, vol. 87, no. 5, pp. 687–693, 1997, doi: 10.3171/JNS.1997.87.5.0687.

[137] S. E. Børgesen and F. Gjerris, “The predictive value of conductance to outflow of CSF in normal pressure hydrocephalus,” *Brain*, vol. 105, no. Pt 1, pp. 65–86, Mar. 1982, doi: 10.1093/BRAIN/105.1.65.

[138] R. P. Mahajan and E. J. Simpson, “Reliability of the Transient Hyperemic Response Test in Detecting Changes in Cerebral Autoregulation Induced by the Graded Variations in End-Tidal Carbon Dioxide,” *Neurosurg. Anesth.*, 1998.

[139] P. Smielewski, M. Czosnyka, V. Iyer, S. Piechnik, H. Whitehouse, and J. Pickard, "Computerised transient hyperaemic response test-A method for the assessment of cerebral autoregulation," *Ultrasound Med. Biol.*, vol. 21, no. 5, pp. 599–611, 1995, doi: 10.1016/0301-5629(94)00154-6.

[140] J. Ekstedt, "CSF hydrodynamic studies in man. 1. Method of constant pressure CSF infusion.," *J. Neurol. Neurosurg. Psychiatry*, vol. 40, no. 2, p. 105, 1977, doi: 10.1136/JNNP.40.2.105.

[141] A. D. Lalou *et al.*, "Shunt infusion studies: impact on patient outcome, including health economics," *Acta Neurochir. (Wien).*, vol. 162, no. 5, pp. 1019–1031, 2020, doi: 10.1007/s00701-020-04212-0.

[142] M. Czosnyka, Z. Czosnyka, S. Momjian, and J. D. Pickard, "Cerebrospinal fluid dynamics," *Physiol. Meas.*, vol. 25, no. 5, 2004, doi: 10.1088/0967-3334/25/5/R01.

[143] J. Oertel and S. Antes, "Infusion studies in hydrocephalus," *Acta Neurol. Scand.*, vol. 127, no. 5, pp. 360–361, May 2013, doi: 10.1111/ANE.12066.

[144] M. Czosnyka *et al.*, "Hemodynamic characterization of intracranial pressure plateau waves in head-injury patients," *J. Neurosurg.*, vol. 91, no. 1, pp. 11–19, 1999, doi: 10.3171/JNS.1999.91.1.0011.

[145] M. L. Daley, C. W. Leffler, M. Czosnyka, and J. D. Pickard, "Plateau waves: Changes of cerebrovascular pressure transmission," *Acta Neurochir. Suppl.*, no. 95, pp. 327–332, 2005, doi: 10.1007/3-211-32318-X_67.

[146] N. LUNDBERG, "Continuous Recording and Control of Ventricular Fluid Pressure in Neurosurgical Practice," *J. Neuropathol. Exp. Neurol.*, vol. 21, no. 3, pp. 489–489, Jul. 1962, doi: 10.1097/00005072-196207000-00018.

[147] M. J. Rosner, S. D. Rosner, and A. H. Johnson, "Cerebral perfusion pressure: management protocol and clinical results," *J. Neurosurg.*, vol. 83, no. 6, pp. 949–962, 1995, doi: 10.3171/JNS.1995.83.6.0949.

[148] O. Doron, Y. Zadka, O. Barnea, and G. Rosenthal, “Interactions of brain, blood, and CSF: a novel mathematical model of cerebral edema,” *Fluids Barriers CNS*, vol. 18, no. 1, pp. 1–14, 2021, doi: 10.1186/s12987-021-00274-z.

[149] A. J. HANSEN and C. E. OLSEN, “Brain extracellular space during spreading depression and ischemia,” *Acta Physiol. Scand.*, vol. 108, no. 4, pp. 355–365, 1980, doi: 10.1111/j.1748-1716.1980.tb06544.x.

[150] F. Ramirez de Noriega *et al.*, “A swine model of intracellular cerebral edema - Cerebral physiology and intracranial compliance,” *J. Clin. Neurosci.*, vol. 58, pp. 192–199, Dec. 2018, doi: 10.1016/J.JOCN.2018.10.051.

[151] K. M. Brady *et al.*, “Positive end-expiratory pressure oscillation facilitates brain vascular reactivity monitoring,” *J. Appl. Physiol.*, vol. 113, no. 9, pp. 1362–1368, 2012, doi: 10.1152/japplphysiol.00853.2012.

[152] X. Liu *et al.*, “Assessment of cerebral autoregulation indices – a modelling perspective,” *Sci. Rep.*, vol. 10, no. 1, pp. 1–11, 2020, doi: 10.1038/s41598-020-66346-6.

[153] E. Syková and C. Nicholson, “Diffusion in brain extracellular space,” *Physiol. Rev.*, vol. 88, no. 4, pp. 1277–1340, 2008, doi: 10.1152/physrev.00027.2007.

[154] N. J. Abbott, “Evidence for bulk flow of brain interstitial fluid: Significance for physiology and pathology,” *Neurochem. Int.*, vol. 45, no. 4, pp. 545–552, 2004, doi: 10.1016/j.neuint.2003.11.006.

[155] S. Hrabětová, J. Hrabe, and C. Nicholson, “Dead-space microdomains hinder extracellular diffusion in rat neocortex during ischemia,” *J. Neurosci.*, vol. 23, no. 23, pp. 8351–8359, 2003, doi: 10.1523/jneurosci.23-23-08351.2003.

[156] J. J. Iliff *et al.*, “Impairment of glymphatic pathway function promotes tau pathology after traumatic brain injury,” *J. Neurosci.*, vol. 34, no. 49, pp. 16180–16193, 2014, doi: 10.1523/JNEUROSCI.3020-14.2014.

[157] A. Eklund *et al.*, "Assessment of cerebrospinal fluid outflow resistance," *Med. Biol. Eng. Comput.*, vol. 45, no. 8, pp. 719–735, 2007, doi: 10.1007/s11517-007-0199-5.

[158] C. Zweifel *et al.*, "Continuous monitoring of cerebrovascular pressure reactivity in patients with head injury," *Neurosurg. Focus*, vol. 25, no. 4, 2008, doi: 10.3171/FOC.2008.25.10.E2.

[159] T. Svedung Wettervik, T. Howells, A. Lewén, and P. Enblad, "Blood Pressure Variability and Optimal Cerebral Perfusion Pressure-New Therapeutic Targets in Traumatic Brain Injury," *Neurosurgery*, vol. 86, no. 3, pp. E300–E309, Mar. 2020, doi: 10.1093/NEUROS/NYZ515.

[160] P. Jakkula *et al.*, "Targeting low-normal or high-normal mean arterial pressure after cardiac arrest and resuscitation: a randomised pilot trial," *Intensive Care Med.*, vol. 44, no. 12, pp. 2091–2101, Dec. 2018, doi: 10.1007/S00134-018-5446-8.

[161] E. J. O. Kompanje *et al.*, "Informed consent procedures for emergency interventional research in patients with traumatic brain injury and ischaemic stroke," *Lancet. Neurol.*, vol. 19, no. 12, pp. 1033–1042, Dec. 2020, doi: 10.1016/S1474-4422(20)30276-3.

[162] M. Czosnyka, P. Smielewski, A. Lavinio, J. D. Pickard, and R. Panerai, "An assessment of dynamic autoregulation from spontaneous fluctuations of cerebral blood flow velocity: A comparison of two models, index of autoregulation and mean flow index," *Anesth. Analg.*, vol. 106, no. 1, pp. 234–239, 2008, doi: 10.1213/01.ane.0000295802.89962.13.

[163] B. Depreitere *et al.*, "Cerebrovascular Autoregulation Monitoring in the Management of Adult Severe Traumatic Brain Injury: A Delphi Consensus of Clinicians," *Neurocrit. Care*, vol. 34, no. 3, pp. 731–738, 2021, doi: 10.1007/s12028-020-01185-x.

[164] R. B. Panerai, "Assessment of cerebral pressure autoregulation in humans - A review of measurement methods," *Physiol. Meas.*, vol. 19, no. 3, pp. 305–338, 1998, doi: 10.1088/0967-3334/19/3/001.

[165] P. Smielewski, M. Czosnyka, P. Kirkpatrick, and J. D. Pickard, "Evaluation of the transient hyperemic response test in head-injured patients," *J. Neurosurg.*, vol. 86, no. 5, pp. 773–778, 1997, doi: 10.3171/JNS.1997.86.5.0773.

[166] R. Chesnut *et al.*, "A management algorithm for adult patients with both brain oxygen and intracranial pressure monitoring: the Seattle International Severe Traumatic Brain Injury Consensus Conference (SIBICC)," *Intensive Care Med.*, vol. 46, no. 5, pp. 919–929, 2020, doi: 10.1007/s00134-019-05900-x.

[167] G. J. Bouma, J. P. Muizelaar, K. Bandoh, and A. Marmarou, "Blood pressure and intracranial pressure-volume dynamics in severe head injury: relationship with cerebral blood flow," *J. Neurosurg.*, vol. 77, no. 1, pp. 15–19, 1992, doi: 10.3171/JNS.1992.77.1.0015.

[168] J. M. K. Lam, J. N. K. Hsiang, and W. S. Poon, "Monitoring of autoregulation using laser Doppler flowmetry in patients with head injury," *J. Neurosurg.*, vol. 86, no. 3, pp. 438–445, 1997, doi: 10.3171/JNS.1997.86.3.0438.

[169] M. Czosnyka, P. Smielewski, P. Kirkpatrick, D. K. Menon, and J. D. Pickard, "Monitoring of cerebral autoregulation in head-injured patients," *Stroke*, vol. 27, no. 10, pp. 1829–1834, 1996, doi: 10.1161/01.STR.27.10.1829.

[170] F. A. Zeiler and P. Smielewski, "Application of robotic transcranial Doppler for extended duration recording in moderate/severe traumatic brain injury: first experiences," *Crit. Ultrasound J.*, vol. 10, no. 1, Dec. 2018, doi: 10.1186/S13089-018-0097-0.

[171] L. A. Steiner, D. Pfister, S. P. Strebel, D. Radolovich, P. Smielewski, and M. Czosnyka, "Near-infrared spectroscopy can monitor dynamic cerebral autoregulation in adults," *Neurocrit. Care*, vol. 10, no. 1, pp. 122–128, Feb. 2009, doi: 10.1007/S12028-008-9140-5.

[172] N. Joram *et al.*, "Continuous Monitoring of Cerebral Autoregulation in Children

Supported by Extracorporeal Membrane Oxygenation: A Pilot Study," *Neurocrit. Care*, vol. 34, no. 3, pp. 935–945, Jun. 2021, doi: 10.1007/S12028-020-01111-1.

[173] F. Tiecks, A. Lam, R. Aaslid, and D. Newell, "Comparison of Static and Dynamic Cerebral Autoregulation Measurements," vol. 26, no. June 1995, pp. 1014–1019, 1995.

[174] F. A. Zeiler, J. Donnelly, D. K. Menon, P. Smielewski, P. J. A. Hutchinson, and M. Czosnyka, "A description of a new continuous physiological index in traumatic brain injury using the correlation between pulse amplitude of intracranial pressure and cerebral perfusion pressure," *J. Neurotrauma*, vol. 35, no. 7, pp. 963–974, 2018, doi: 10.1089/neu.2017.5241.

[175] M. J. H. Aries *et al.*, "Continuous monitoring of cerebrovascular reactivity using pulse waveform of intracranial pressure," *Neurocrit. Care*, vol. 17, no. 1, pp. 67–76, 2012, doi: 10.1007/s12028-012-9687-z.

[176] P. M. Lewis, P. Smielewski, J. D. Pickard, and M. Czosnyka, "Dynamic cerebral autoregulation: Should intracranial pressure be taken into account?," *Acta Neurochir. (Wien).*, vol. 149, no. 6, pp. 549–555, 2007, doi: 10.1007/s00701-007-1160-y.

[177] M. Czosnyka, P. Smielewski, S. Piechnik, L. A. Steiner, and J. D. Pickard, "Cerebral autoregulation following head injury," *J. Neurosurg.*, vol. 95, no. 5, pp. 756–763, 2001, doi: 10.3171/JNS.2001.95.5.0756.

[178] M. Hiler *et al.*, "Predictive value of initial computerized tomography scan, intracranial pressure, and state of autoregulation in patients with traumatic brain injury," *J. Neurosurg.*, vol. 104, no. 5, pp. 731–737, May 2006, doi: 10.3171/JNS.2006.104.5.731.

[179] J. A. Claassen *et al.*, "Transfer function analysis of dynamic cerebral autoregulation: A white paper from the International Cerebral Autoregulation Research Network," *J. Cereb. Blood Flow Metab.*, vol. 36, no. 4, pp. 665–680, 2015, doi: 10.1177/0271678X15626425.

[180] X. Liu *et al.*, "Comparison of frequency and time domain methods of assessment of cerebral autoregulation in traumatic brain injury," *J. Cereb. Blood Flow Metab.*, vol. 35, no. 2, p. 248, Feb. 2015, doi: 10.1038/JCBFM.2014.192.

[181] M. L. Sanders *et al.*, "Dynamic cerebral autoregulation reproducibility is affected by physiological variability," *Front. Physiol.*, vol. 10, no. JUL, p. 461520, Jul. 2019, doi: 10.3389/FPHYS.2019.00865/BIBTEX.

[182] J. D. Smirl, K. Hoffman, Y. C. Tzeng, A. Hansen, and A. P. N. Ainslie, "Methodological comparison of active- and passive-driven oscillations in blood pressure; implications for the assessment of cerebral pressure-flow relationships," *J. Appl. Physiol.*, vol. 119, no. 5, pp. 487–501, Sep. 2015, doi: 10.1152/JAPPLPHYSIOL.00264.2015.

[183] F. G. Brodie, E. R. Atkins, T. G. Robinson, and R. B. Panerai, "Reliability of dynamic cerebral autoregulation measurement using spontaneous fluctuations in blood pressure," *Clin. Sci. (Lond).*, vol. 116, no. 6, pp. 513–520, Mar. 2009, doi: 10.1042/CS20080236.

[184] E. D. Gommer, E. Shijaku, W. H. Mess, and J. P. H. Reulen, "Dynamic cerebral autoregulation: different signal processing methods without influence on results and reproducibility," *Med. Biol. Eng. Comput.*, vol. 48, no. 12, pp. 1243–1250, Dec. 2010, doi: 10.1007/S11517-010-0706-Y.

[185] R. B. Panerai, J. M. Rennie, A. W. R. Kelsall, and D. H. Evans, "Frequency-domain analysis of cerebral autoregulation from spontaneous fluctuations in arterial blood pressure," *Med. Biol. Eng. Comput.*, vol. 36, no. 3, pp. 315–322, 1998, doi: 10.1007/BF02522477.

[186] R. B. Panerai, P. J. Eames, and J. F. Potter, "Variability of time-domain indices of dynamic cerebral autoregulation," *Physiol. Meas.*, vol. 24, no. 2, pp. 367–381, 2003, doi: 10.1088/0967-3334/24/2/312.

[187] S. Brasil *et al.*, “Contribution of intracranial pressure to human dynamic cerebral autoregulation after acute brain injury,” *Am. J. Physiol. Integr. Comp. Physiol.*, vol. 324, no. 2, pp. R216–R226, 2023, doi: 10.1152/ajpregu.00252.2022.

[188] R. B. Panerai, “Cerebral autoregulation: from models to clinical applications,” *Cardiovasc. Eng.*, vol. 8, no. 1, pp. 42–59, Mar. 2008, doi: 10.1007/S10558-007-9044-6.

[189] E. M. Wagner and R. J. Traystman, “Cerebrovascular transmural pressure and autoregulation,” *Ann. Biomed. Eng.*, vol. 13, no. 3–4, pp. 311–320, May 1985, doi: 10.1007/BF02584249.

[190] G. E. Cold and F. T. Jensen, “Cerebral autoregulation in unconscious patients with brain injury,” *Acta Anaesthesiol. Scand.*, vol. 22, no. 3, pp. 270–280, 1978, doi: 10.1111/J.1399-6576.1978.TB01301.X.

[191] G. E. Cold, “Cerebral blood flow in the acute phase after head injury. Part 2: Correlation to intraventricular pressure (IVP), cerebral perfusion pressure (CPP), PaCO2, ventricular fluid lactate, lactate/pyruvate ratio and pH,” *Acta Anaesthesiol. Scand.*, vol. 25, no. 4, pp. 332–335, 1981, doi: 10.1111/J.1399-6576.1981.TB01662.X.

[192] J. Sahuquillo *et al.*, “False autoregulation (pseudoautoregulation) in patients with severe head injury. Its importance in CPP management,” *Acta Neurochir. Suppl.*, vol. 76, pp. 485–490, 2000, doi: 10.1007/978-3-7091-6346-7_102.

[193] R. B. Panerai, J. M. Rennie, A. W. R. Kelsall, and D. H. Evans, “Grading of Cerebral Dynamic Autoregulation From Spontaneous Fluctuations in Arterial Blood Pressure,” *Med. Biol. Eng. Comput.*, vol. 36, no. 3, pp. 315–322, 1998, doi: 10.1007/BF02522477.

[194] J. Tas *et al.*, “Inducing oscillations in positive end-expiratory pressure improves assessment of cerebrovascular pressure reactivity in patients with traumatic brain injury,” *J. Appl. Physiol.*, vol. 133, no. 3, pp. 585–592, Sep. 2022, doi:

10.1152/JAPPLPHYSIOL.00199.2022.

[195] I. Timofeev *et al.*, "Effect of decompressive craniectomy on intracranial pressure and cerebrospinal compensation following traumatic brain injury," *J. Neurosurg.*, vol. 108, no. 1, pp. 66–73, Jan. 2008, doi: 10.3171/JNS/2008/108/01/0066.

[196] F. A. Zeiler *et al.*, "Statistical Cerebrovascular Reactivity Signal Properties after Secondary Decompressive Craniectomy in Traumatic Brain Injury: A CENTER-TBI Pilot Analysis," *J. Neurotrauma*, vol. 37, no. 11, p. 1306, Jun. 2020, doi: 10.1089/NEU.2019.6726.

[197] S. Bratton, R. Chestnut, J. Ghajar, F. McConnell Hammond, O. Harris, and R. Hartl, "Guidelines for the management of severe traumatic brain injury. IX. Cerebral perfusion thresholds," *J. Neurotrauma*, vol. 24 Suppl 1, no. SUPPL. 1, 2007, doi: 10.1089/NEU.2007.9987.

[198] E. Beqiri *et al.*, "The lower limit of reactivity as a potential individualised cerebral perfusion pressure target in traumatic brain injury: a CENTER-TBI high-resolution sub-study analysis," *Crit. Care*, vol. 27, no. 1, Dec. 2023, doi: 10.1186/S13054-023-04485-8.

[199] S. Park, E. Beqiri, P. Smielewski, and M. Aries, "Inaugural State of the Union: Continuous Cerebral Autoregulation Monitoring in the Clinical Practice of Neurocritical Care and Anesthesia," *Neurocrit. Care*, pp. 1–10, Oct. 2023, doi: 10.1007/S12028-023-01860-9/METRICS.

[200] E. Needham, C. McFadyen, V. Newcombe, A. J. Synnot, M. Czosnyka, and D. Menon, "Cerebral Perfusion Pressure Targets Individualized to Pressure-Reactivity Index in Moderate to Severe Traumatic Brain Injury: A Systematic Review," *J. Neurotrauma*, vol. 34, no. 5, pp. 963–970, Mar. 2017, doi: 10.1089/NEU.2016.4450.

[201] E. Sorrentino *et al.*, "Critical thresholds for cerebrovascular reactivity after traumatic brain injury," *Neurocrit. Care*, vol. 16, no. 2, pp. 258–266, Apr. 2012, doi:

10.1007/S12028-011-9630-8.

[202] A. G. Kolias *et al.*, “Decompressive craniectomy following traumatic brain injury: developing the evidence base,” *Br. J. Neurosurg.*, vol. 30, no. 2, pp. 246–250, Mar. 2016, doi: 10.3109/02688697.2016.1159655.

[203] H. Alvis-Miranda, S. Milena Castellar-Leones, L. Rafael Moscote-Salazar, and L. Rafael Moscote, “Decompressive Craniectomy and Traumatic Brain Injury: A Review,” *Bull. Emerg. Trauma*, vol. 1, no. 2, p. 60, Apr. 2013, Accessed: Feb. 04, 2024. [Online]. Available: /pmc/articles/PMC4771225/.

[204] D. K. Radolovich *et al.*, “Pulsatile intracranial pressure and cerebral autoregulation after traumatic brain injury.,” *Neurocrit. Care*, vol. 15, no. 3, pp. 379–386, Dec. 2011, doi: 10.1007/S12028-011-9553-4.

[205] M. Czosnyka *et al.*, “Concept of ‘true ICP’ in monitoring and prognostication in head trauma,” *Acta Neurochir. Suppl.*, vol. 95, no. 95, pp. 341–344, 2005, doi: 10.1007/3-211-32318-X_70.

[206] J. Diedler *et al.*, “The limitations of near-infrared spectroscopy to assess cerebrovascular reactivity: the role of slow frequency oscillations,” *Anesth. Analg.*, vol. 113, no. 4, pp. 849–857, 2011, doi: 10.1213/ANE.0B013E3182285DC0.

[207] F. A. Zeiler *et al.*, “Continuous Autoregulatory Indices Derived from Multi-Modal Monitoring: Each One Is Not Like the Other,” *J. Neurotrauma*, vol. 34, no. 22, pp. 3070–3080, 2017, doi: 10.1089/neu.2017.5129.

[208] J. Donnelly *et al.*, “Observations on the Cerebral Effects of Refractory Intracranial Hypertension After Severe Traumatic Brain Injury,” *Neurocrit. Care*, vol. 32, no. 2, p. 437, Apr. 2020, doi: 10.1007/S12028-019-00748-X.

[209] M. Balestreri *et al.*, “Intracranial hypertension: what additional information can be derived from ICP waveform after head injury?,” *Acta Neurochir. (Wien).*, vol. 146, no. 2, pp. 131–141, Feb. 2004, doi: 10.1007/S00701-003-0187-Y.

[210] M. Czosnyka, D. J. Price, and M. Williamson, “Monitoring of cerebrospinal dynamics using continuous analysis of intracranial pressure and cerebral perfusion pressure in head injury,” *Acta Neurochir. (Wien).*, vol. 126, no. 2–4, pp. 113–119, Jun. 1994, doi: 10.1007/BF01476419.

[211] J. Donnelly *et al.*, “Cerebral haemodynamics during experimental intracranial hypertension,” *J. Cereb. Blood Flow Metab.*, vol. 37, no. 2, p. 694, 2017, doi: 10.1177/0271678X16639060.

[212] A. Hall and R. O’Kane, “The best marker for guiding the clinical management of patients with raised intracranial pressure—the RAP index or the mean pulse amplitude?,” *Acta Neurochir. (Wien).*, vol. 158, no. 10, pp. 1997–2009, Oct. 2016, doi: 10.1007/S00701-016-2932-Z/FIGURES/5.

[213] D. J. Kim *et al.*, “Index of cerebrospinal compensatory reserve in hydrocephalus,” *Neurosurgery*, vol. 64, no. 3, pp. 494–501, Mar. 2009, doi: 10.1227/01.NEU.0000338434.59141.89.

[214] Y. Yang, Y. Pan, C. Chen, P. Zhao, and C. Hang, “Clinical Significance of Multiparameter Intracranial Pressure Monitoring in the Prognosis Prediction of Hypertensive Intracerebral Hemorrhage,” *J. Clin. Med.*, vol. 11, no. 3, Feb. 2022, doi: 10.3390/JCM11030671.

[215] Y. Pan, Y. Xue, P. Zhao, J. Ding, Z. Ren, and J. Xu, “Significance of ICP-related parameters for the treatment and outcome of severe traumatic brain injury,” *J. Int. Med. Res.*, vol. 48, no. 8, Aug. 2020, doi: 10.1177/0300060520941291.

[216] A. Vik *et al.*, “Relationship of ‘dose’ of intracranial hypertension to outcome in severe traumatic brain injury: Clinical article,” *J. Neurosurg.*, vol. 109, no. 4, pp. 678–684, Oct. 2008, doi: 10.3171/JNS/2008/109/10/0678.

[217] E. R. Zanier, F. Ortolano, L. Ghisoni, A. Colombo, S. Losappio, and N. Stocchetti, “Intracranial pressure monitoring in intensive care: clinical advantages of a

computerized system over manual recording," *Crit. Care*, vol. 11, no. 1, 2007, doi: 10.1186/CC5155.

[218] F. Caire and J. J. Moreau, "Méthode et résultats du test de perfusion dans l'hydrocéphalie à pression normale : revue de la littérature," *Rev. Neurol. (Paris).*, vol. 166, no. 5, pp. 494–501, May 2010, doi: 10.1016/J.NEUROL.2009.10.007.

[219] G. V. Varsos, M. Kasprowicz, P. Smielewski, and M. Czosnyka, "Model-based indices describing cerebrovascular dynamics," *Neurocrit. Care*, vol. 20, no. 1, pp. 142–157, 2014, doi: 10.1007/s12028-013-9868-4.

[220] Z. Czosnyka, M. Czosnyka, A. Lavinio, N. Keong, and J. D. Pickard, "Clinical testing of CSF circulation," *Eur. J. Anaesthesiol.*, vol. 25, no. SUPPL. 42, pp. 142–145, 2008, doi: 10.1017/S0265021507003249.